Doctoral Dissertation

Study on Natural Circulation of the Reactor Pool under RVACS Operation using Fluid to Fluid Model Simulating Experiment

Min Ho Lee

Department of Nuclear Engineering

Graduate School of UNIST

2020

Study on Natural Circulation of the Reactor Pool under RVACS Operation using Fluid to Fluid Model Simulating Experiment

A dissertation
submitted to the Graduate School of UNIST
in partial fulfillment of the
requirements for the degree of
Doctor of Philosophy of Science

Min Ho Lee

04. 16. 2020

Approved by

Advisor

In Cheol Bang

Study on Natural Circulation of the Reactor Pool under RVACS Operation using Fluid to Fluid Model Simulating Experiment

Min Ho Lee

This certifies that the dissertation of Min Ho Lee is approved.

04. 16. 2020

signature

Advisor: In Cheol Bang

signature

Dong Wook Jerng

signature

Eung Soo Kim

signature

Ji Hyun Kim

signature

Eisung Yoon

Abstract

Passive safety becomes more and more important under station black out situation like Fukushima, providing trustworthy countermeasure for the accident. Importance of the passive safety is emphasized in the generation-IV reactors which are under development. Among the gen-IV reactors, lead-cooled fast reactor and sodium-cooled fast reactor have advantages to apply passive safety system driven by natural circulation due to superior thermal properties of the liquid metal coolant. For design and performance evaluation of natural circulation driven passive safety systems, experimental approach is necessary. However, liquid metal natural circulation itself has many difficulties like high temperature, toxicity, handling, cost, etc. Therefore, simulating experiment is required for the liquid metal natural circulation. In this research, experimental validation was conducted with liquid metal and non-metallic fluid, water. And based on the result of the validation experiment, natural circulation behavior under reactor vessel auxiliary cooling system (RVACS) operation condition was investigated, changing decay heat and boundary condition.

For the validation of the similarity law, Wood's metal, which is alloy of bismuth, lead, tin and cadmium, was selected as a representative for the liquid metal and water was selected as a simulant of liquid metal. In this experiment, it was concluded that water experiment could simulate temperature field of liquid metal natural circulation with reasonable error, and could simulate velocity field with moderate error.

Based on the validation experiment, 2-D slab model was designed for RVACS performance evaluation. Effect of decay heat and boundary condition on the temperature distribution inside of the reactor pool were observed in the experiment. It was concluded that change of the decay heat affected slightly to the normalized temperature distribution and boundary condition made global shift of the temperature in the whole reactor pool.

Contents

List of figures

List of tables

Nomenclature

A_{eq}	: equivalent area	[m]
Bo’	: modified Boussinesq number	[1]
Gr’	: modified Grashof number	[1]
L	: characteristic length	[m]
Nu	: Nusselt number	[1]
P	: pressure	[Pa]
Q	: heat generation rate	[W]
Q”, q”	: heat flux	[W/m^2]
Q_0	: volumetric heat generation rate	[W/m^3]
T	: temperature	[K]
T_0	: temperature at the arbitrary reference point	[K]
T^*	: non-dimensionalized temperature	[1]
c_p	: specific heat	[J/kg.K]
g	: gravitational acceleration	[m/s^2]
h	: heat transfer coefficient	[W/m^2.K]
$\dot{m}$	: mass flow rate	[kg/s]
t	: time	[s]
t^*	: non-dimensionalized time	[1]
u_i	: velocity	[m/s]
u_i^*	: non-dimensionalized velocity	[1]
x_i	: Cartesian co-ordinates	[m]
x_i^*	: non-dimensionalized Cartesian co-ordinates	[m]
ΔP	: Pressure drop	[Pa]
ΔT	: Temperature difference	[K]
Δx	: Thickness	[m]
α	: thermal diffusivity	[m^2/s]
β	: volumetric thermal expansion coefficient	[1/K]
δ_{ij}	: Kronecker's delta	[1]
θ	: Non-dimensionalized temperature	[1]

ν	: kinematic viscosity	$[m^2/s]$
ρ	: density	$[kg/m^3]$
ζ	: Pressure drop coefficient	[1]

Chapter 1. Introduction

1.1. Research background and motivation

The meaning of the word ‘safety’ has something in common in the nuclear safety and military. During most of the operation time, their importance could be forgettable, because a probability of accident is very low. However, when the accident happens, the safety system, which could mitigate the result of the accident, becomes extremely important. In the point of the guaranteed activation of the safety system, reliability of the safety system is the most important thing. Safety systems should be activated as designed whenever it is required under extreme conditions.

I usually use metaphor of the safety and integrity of the nuclear system as a diaper. The best thing is the diaper kept clean, which corresponds to no core damage in nuclear accident. However, once the core was damaged, maintaining the integrity of the boundary is important to prevent leakage of the radioactive material into the environment, like the diaper. The boundary was damaged by accumulation of the thermal energy, which was mainly caused by decay heat, the most unique point of the nuclear power. To prevent the accumulation of the thermal energy, safety systems operate in two ways; controlling heat generation of the reactor core and cooling the heat from the core. The research scope of the dissertation is about cooling of the decay heat.

To secure its activation under extreme conditions, the nuclear safety systems have evolved in the direction of using passiveness, which provide a naturally occurring deriving force for its activation. This kind of the deriving forces employs simple principle from the nature. Because they were derived without any external power, activation of the passive safety system could be secured under station black out (SBO) circumstance. Generally, forced convection is the best way to deliver heat, however, it requires power for the activation of the pump. The dependence on the active safety system has been proof by Fukushima accident. Safety systems were failed under SBO condition and the Fukushima provided us a lesson: the importance of the passive safety. Therefore, for the passiveness, passive systems employing natural circulation as their deriving force have been received attention. For the general pressurized water reactor (PWR), various passive injection systems and heat exchanger have been researched focusing on supplying coolant into the core, which removes heat from the core by phase change.

The trend to use passive safety system was also applied to the developing reactors like the LMRs. Therefore, to remove heat passively, natural circulation was employed in the LMRs, whose coolant has favorable characteristics for the natural circulation. In case of the PWR, simply, supply of the coolant is important because of boiling is the main heat removal mechanism. However, for the LMRs, coolant temperature is very important for positive void coefficient and structural integrity. Different to

water, liquid metals have high boiling point so that under single-phase natural circulation, integrity of the structure could be threatened. In case of the sodium-cooled fast reactor (SFR), boiling phenomena should also be considered because of its relatively low boiling point. If the sodium coolant temperature increases more than its boiling temperature, boiling occurs, and corresponding positive reactivity is related to re-criticality. Therefore, during passive heat removal by natural circulation in the LMRs, temperature distribution of the coolant is very important.

There are various decay heat removal systems (DHRS) using natural circulation. They could be divided into two groups; one is the additional heat exchanger and the other is reactor vessel auxiliary cooling system (RVACS). The additional heat exchanger type DHRSs needs additional heat transfer systems for transfer heat from the heat exchanger to the final heat sink. Thus, in the aspect of simplicity and reliability, they are worse than that of the RVACS, which only requires additional opening of the damper in the air duct for its activation. The RVACS could have another advantage in the aspect of reactivity because relative insert depth of the control rod is affected by the reactor vessel (RV) temperature. So that the RVACS is superior in the aspect of passive safety.

In summary, the passive safety system RVACS was researched in the aspect of the temperature distribution of the reactor pool under natural circulation. It was conducted in the experimental way with simulating experiments because using simulant has more advantages than directly using liquid metal. Theoretical base of the similarity law of the temperature field of the natural circulation is introduced, and the similarity law was validated by the validation experiment. Finally using the similarity law, the reactor pool temperature distribution under RVACS operation was experimentally analyzed with a reference reactor, prototype generation-IV sodium-cooled fast reactor (PGSFR).

1.2. Literature review on the DHRSs in the LMRs

The definition of the nuclear safety is protection of the human being and environment from the probable radiation hazard. To isolate radioactive materials in the reactor system boundary, integrity of the system should be secured by proper cooling. As briefly mentioned before, boiling of coolant in the LMRs is not allowed for the coolant temperature itself and positive reactivity followed by the void. Fortunately, the liquid metal coolant has several favorable features for the passive heat transfer, specifically, the natural circulation. Its thermal conductivity is more than an order higher than the traditional coolant, water. Considering operation temperature, the viscosity of the liquid metals is approximately several mPa.s, which is similar to that of water higher than 80°C. Therefore, LMRs employed single-phase natural circulation for its passive heat removal.

Experimental breeder reactor -II (EBR-II) was a pool-type SFR with 62.5 MWth power. A shutdown cooler was installed in the EBR-II and could remove 0.5 % of the total power[1]. Various tests

were conducted in the EBR-II for the successful shutdown of the reactor and proper cooling of the decay heat[2-6]. The combination of the secondary side heat removal and decay heat removal by the shutdown heat exchanger showed their capability to cool the reactor sufficiently under loss of flow or heat sink accident, even in unprotected case.

Fast flux test facility (FFTF) was a test reactor for testing various concept of the loop-type SFR, which was built in 1978. It had the higher power than the EBR-II, as 400 MWth. The concept of the passive decay heat removal was already applied in this early age[7-9]. Decay heat was removed by dump heat exchangers, which were already used in the normal operation for the balance of heat generation and removal because the FFTF did not generate electricity. The FFTF had a unique reactivity control system, gas expansion module, which increases leakage of the neutron by changing sodium surrounding the core to the inert gas. The passive decay heat removal concept was validated in the FFTF facility.

Joyo was a loop type, prototype SFR in Japan which had 100 MWth of power. It had indirect DHRS through the intermediate heat exchanger (IHX). If primary and secondary pumps were stopped after scram, DHRS could remove sufficient amount of heat in the loss of flow and loss of heat sink accident. However, this system was partially passive because blower in the final dump heat exchanger required external power for its operation[10-13].

Monju was another loop type, prototype SFR in japan which had approximately 700MWth of power. Also, the Monju had similar DHRS to Joyo. The DHRS of the Monju was natural circulation loop installed in the secondary loop, with air heat exchanger[14-15]. It also required power for the blower operation.

PRISM is the abbreviation of power reactor innovative small module, which is based on the EBR-II design. It is a pool-type demonstration reactor of SFR with 840 MWth power. It has not been constructed yet, however, its design gives insights to other developing SFRs. The PRISM has an additional heat exchanger for decay heat removal, which is immersed in the reactor pool[16-17]. RVACS is also applied for the PRISM. These DHRS concept have been adopted in many other LMRs[18]. Under current design, RVACS of the PRISM can successfully remove decay heat of the core. Additionally, it was revealed that combination of the RVACS and decay heat exchanger (DHX) could shutdown the reactor inherently and cool the reactor properly even in unprotected conditions[17].

PGSFR is an SFR under development in Korea, which is the abbreviation of prototype generation-IV sodium cooled fast reactor. It is prototype pool-type reactor which has 392 MWth of power. It has similar DHRS to PRISM; DHX and RVACS. Passiveness of the DHX has been improved form the design of the PRISM because heat exchanger at the air side of the DHX loop includes partially natural circulation[19]. The design of the RVACS is basically the same with the PRISM. The safety systems showed good performance even under unprotected conditions[20-21], and RVACS could give additional

safety margin in the aspect of both reactivity and cooling[22].

ASTRID is a pool type prototype SFR under development by collaboration of France and Japan. Its abbreviation is advanced sodium technological reactor for industrial demonstration, and it has 1500 MWth power. Because it has larger power than other reactors, there are three kinds of DHRS in the ASTRID, named RRA, RRB, RRC respectively. RR means residual heat removal and A, B, and C mean numbering of each system[23-25]. RRA and RRB are similar to DHX of other pool type SFRs. RRA requires electrical power for its operation, while RRB does not. RRC is a kind of external vessel cooling, however, different to PWR, it is operated by oil and pump. Instead of RVACS, the ASTRID selected RRC.

The lead cooled fast reactor (LFR) is another reactor type using liquid metal coolant. Compared to SFR, thermal conductivity is relatively lower, density is much higher, and boiling point is much higher than sodium. The LFR is still under development so that there is no prototype or demonstration reactor, except for the engine of submarine. All the LFRs under development is pool-type reactor and adopted DHX[26-28]. RVACS is under consideration, though, LFR has favorable structures for the application of the RVACS, RVACS is one of the promising for the safety system of the LFR.

To summarize, DHRSs of the reactor could be categorized by whether it is pool-type or loop-type. Regardless of its coolant, only geometry of the reactor determines the type of the DHRSs. For the loop type reactors, DHRSs were installed in the IHX and acted like auxiliary secondary side of the reactor, which could remove the heat from the primary system. For the loop-type reactors, there is no space for installation of the DHRS directly in the primary system. Therefore, DHRSs were installed at the IHX, where is the nearest point in the aspect of the heat transfer chain and favorable point for the natural circulation of the primary side. For this kind of the natural circulation, which occurred in the loop, phenomena in the natural circulation could be simplified as 1-D and relatively easily analyzed by system code. However, in case of the DHRSs of the pool-type reactors, DHRSs were installed in the reactor pool. Therefore, complex natural circulation phenomena occur in the reactor pool. Because the natural circulation flow is not confined by the loop, the natural circulation in the reactor pool is very complexed. According to the type of the DHRS, whether it is the DHX or RVACS, natural circulation phenomena could be totally different. Install position of the DHX also could affect the natural circulation phenomena, which is in the cold pool or hot pool.

Currently developing reactors like all the LFRs, PGSFR, and ASTRID, they adopted pool-type design because it has more advantages than loop-type design. Even for the loop-type design adopted pool-type like design features like increased vessel size considering thermal inertial, and adopted DHX in the primary system because of the safety issue[29-30]. Even hybrid reactors of the pool and loop-type reactor are under discussion[31]. In case of the SFR, there are more advantages in the pool-type SFR in the aspect of the inherent safety like large thermal inertia and void coefficient[32-35]. Its thermal

inertia is much larger than that of the loop-type SFR. In the viewpoint of the efficiency of the heat removal from the core, DHRSs of the pool-type reactor are more efficient than those of the loop-type because they are installed closer to the core in the thermal circuit.

To analyze complex natural circulation phenomena in the pool-type reactors, various experimental apparatus has been developed. However, most of them are focused on the DHX and corresponding natural circulation phenomena. The natural circulation under the RVACS operation has unique characteristics in the aspect of heat sink term and distribution of the natural circulation, thus, it should be independently researched.

1.3. Uniqueness of the present study

As mentioned before, DHRSs installed in the reactor pool accompany with complex natural circulation. The DHRSs in the reactor pool have various name like RRA and RRB in the ASTRID, direct reactor auxiliary cooling system (DRACS) in the Japanese SFR (JSFR), and just DHX in the PGSFR. In detail, RRA and RRB are installed in the boundary of the cold pool and hot pool, DHX is installed in the cold pool, and DRACS is installed in the hot pool. Therefore, the natural circulation by the RRA, RRB, DHX occurred in the whole pool, while the natural circulation by the DRACS occurred in the only hot pool. However, in the aspect of the heat sink, they have many things in common, only circulation path is different. Heat sink, in other words cooling, is related to the heat exchanger, which is relatively small region compared to the whole reactor pool. Therefore, it could be simplified as volumetric heat sink in the heat sinking region, similar to the volumetric heat source of decay heat in the active fuel region.

On the other hand, the RVACS showed totally different in the aspect of the heat sink term. The heat source term is the same because it is the decay heat. However, cooling of the RVACS occurs at the RV. It means that cooling of the RVACS occurs through the large region and it could not be simplified like volumetric heat sink in the DHXs. Considering heat removal characteristics of the RVACS, the heat sink term should be heat flux term near the wall.

The difference of the heat sink term between the volumetric heat sink and the areal heat sink showed significant difference in the aspect of similarity. For heat exchanger type DHRS, combination of the geometrical similarity and volumetric heat generation or removal rate could easily assure similarity between the model and the prototype. The heat removal profile, in other words, distribution of the volumetric heat sink could be negligible because heat is removed only small region in the reactor pool. Thus, distribution of the cooling in the small heat exchanger region could be negligible in the aspect of overall natural circulation. However, in case of the RVACS, its distribution could not be neglected. For the natural circulation, deriving force of the natural circulation could be simplified

using distance between the thermal center, which means heating center and cooling center. The location of the cooling center could be affected by the distribution of the cooling heat flux. Even with the same cooling thermal center, the distribution of the cooling heat flux easily has effect on the natural circulation due to complex internal structures in the reactor pool.

Additionally, realistic boundary condition of the RVACS have not been clearly researched. There are various researches about the RVACS[22,36-38], however, they usually focused on the performance of the external air natural circulation, which is final heat sink. Schematic of the RVACS was illustrated in the figure 1-1. In the aspect of the thermal circuit of the RVACS, it could be summarized like the figure 1-2. Heat from the core is removed by the liquid metal coolant natural circulation, where the cooling boundary is the RV. Heat from the RV is removed by the containment vessel (CV) through conduction and radiation. Finally, external air natural circulation removes heat from the CV. Here, CV and RV are conjugated with radiation and conduction. Moreover, heat removal at the RV in the viewpoint of the sodium natural circulation, is conjugated heat source at the CV to the external air. Therefore, two natural circulation (the liquid metal and the air) are closely conjugated and interact each other.

For these complex and important phenomena related to cooling boundary condition of the liquid metal natural circulation, there is no complete research for the effect of the boundary condition. Moreover, for the experimental approach, issues related to similarity law for the temperature field of the natural circulation have not been clearly validated by the direct comparing experiment. The issues were described in more detail in the following chapter. Based on the similarity law, the effect of the boundary condition was experimentally analyzed, in addition to the effect of decay heat level.

In summary, there are some unique points in the present study. Regard to the similarity law, cooling boundary condition as surface heat sink was considered in addition to conventional volumetric heat sink or source. Consequently, the effect of the boundary condition was experimentally analyzed. Most of all, fully experimental validation of the similarity law is the most unique point of the present study. It is necessary to strictly validate the law, however, it has not been conducted yet. The author conducted strict validation of the similarity law for the first time in the world.

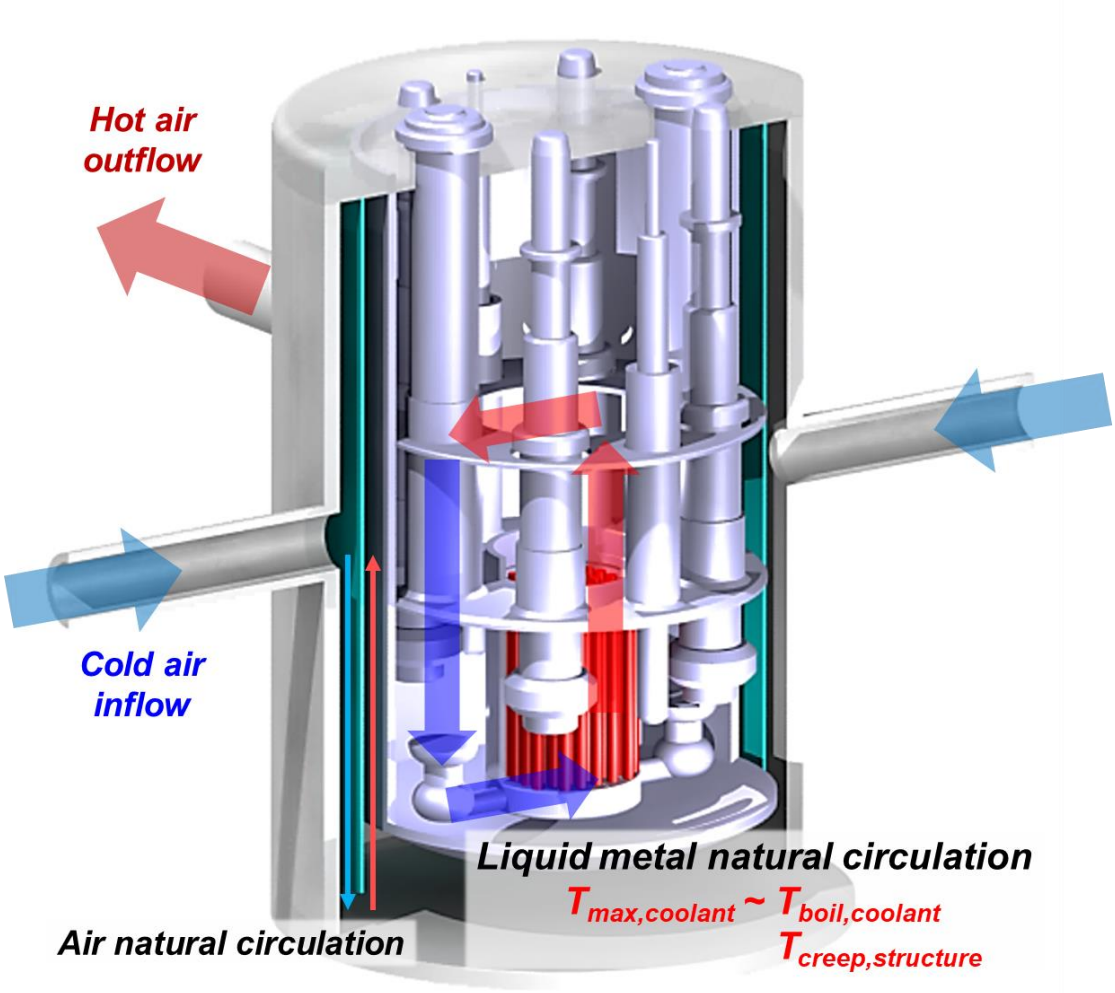

Figure 1-1. Schematic of the thermal circuit of the RVACS

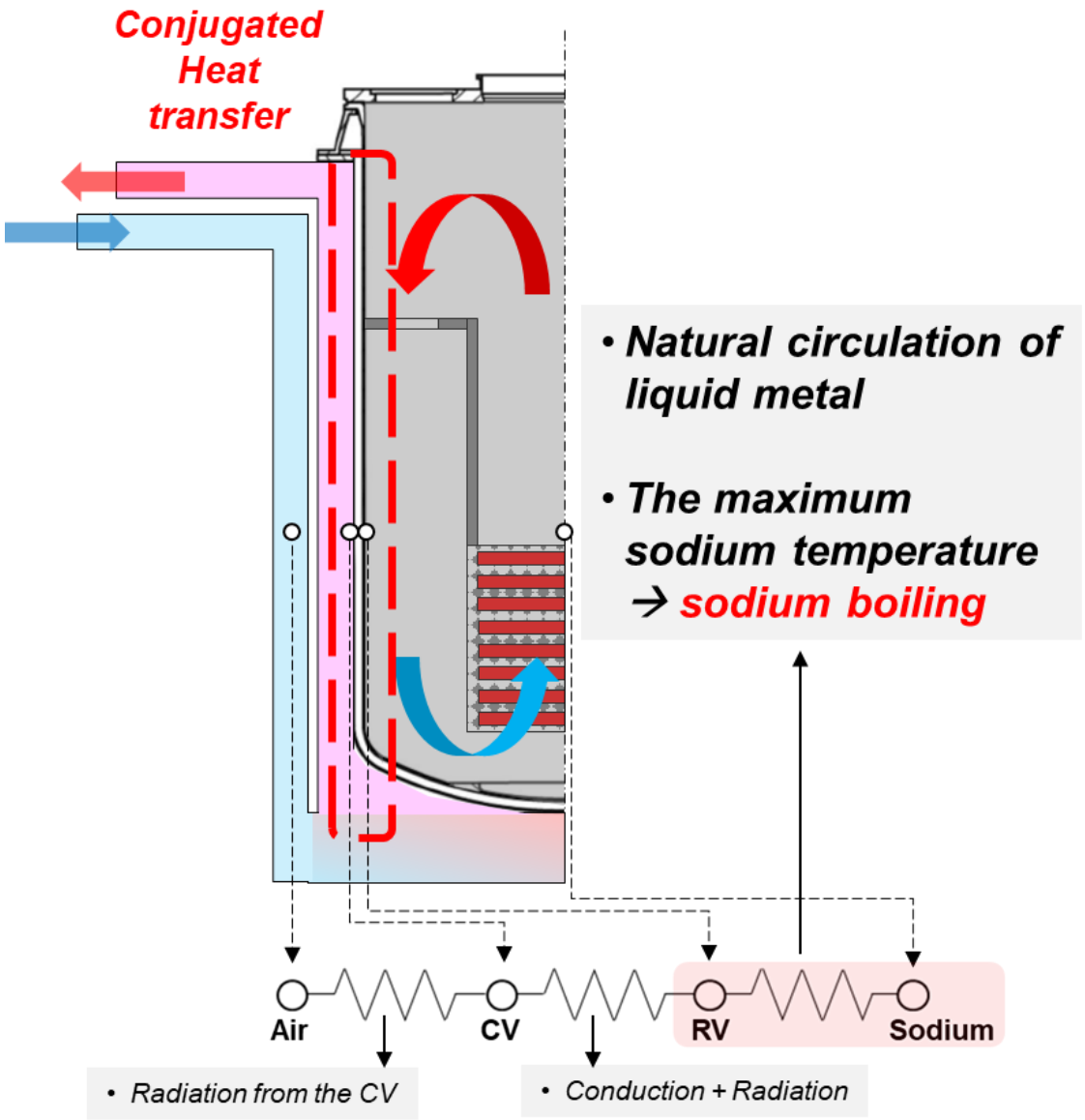

Figure 1-2. Schematic of the thermal circuit of the RVACS

1.4. Research objectives and scope

The final goal of the present study is to evaluate natural circulation phenomena under RVACS operation. To obtain that results, experimental approach was used based on the similarity law. This similarity law was experimentally validated including boundary condition effect. The process of the research is summarized.

(1) To revisit similarity law with unique approach for the boundary condition

(2) To validate similarity law in the fully experimental way

(3) Based on the similarity law, another experiment for observing boundary condition effect was designed.

(4) Validate experimental results with computational methods

(5) Analyze phenomena and evaluate the effect of the boundary condition on the natural circulation

The experiments were conducted in the series of the experimental facility named SINCRO, which is the abbreviation of the simulating natural circulation of reactor pool under the RVACS operation.

Chapter 1 is introduction of the present study and the RVACS including the importance and necessity of the present study. The uniqueness of the present study is summarized compared to the other research.

Chapter 2 is about theoretical derivation of the similarity law about the temperature field of the natural circulation and data interpretation method.

Chapter 3 is about the validation experiment for the similarity law. Wood's metal and water were selected as representative fluid to validate similarity law and temperature distribution was analyzed in both quantified and qualified manner.

Chapter 4 is the main experiment, which was observing the effect of the boundary condition effect in the realistic geometry. The experimental facility designed based on the PGSFR and simplified as 2-D slab model. Its results were also compared to the numerical results which were obtained by commercial CFD software ANSYS-CFX and system code MARS-KS.

The summary and the conclusions of the present study are described in the chapter 5.

Finally, this research would contribute to the safety analysis of the SFR. The performance evaluation of the RVACS is conducted by transient analysis through the system code like MARS-KS. Regard to the validity of the system code, my research could give experimental results for the validation of the code under steady state.

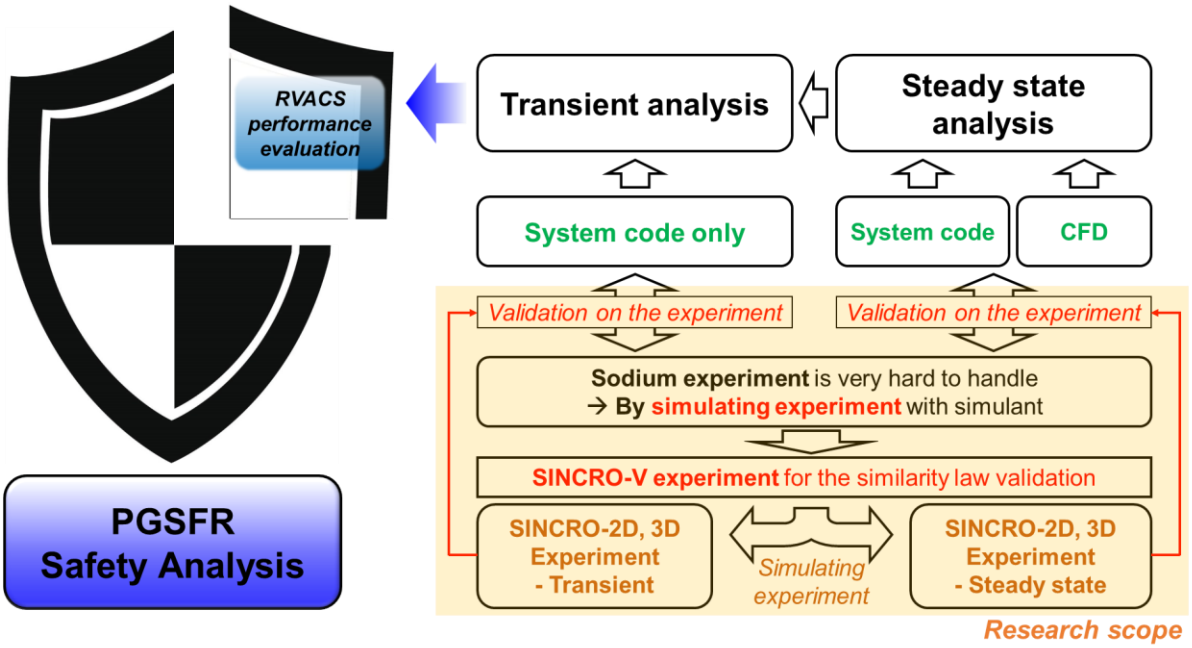

Figure 1-3. Scope of the research

Chapter 2. Theoretical base for the natural circulation similarity

2.1. Introduction to Bo' based similarity law

Importance of the liquid metal natural circulation was introduced in the previous section. Therefore, experiments for the liquid metal are required for validation of the numerical results and system codes. However, the liquid metals have severe disadvantages for their handling. In case of sodium, it should be isolated from the air or water due to its extremely high reactivity. In case of lead, it could be relatively free from the reactivity issue, however, it has a corrosive effect with most of the structural metals. Including corresponding system, the liquid metal experiment has more disadvantages. For the similarity, the size of the original system could not be significantly reduced, which regards to the large experimental system and corresponding high capacity of the power, insulation, system weight, etc. The experiments using liquid metal directly have many disadvantages, thus, simulating experiment with simulant should be considered.

In general, the Grashof number and Rayleigh number are usually considered as main parameter for the similarity. The Grashof number is the ratio of viscous force to inertial force, which is related to the flow regime of the natural circulation flow. The Rayleigh number is multiplication of the Grashof number and Prandtl number, and the ratio of the time scale of the conduction to the convection. In other words, if the Rayleigh number is larger than certain value, the convective time scale is smaller than the conductive time scale. Therefore, the Rayleigh number is related to the magnitude of the natural circulation heat transfer.

To consider the meaning of the general natural circulation similarity law, review of the derivation of the similarity law is required. Three governing equation for the continuity, momentum, and energy were non-dimensionalized with reference parameters. For the non-dimensionalization, references for the velocity and temperature were used as external values, like u infinite and T infinite. From this kind of reference selection, it could be concluded that scope of the Grashof and Rayleigh number-based similarity law is focused in the near wall region, where infinite values exist. A lot of heat transfer correlations have been developed based on the Grashof and Rayleigh number-based similarity law. In summary, traditional, general similarity law is focused on the near-wall phenomena, in other words, heat transfer.

However, modified Boussinesq number (Bo') based similarity law has different fields of view to the traditional similarity law. The Bo' based similarity law is focus on the overall behavior of the natural circulation system. Basically, three governing equations are the same with the traditional similarity law. The derivation of non-dimensionalization and corresponding important non-dimensional numbers are the same.

The basis of similarity was proposed by Grewal et al.; they suggested that water simulation of sodium natural circulation is better than the scaled sodium test[39]. Preliminary analysis of the design concept was conducted by comparing scaled and working fluids in terms of nondimensional numbers[40]. It was revealed that a similar experiment using water has many advantages over liquid metal experiments in reduced scale. Eguchi et al. evaluated the similarity law by comparing water experiments and computational fluid dynamics (CFD) data. The temperature showed 7% to 30% discrepancy with CFD data because of insulation[41].

Most of the sodium natural circulation experiment were conducted using water as simulant based on the Bo' based similarity law. To analyze natural circulation phenomena under direct heat exchanger (DHX) operation condition, RAMONA and NEPTUN experimental facility were built, and they were scaled-down by 1/20 and 1/5, respectively[42-45]. Various simulations of upper internal structures were conducted in RAMONA. For the NEPTUN facility, there were unique phenomena named inter-wrapper flow, which is a reverse flow into the outer core region from the upper plenum. Water experiment with the 1/8 scaled-down model showed good agreement with temperature drop rate; however, the temperature gradient did not match actual plant data[46]. Akutsu et al. experimented with the same 1/8 model. The direct reactor ACS (DRACS) and primary reactor ACS (PRACS) were tested, and the data were used to develop multidimensional system analysis codes[47]. Takeda et al. performed water experiment on a 1/20, 2-D slab model and observed the fluctuations of both velocity and temperature[48]. After the 2-D model experiment, they extended their work to the 3-D model, which had 1/20 and 1/6 scale, and compared the results[49]. They concluded that the effect of the modified Grashof number (Gr') could be negligible, while that of modified Boussinesq number (Bo') should be into consideration. In AQUARIUS, which has 2-D slab shape in 1/20 scale, the effect of DHX location was investigated[50]. Recently, the spatial distribution of the phenomena was investigated by Mente et al.[51]. Flow distribution under DHX operation was observed and fuel assemblies in the outer core were more effectively cooled by direct downward flow from the DHX. The similarity law was also applied to loop-type reactors. The primary flow rate and temperature were investigated in a 1/10 scaled-down facility of a reactor named Japanese SFR[52]. The PHEASANT facility focused on velocity distribution as well as temperature, and visualized flow during DHX operation conditions[53]. In the case of LFR, the MYRRAHABELLE facility has been developed, which is a 1/5-scale 3-D model of the MYRRHA, and temperature behavior in various transient situations were investigated[54].

Difference between the Bo' based similarity law and the general similarity law is selection of the reference point for non-dimensionalization. In case of the general similarity law, reference point is bulk fluid, thus, the similarity law has focus near wall phenomena comparing with bulk fluid, like heat transfer phenomena. However, Bo' based similarity law has unique references for non-dimensionalization. Rather than infinite value, the reference parameters in the Bo' based similarity

law were derived from the characteristics of the natural circulation system. In the aspect of overall system, temperature difference, velocity, and time could not be defined without considering the system properties. For example, in case of the same pair of system, if power of the one system is higher than the other system, reference properties should be differed from each other. If two system have the same geometrical characteristics with different scale, reference properties should be changed along the scale of the system. Additionally, for the same pair of system with different working fluid, the reference parameters in the systems should be differed. To reflect this kind of system properties and working fluid's properties, reference parameters of the Bo' based similarity law were derived from combinations of the system and workings fluid's properties. Briefly, using characteristics of the natural circulation and balances in the system, the reference properties were derived. Thereby, Bo' based similarity law could focus on the over behavior of the system under the natural circulation. From the next section, detailed derivation process and its application would be analyzed.

2.2. Derivation of the Bo' based similarity law

As mentioned before, similarity law was derived from the non-dimensionalization of the governing equations like general similarity law with Grashof and Rayleigh number. However, Bo' base similarity law has different point of view owing to its reference considering overall system. In this section, deriving reference parameters for the natural circulation was introduced, and based on the reference, important non-dimensionalized numbers were derived based on the non-dimensionalization of the governing equation. Then, discussion on the priority and meaning of the non-dimensionalized numbers were described.

2.2.1. Setting reference values for the natural circulation

In the natural circulation system, there is no specific references for some parameters. In the traditional similarity law, infinite values were used as references, like T infinite and u infinite. However, in the aspect of the overall system, there is no infinite value or certain reference for the temperature difference or velocity in the natural circulation system. Therefore, in the Bo' based similarity law, reference parameters were derived considering properties of the working fluid and system properties including scale.

In the natural circulation system, there is one clear reference, the length scale. Therefore, the other references such as the velocity, time, and temperature difference should be defined by functions of the other, clear parameters. To derive relationship between parameters and to express undefined reference, first, balance between the kinetic energy and buoyancy potential energy could be used. Under the

steady state of the natural circulation, the deriving forces of the system equals to the loss of the energy during natural circulation, which makes flow do not change. It could be expressed like equation (2-1). The left-hand side of equation (2-1) represent the buoyancy potential energy of the natural circulation system, which was defined as a multiplication of the density difference, gravitational acceleration, and length scale. The right-hand side of equation (2-1) represent the kinetic energy of the natural circulation, whose velocity was the reference velocity of the system.

Here, using the Boussinesq approximation, which is that the density difference could be expressed as a multiplication of the reference density and the volumetric expansion coefficient, left-hand side of equation (2-1) could be modified as equation (2-2). Then, neglecting constant, and re-arrange equation (2-2) as a function of u, equation (2-3) could be derived.

$$\Delta\rho g L \sim \frac{1}{2}\rho u_{ref}^2 \tag{2-1}$$

$$\rho g\beta\Delta T_{ref} L \sim \frac{1}{2}\rho u_{ref}^2 \tag{2-2}$$

$$u_{ref} = \left(g\beta\Delta T_{ref} L\right)^{1/2} \tag{2-3}$$

Basically, this process has the same meaning with an assumption that Richardson number was 1. The Richardson number means the ratio of buoyancy force to inertia force of the working fluid, in other words, the driving force of the natural circulation to the kinetic energy of the system. Therefore, the balance between the buoyancy potential energy and the kinetic energy could be expressed in more strict manner. The Richardson number was assumed as 1.

$$Ri = \frac{g\beta\Delta T_{ref} L}{u_{ref}^2} = 1 \tag{2-4}$$

In equation (2-3), it was success that expressing uncertain reference velocity with other parameters. However, as shown in the right-hand side of equation (2-3), it still had an uncertain parameter as the reference temperature difference. To eliminate this uncertain parameter in the expression of the velocity, one more relationship between the heating and convective heat transfer in the heating region was used. Equation (2-5) is the general energy conservation equation with internal source. Here, two terms in the general governing equation were assumed as zero: the transient term and the diffusion term. Neglecting these terms has two meaning. One is the steady state, and the other is neglecting diffusive heat transfer, which is dominant in the region having a high temperature gradient, especially, near wall region.

After neglecting two terms, equation (2-5) was changed to equation (2-6). Here, we could use a concept of the total heat generation. Because Q_0 is volumetric heat generation in the unit volume, total heat generation Q_{total} could be expressed as Q_0L^3 under isotropic scaling. By doing so, Equation (2-6) could be manipulated as (2-7), which is the description of Q_0 as a function of other properties. Each parameter in the equation (2-7) was treated as reference parameter. It is the balance between heating and convective cooling.

$$\frac{\partial T}{\partial t} + u_j \frac{\partial T}{\partial x_j} = \alpha \frac{\partial^2 T}{\partial x_j^2} + \frac{Q_0}{\rho c_p} \tag{2-5}$$

$$u_j \frac{\partial T}{\partial x_j} = \frac{Q_0}{\rho c_p} \tag{2-6}$$

$$Q_{total} = \rho c_p u_{ref} \Delta T_{ref} L^2 \tag{2-7}$$

Here, we obtained another relationship between the reference velocity and the reference temperature difference. By using equation (2-3) and (2-7) we could express the other parameters with clear, defined parameters. The reference time was expressed as length scale over reference velocity, which has a dimension of time. The reference velocity, the reference time, and the reference temperature difference were summarized in the equation (2-8) to (2-10) respectively. And comparisons of the reference parameters to the general, forced convection situation were summarized in the table 2-1.

$$u_{ref} = \left(\frac{\beta g}{\rho c L} \right)^{1/3} Q^{1/3} \tag{2-8}$$

$$t_{ref} = \left(\frac{\rho c L^4}{\beta g} \right)^{1/3} Q^{-1/3} \tag{2-9}$$

$$\Delta T_{ref} = \left(\beta g \rho^2 c^2 L^5 \right)^{-1/3} Q^{2/3} \tag{2-10}$$

2.2.2. Non-dimensionalization of the governing equations

Three governing equations; the mass, momentum, and energy conservation equation, are non-dimensionalized by the reference parameters obtained in the previous section. The three conservation equations are summarized in the equation (2-11) – (2-13-1) respectively. Equation (2-13) is the general energy conservation equations including both heat source and sink term, while equation (2-13-

1) is the energy conservation equation without the source and sink term, which would be applied for the not heated and cooled region.

$$\frac{\partial u_i}{\partial x_i} = 0 \tag{2-11}$$

$$\frac{\partial u_i}{\partial t} + u_j \frac{\partial u_i}{\partial x_j} = \nu \frac{\partial^2 u_i}{\partial x_j^2} - \beta \Delta T g \delta_{i3} - \frac{1}{\rho} \frac{\partial P}{\partial x_i} \tag{2-12}$$

$$\frac{\partial T}{\partial t} + u_j \frac{\partial T}{\partial x_j} = \alpha \frac{\partial^2 T}{\partial x_j^2} + \frac{Q_0}{\rho c_p} - \frac{Q''}{\rho c_p L} \tag{2-13}$$

$$\frac{\partial T}{\partial t} + u_j \frac{\partial T}{\partial x_j} = \alpha \frac{\partial^2 T}{\partial x_j^2} \tag{2-13-1}$$

By the reference parameters, non-dimensionalized governing equations are summarized in equation (2-14) – (2-16-1). Here, the heat source term could be treated as 1 (unity) as long as volumetric heat generation rate was maintained. Regard to the volumetric heat generation, it could be changed. However, if it is decreased, quality of the experimental data become degraded because overall magnitude of the parameter decreases, and relative error is increased. Otherwise, it could not be increased considering specification of the cartridge heater. Therefore, the volumetric heat generation rate was the same with prototype. Thus, the heat source term in equation (2-16) was evaluated as unity by Richardson number assumption, which is balance between convective cooling and heating. Therefore, similarity for the heating could be achieved by making the volumetric heat generation rate identical for the heating region. Regard to the heat sink term, it could be characterized to cooling heat flux. For ideal similarity, cooling heat flux should be applied with similar distribution characteristics. However, by simple Fourier's law, the conductive heat flux could be expressed as function of temperature difference between two points. It means that the temperature of the cooling boundary is properly simulated, temperature difference between the cooling boundary and pool, and corresponding cooling heat flux could be simulated. Regard cooling, boundary temperature is pretty much easier to control than heat flux. Therefore, it is better to apply temperature boundary condition to get similarity for the heat sink number considering practical application. The heat source term and sink term would be discussed in more detail in the following part.

$$\frac{\partial u_i^*}{\partial x_i^*} = 0 \tag{2-14}$$

$$\frac{\partial u_i^*}{\partial t^*} + u_j^* \frac{\partial u_i^*}{\partial x_j^*} = \frac{1}{Gr'^{1/2}} \frac{\partial^2 u_i^*}{\partial x_j^{2*}} - \frac{\beta g \Delta T_{ref} L}{u_{ref}^2} T^* \delta_{i3} - \frac{\Delta P}{\rho u_{ref}^2} \frac{\partial P^*}{\partial x_i^*} \quad (2\text{-}15)$$

$$\frac{\partial T^*}{\partial t^*} + u_j^* \frac{\partial T^*}{\partial x_j^*} = \frac{1}{Bo'^{1/2}} \frac{\partial^2 T^*}{\partial x_j^{2*}} + \frac{Q_0 L}{\rho c_p u_{ref} \Delta T_{ref}} - \frac{Q''}{\rho c_p u_{ref} \Delta T_{ref}} \quad (2\text{-}16)$$

$$\frac{\partial T^*}{\partial t^*} + u_j^* \frac{\partial T^*}{\partial x_j^*} = \frac{1}{Bo'^{1/2}} \frac{\partial^2 T^*}{\partial x_j^{2*}} \quad (2\text{-}16\text{-}1)$$

Here, two important non-dimensional numbers were derived in the diffusion term in the right-hand side of equation (2-15) and (2-16). One is the modified Grashof number (Gr'), the other is the Bo', which we continuously discussed about. Their definitions are given in equations (2-17) and (2-18), respectively. As shown in its name, modified Grashof number, Gr' has similar meaning to the original Grashof number, which is the ratio between the buoyancy force to the viscous force. However, Bo' has similar but different meaning with the Rayleigh number. Because its reference is the overall system, Bo' represents the ratio of the amount of the heat transfer by the natural circulation to conduction.

$$Gr' = \left(\frac{\beta g}{\rho c_p} \right)^{2/3} \frac{L^{4/3} Q^{2/3}}{\nu^2} \quad (2\text{-}17)$$

$$Bo' = \left(\frac{\beta g}{\rho c_p} \right)^{2/3} \frac{L^{4/3} Q^{2/3}}{\alpha^2} \quad (2\text{-}18)$$

Table. 2-1 Summary and comparison of the reference parameters for non-dimensionalization

Parameter	**Reference**	
	Forced circulation	Natural circulation
x (length scale)	L	L
u (velocity)	u_∞	$u_{ref} = \left(\frac{\beta g}{\rho c L} \right)^{1/3} Q^{1/3}$
t (time)	L/u_∞	$t_{ref} = \left(\frac{\rho c L^4}{\beta g} \right)^{1/3} Q^{-1/3}$
T (Temperature)	T_∞	$\Delta T_{ref} = \left(\beta g \rho^2 c^2 L^5 \right)^{-1/3} Q^{2/3}$

2.3. Meaning and priority of the similarity parameters

In this section, detailed similarity parameters in the non-dimensionalized equations would be discussed including meaning of the two important non-dimensional numbers; Gr' and Bo'. Then, based on their meaning, relative importance of the parameters is determined considering realistic simulants and the liquid metal. After that, not only for the Gr' and Bo', other similarity parameters in the governing equation are discussed.

2.3.1. Similarity parameters in the momentum conservation equation

$$\frac{\partial u_i^*}{\partial t^*} + u_j^* \frac{\partial u_i^*}{\partial x_j^*} = \frac{1}{Gr'^{1/2}} \frac{\partial^2 u_i^*}{\partial x_j^{2*}} - \frac{\beta g \Delta T_{ref} L}{u_{ref}^2} T^* \delta_{i3} - \frac{\Delta P}{\rho u_{ref}^2} \frac{\partial P^*}{\partial x_i^*} \qquad (2\text{-}15)$$

$$Ri = \frac{g\beta \Delta T_{ref} L}{u_{ref}^2} = 1 \qquad (2\text{-}4)$$

The non-dimensionalized momentum conservation equation is in equation (2-15). Terms in the left-hand side consist of non-dimensionalized parameters like u_i^*, t^*, and x^*. Therefore, they could be excluded from the similarity issue. The three terms in the right-hand side of the equation includes parameters like system properties and material properties. Discussion is continued with these three terms with their meaning and order of magnitude, in other words, the relative importance.

The first term is regard to diffusion phenomena and includes Gr'. As described before, Gr' is the ratio of buoyancy force to viscous force and determines flow regime in the natural circulation. It has the similar meaning to the Reynolds number in the forced flow condition, which determines flow regimes in common. Because Gr' is related to flow regime of the natural circulation, it could be compromised as preservation of the flow regime.

The balance between the buoyancy potential energy and inertial force is described in the second term. In the derivation procedure, the author assumed the balance between the buoyancy potential energy of the natural circulation and the kinetic energy of the natural circulation flow, and it corresponds to assumption that Richardson number is unity, in more mathematical expression. The Richardson number is added in front of the multiplication of non-dimensionalized temperature difference and Kronecker delta. Therefore, similarity issue related to the second term in the right-hand side could be summarized that Richardson number was assumed as 1.

Third term includes dimensional parameter as pressure drop over kinetic energy of the natural circulation flow, which is the definition of the pressure drop coefficient. It means that the pressure drop coefficient each part should be matched to secure the similarity in the aspect of the flow. The

pressure drop coefficient could be matched by modifying a cross sectional area of the component like orifice. Therefore, this term could be matched independently with other terms.

2.3.2. Similarity parameters in the energy conservation equation

$$\frac{\partial T^*}{\partial t^*} + u_j^* \frac{\partial T^*}{\partial x_j^*} = \frac{1}{Bo'^{1/2}} \frac{\partial^2 T^*}{\partial x_j^{2*}} + \frac{Q_0 L}{\rho c_p u_{ref} \Delta T_{ref}} - \frac{Q''}{\rho c_p u_{ref} \Delta T_{ref}} \qquad (2\text{-}16)$$

Equation (2-16) indicates the non-dimensionalized energy conservation equation. Similar to the non-dimensionalized momentum conservation equation, two terms in the left-hand side do not includes dimensional parameters. Therefore, similarity issue on the energy conservation equation would be discussed in the only three terms in the right-hand side of the equation.

The diffusion term in the first includes Bo', which is the main similarity parameter in the present similarity law of the temperature distribution of the natural circulation. The Bo' is the ratio of the heat transferred amount by natural circulation to that by the conduction. It is similar to the Peclet number in the forced convection situation, however, Bo' concentrates on the overall system. It is the key parameter for the similarity law, so that the Bo' of the model should be identical to that of the original system.

The second term is related to the heat source of the natural circulation, which was given as the volumetric heat generation. By replacing the reference velocity and the reference temperature to their definition in equation (2-8) and (2-10) respectively, this term treated as unity. For the same volumetric heat generation rate, it remains unity. In case of the volumetric heat generation rate change, corresponding reference parameters are changed automatically, and this term steel remains unity. Therefore, this term is kept as unity in every situation and similarity about the source term could be automatically secured.

Last term is regard to cooling of the natural circulation. This is unique boundary condition because the RVACS showed different cooling characteristics compared to the DHX or other decay heat exchanger. This term could be considered in two ways. First, in the aspect of the overall system, heat flux could be expressed in the form of the total power over area if heat balance of the system maintained, like (Q_0L^3/L^2). And this term could be reduced to Q_0L and the heat sink term has the same form with the heat source term. Here, isotropic scaling was assumed in the expression of Q" in another form and reduction. Thus, in the aspect of the overall system, similarity of the cooling boundary condition could be achieved by isotropic scale reduction. Second, for heat transfer phenomena near boundary, heat flux term could be expressed as $k\Delta T_{ref}/L$, using the concept of the

Fourier's law. Thereby, the heat sink term could be reduced to ($\alpha/u_{ref}L$). By using relationship between u_{ref} and t_{ref}, it could be changed to ($\alpha t_{ref}/L^2$), which is the same form with Fourier number. Fourier number means the ratio between the amount of the heat transfer to heat storage, thus, it should have value as 1 for both Wood's metal and water under steady state. Even under unsteady state, it could have the same value for both Wood's metal and water. By replacing u_{ref} to its definition in the equation (2-8), the heat sink term summarized as $Bo'^{3/2}$, which could be identical between Wood's metal and water by matching the main similarity criterion for the similarity law, Bo'. Here, ΔT and Δx term in the Fourier's law was expressed by the ΔT_{ref} and L, which is reference temperature difference and length scale. It means that temperature profile in the cooling boundary should be linearly proportional to the reference temperature difference, and boundary layer thickness should be reduced in the isotropic manner, having same reduction ratio with the general length. In summary, similarity of the cooling region could be achieved by isotropic scale reduction, matching Bo' and assumption of temperature profile and thickness of the boundary layer. Even it could be valid under unsteady state if heat balance of the system is similar.

For the volumetric heat sink term, which could be applied to the DHX, distribution could be neglected because cooling region is very small compared to the overall reactor pool. Therefore, heat flux sink term is one of the unique points in the present study. The heat flux boundary concept was derived from the characteristics of the RVACS, whose cooling is achieved by the RV wall, having considerable cooling region compared to the overall reactor pool. The heat sink term described cooling of the working fluid during going downward through the cooling wall. Dimension of the equation (2-13) and (2-13-1) was [K/s], which was temperature change rate. To derived cooling term, schematic of the cooling phenomena and corresponding mathematical description were summarized in figure 2-1. Here, balance between temperature change of the working fluid and the cooling could be expressed like equation (2-19) and (2-20), where $\Delta T_{in,out}$ represents $T_{in} - T_{out}$.

$$Q_{out} = \rho c_p uwd\left(T_{in} - T_{out}\right) \tag{2-19}$$

$$q''wh = \rho c_p uwd\Delta T_{in,out} \tag{2-20}$$

$$q''L^2 = \rho c_p uL^2\Delta T_{in,out} \tag{2-21}$$

It could be simplified as equation (2-21) by replacing w, d, and h by representative length scale L. Because isotropic scale reduction was assumed, it could be represented by the common parameter as the length scale L. Velocity term u could be modified as (L/t) because it has the dimension of the length over time. Then, arranging both sides of the equation (2-21), equation (2-22) could be derived.

From equation (2-22) we could obtain temperature change rate over time like equation (2-23), which is the cooling term in the equation (2-13) in the previous section.

$$q'' = \rho c_p L \Delta T_{in,out} / t \tag{2-22}$$

$$\Delta T_{in,out} / t = \frac{q''}{\rho c_p L} \tag{2-23}$$

If system is under steady state, the amount of heating and cooling is equal. Therefore, in the aspect of average heat flux, similarity about non-dimensional cooling heat flux is automatically achieved without a particular cooling methodology. Furthermore, the author intended to control cooling condition in more detail, which could be represented as its distribution. In case of the DHX cooling experiment, total cooling could be measured by using temperature increment in the cooling loop. Size of the DHX is smaller than that of the pool, therefore, detailed distribution of the cooling heat flux through the DHX could be ignored in the aspect of the overall temperature distribution inside the pool. However, in case of the RVACS, where all the RV wall is the cooling wall, its distribution could not be neglected. Therefore, the author intended to control distribution of the cooling. However, in the point of heat flux distribution control in the experiment, it is not easy to achieve. Otherwise, in case of the heating, both heat flux (power) and temperature could be easily achieved because heat flux could be directly controlled by power change and temperature could be monitored in real-time. However, heat flux distribution control in cooling could not be clearly given. The temperature cooling condition could be given in more detail by monitoring cooling wall temperature. Moreover, in the real RVACS situation, boundary condition would be given as temperature of the RV wall. The most important reason is that the heat flux distribution could be indirectly quantified by temperature distribution along the wall. Referring figure 2-1, outward heat flux (cooling) could be expressed like equation (2-24)

$$q'' = h\left(T_{fluid} - T_{wall}\right) \tag{2-24}$$

As described in the equation (2-13), parameter which has direct effect on the fluid temperature was cooling heat flux. Objective of the temperature boundary condition is to simulate distribution of the heat flux. To control heat flux, control of three terms in the right-hand side is required. Here, the heat transfer coefficient h could not be modified because operating condition and working fluid were already fixed. The fluid temperature T_{fluid} could automatically have similarity because similarity of the temperature distribution in the pool was already satisfied by the Bo'. Last term is wall temperature,

which was the main concern in the discussion. In the practical point of view, by controlling wall temperature at an arbitrary point, heat flux could be controlled at the point.

The total cooling amount must be the same under steady state as discussed in the first part of the comment. Therefore, controlling of distribution of the heat flux along the cooling wall could make same cooling boundary condition in the aspect of the heat flux, and it could be achieved by the cooling wall temperature control. Furthermore, change of the heat transfer coefficient along the wall could be sufficiently reflected by changing wall temperature theoretically. General Nusselt number for the laminar, vertical wall natural circulation is like equation (2-25). g(Pr) means a function of Prandtl number, which was described in the right-hand side. Under isotropic scaling condition, x could be properly scaled. Prandtl number is already determined according to simulant. The most important parameter determining distribution of Nusselt number was temperature difference term. It could be properly simulated by controlling wall temperature. In conclusion, the author insist that cooling condition should be applied as temperature boundary condition. The reason is that the temperature boundary condition is more practical in the point of distribution and heat flux distribution could be scaled based on the temperature-based approach.

$$Nu_x = \left(\frac{Gr_x}{4}\right)^{1/4} g(Pr) = \left(\frac{g\beta(T_\infty - T_{wall})x^3}{4\nu^2}\right)^{1/4} \frac{0.75\,Pr^{1/2}}{\left(0.609 + 1.221\,Pr^{1/2} + 1.238\,Pr^{1/4}\right)} \quad (2\text{-}25)$$

2.3.3. Practical limitation for simulating with real materials

To obtain the perfect similarity, all the non-dimensional numbers should be identical between the original system and model. However, as shown in equation (2-17) and (2-18), the two numbers have many parameters in common. It means that Gr' and Bo' could not be independently modified by changing its system or working fluid. Therefore, we should select a one parameter between Gr' and Bo'. It would be discussed in the following section in more detail, but briefly, there is no material satisfying both Bo' and Gr simultaneously. Between Gr' and Bo', with regard to the temperature field of natural circulation, Bo' is more important because it denotes the ratio of the amount of heat transferred by natural circulation to that of conduction. A lot of previous research indicated that identical Bo' with compromised Gr' ensures the similarity of the temperature field[43,46,49,53]. Therefore, the Bo' was selected as main similarity parameters in the study.

For the compatibility of the identical Bo' and the identical Gr' between the original system and the model, the author obtained proper length scale for the identical Bo'. Based on the discussion on Bo', and scale for the identical Bo', corresponding Gr' at that condition would be discussed. Here, Bo' was assumed as a solely function of the length scale for a single material. Considering the definition of the

Bo' in equation (2-18), the volumetric heat generation rate could be changed, in addition to the length scale. However, it was fixed as constant as other literatures did[40-49,51-53]. There are two reasons for the fixed volumetric heat generation rate. Here, a working fluid of the system was assumed as the sodium and simulant was assumed as the water. First one is related to increasing the volumetric heat generation rate. Actually, the average volumetric heat generation rate of a certain SFR (PGSFR) was 213.4MW/m^3 (213.4W/cm^3). In case of 1% of the decay heat, 2.13W/cm^3 of the heat should be generated as the q''' was maintained. This value was average power density for the whole core so that net power density should be considered excluding flow region. Then, the power density became quite high-power density for the heater, which was nearly manufacturing limit for the heater. Therefore, increasing power density in the experimental facility was hard to be considered.

$$\Delta T_{Sodium} = \frac{\Delta T_{reference,Sodium}}{\Delta T_{reference,water}} \times \Delta T_{water} \tag{2-26}$$

Otherwise, decreasing power density also has problem. As described in the definition of the Bo', if volumetric heat generation (equivalent to total heat generation under isotropic scaling) decrease, length scale for the identical Bo' is increased. In case of sodium-water simulation, scale-down ratio for water facility is 1/25 for the same volumetric heat generation and 1/17 for the 1/10 reduced volumetric heat generation. The most important problem is drastically decreased ΔT_{ref}, which cause increase of error. It would be discussed in more detail in section 2.4, however, to briefly discuss disadvantages of reducing the volumetric heat generation rate, it was simply referred. ΔT_{ref} is used as numerator in the data interpretation formula, equation (2-26). Error in the predicted sodium temperature was calculated assuming that uncertainty of the temperature in the experiment was 1.5°C. Exact calculation was summarized in the table 2-2 and ΔT_{ref} for sodium was 1.636°C. If the volumetric heat was reduced to 1/10 and the facility was designed based on that parameter, size of the facility could be increased approximately 1.5 times. It is a clear advantage of the scaling up by reducing the volumetric heat generation. However, as mentioned before, error in the predicted sodium temperature was increased. Originally, the error was 10°C, which could be acceptable. However, after size reduction, the error was increased approximately 4 times, approximately 40°C. This is an obvious disadvantage for reducing the volumetric heat generation. In conclusion, increase of the volumetric heat generation rate is hard to achieve because of the specification limit of the cartridge heater. Reduction of the volumetric heat generation rate was possible, however, there was a significant disadvantage. 1/10 times of the reduction of the volumetric heat generation rate made scale of the experimental facility approximately 1.5 times larger, while error range was increased approximately 4

times. Therefore, do not change the volumetric heat generation rate, and using the same volumetric heat generation rate is the best.

Therefore, Bo' becomes a solely function of the length scale. Figure 2-2 showed relative length scale for identical Bo', while water was set as reference as a length scale of unity. It means that compared to the water system, the length scale of the other system should be increased or decreased to the corresponding scale. For example, if someone want to simulate water natural circulation by the ethanol, the size of the ethanol system should be 0.35 times of the water in the aspect of the length scale. And, to simulate natural circulation of the Field's metal by the water, the size of the water facility is 7.3 times smaller than that of the Field's metal facility in the perspective of the length scale.

To simulate natural circulation of the liquid metals by non- metallic fluids, the non-metallic fluid could be categorized as 4 groups: heat transfer oils, liquid metals, heat transfer salts, refrigerants, and the water. For heat transfer oils, which is light brown colors in figure 2-2, to match Bo', the scale should be less than 1/50. Moreover, the ratio of Gr' number has much smaller value than other liquid so that the flow regime would be significantly changed. Because of the highest viscosity and lowest thermal conductivity among the candidates, heat transfer oils are not suitable for simulant of liquid metals. Liquid metals, which are in the right side of the figure 2-2 have similar properties with original coolant, sodium, except for density. These similar properties have some advantages in scale difference, however, have disadvantages in scale-down. The liquid metal system, more precisely, the reactor pool is too large to directly conduct experiment without scale-down. Toxicity and economy are the other problems for liquid metals. Therefore, liquid metal was excluded. Heat transfer salts, which are green in figure 2-2, requires smaller length scale than water and they are also opaque. Refrigerants are blue letters in figure 2-2. They are transparent, however, requires smaller length scale for identical Bo'. So that there is no advantage than water in refrigerant and it is same for ethanol. The water is the fluid whose properties are most well-known, however, the water could not make both the Bo' and Gr' identical with liquid metals simultaneously. All kinds of the simulants for the liquid metal natural circulation were reviewed, however, there was no simulant to satisfy similarity for both the Bo' and the Gr' simultaneously. Therefore, we cannot make perfect similarity by matching all kinds of the non-dimensional numbers. Object of the similarity law is to simulate temperature distribution of the liquid metal natural circulation. Between the Bo' and Gr', for simulating temperature distribution, it was known that Bo' is more important that Gr'[41,46,49,50]. Gr' is related to natural circulation flow regime, such as laminar or turbulent. Moreover, concentrating on Bo' could provide rough similarity for the flowrate because the temperature distribution is the driving force of the natural circulation[41,52]. Therefore, in this similarity law, as its named, Bo' was considered as the core similarity parameter.

2.3.4. Priority analysis using order of magnitude

As reviewed in the section 2.2.1 and 2.2.2, various parameters related to the similarity issue were discussed. In case of the energy conservation equation, the Bo' should be matched because it is the main similarity parameters. The similarities in the heat source and sink could be matched independent to matching the Bo' because the heat source term is always unity and the heat sink term could be matched by modifying boundary condition, which is independent to the Bo'. Therefore, similarity issues in the energy conservation equation are solved.

However, for the momentum conservation equation, the Gr' cannot be identical to the original system as long as Bo' is identical. The second term including the Richardson number is always unity because the Richardson number was assumed as 1 during the derivation. The last term is related to pressure drop coefficient, which could be matched independent to the Bo' or the Gr' by modifying the cross section of flow channels. In this section, the author wanted to clarify the meaning and importance of the pressure drop coefficient in the viewpoint of the overall flow similarity. For the overall flow similarity, relative importance of the Gr' and the pressure drop coefficient are discussed in the present section.

The order of magnitude method was used in this section, which simply compare the order of magnitude of each term by combination of the order of magnitude of each parameter. The order of magnitude of each parameter is summarized in table 2-3. Considerable order of magnitude was expressed as 1 and negligible order of magnitude was expressed as epsilon (ε). Non-dimensionalized parameter like non-dimensionalized velocity, temperature difference, and pressure have an order of 1 because they were already non-dimensionalized to have an order of 1. For the derivatives, along the parallel direction to the flow direction, there is no significant change of the parameters except for the pressure difference, which is the deriving force of the flow. Along the perpendicular direction to the flow direction, the situation is reversed from the that of the parallel direction. Therefore, only the pressure derivative has an order of ε and the other terms have an order of 1. Gr' of the PGSFR is about 3.55×10^{12}, and 2.18×10^{6} in the SINCRO-2D facility, which is a 2-D slab model facility of the PGSFR. Therefore, Gr' is assumed as $1/\varepsilon$, which represents a large number. δ is Kronecker delta, which have values of 0 or 1 regard to the basis of the tensor. The pressure drop coefficient surely has an order of 1 because it has a meaningful order of magnitude, however, not as big as Gr'. Based on the order of magnitude of each parameter as discussed, equation (2-27) summarized the order of magnitude term by term.

$$\underset{\{0\}}{\frac{\partial u_i^*}{\partial t^*}} + \underset{\{1*1*1\}}{u_j^* \frac{\partial u_i^*}{\partial x_j^*}} = \underset{\{\varepsilon^{1/2}*1*1*1\}}{\frac{1}{Gr'^{1/2}} \frac{\partial^2 u_i^*}{\partial x_j^{2*}}} - \underset{\{1*1*1\}}{\frac{\beta g \Delta T_{ref} L}{u_{ref}^2} T^* \delta_{i3}} - \underset{\{1*1*1\}}{\frac{\Delta P}{\rho u_{ref}^2} \frac{\partial P^*}{\partial x_i^*}} \quad (2\text{-}27)$$

The left-hand side has an order of 1 by adding 0 and 1, while the right-hand side has an order of 1 by summation of $\varepsilon^{1/2}$,1 and 1. It could be verified that the order of magnitude of each parameter was properly assumed because order of the left-hand side and the right-hand side is equal. Here, about the order of the magnitude of the terms in the right-hand side, there is a clue for the importance of each term in the viewpoint of the overall similarity. Excluding the second term in the right-hand side, which is related to the Richardson number, the order of magnitude of the first term and the third term is different. The Gr' related term has an order of $\varepsilon^{1/2}$ and the pressure drop coefficient related term has an order of 1. The order of magnitude of the pressure drop term is larger than that of the Gr' term. It means that relative importance of the pressure drop coefficient is bigger than that of the Gr'. It suggests an importance priority of the flow similarity. As discussed before, the Bo' is the most important parameter for the natural circulation flow because it is related to the temperature distribution, which is the driving force of the natural circulation. And then, the second important parameter is the pressure drop coefficient. The Gr' is the third important parameter according to the order of magnitude analysis. This kind of the priority gives justification of the compromise of the Gr' for identical Bo'. Although the Gr' is not matched with that of the original system, by matching the Bo' and the pressure drop coefficient, the flow similarity could be achieved because the Bo' and the pressure drop coefficient are more important than the Gr'. Therefore, the similarity issue related to the Gr' could be relatively free as long as the flow regime maintained.

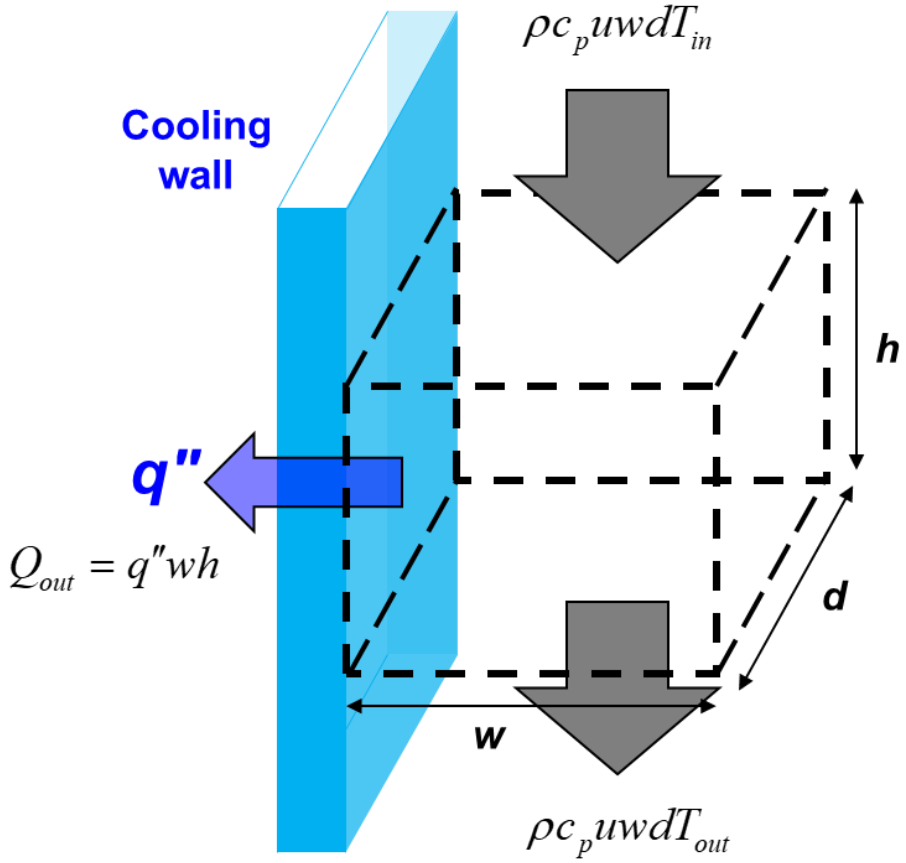

Figure 2-1. Schematic of the cooling boundary condition

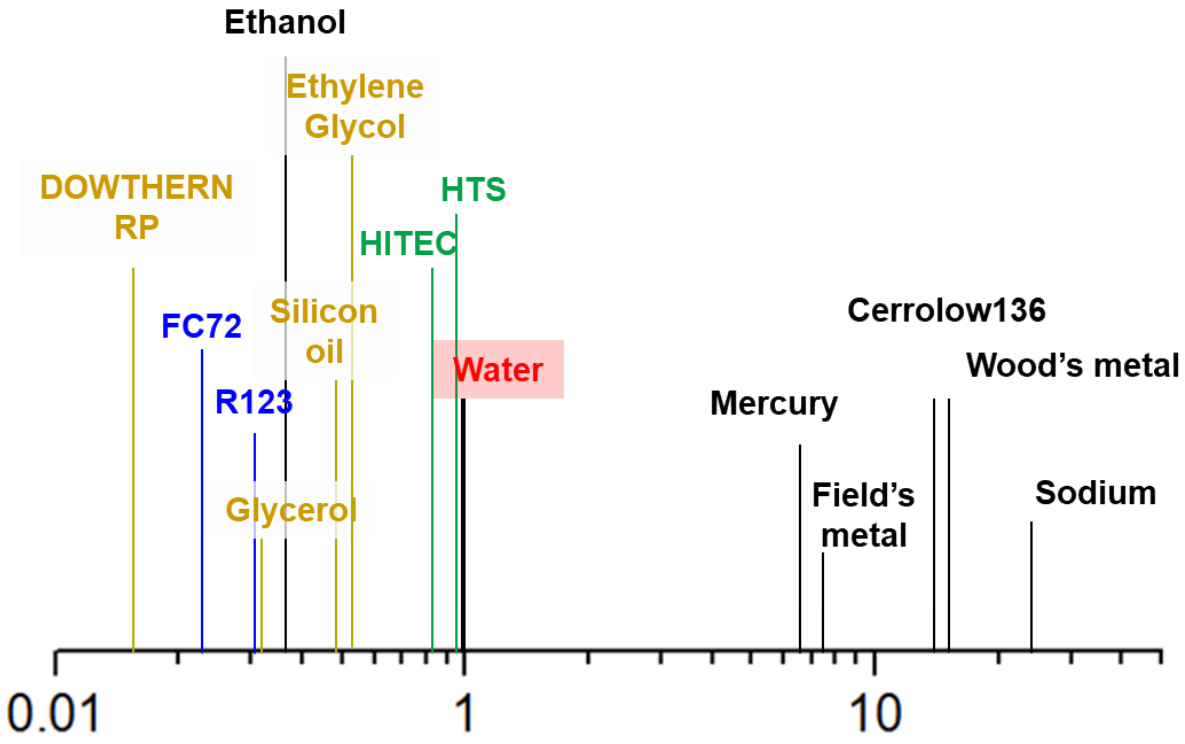

Figure 2-2. Relative length scale for identical Bo'

Table. 2-2 Summary of the parameter change by q''' change

	q''' = q''' sodium	**Q'''= 1/10 q'''sodium**	**Ratio** f(1/10q''')/f(q''')
Scale for identical Bo'	1 / 25	1 / 17	1.471
ΔT_{ref}	0.2420°C	0.0607°C	0.251
Error in the predicted sodium temperature ($T_{uncertainty,experiment}$ = 1.5°C)	10.14°C	40.41°C	3.986

Table. 2-3 Summary of the order of magnitude in the momentum conservation equation

Parameter	**Meaning**	**Order of magnitude**
u_i *	Non-dimensionalized velocity	1
$\frac{\partial}{\partial x_i}$	Change along the parallel direction to the flow	For pressure: 1 For the others: ε
$\frac{\partial}{\partial x_j}$	Change along the perpendicular direction to the flow	For pressure: ε For the others: 1
Gr’	Modified Grashof number	1/ε (large number)
T*	Non-dimensionalized temperature difference	1
P*	Non-dimensionalized pressure difference	1
δ	Kronecker delta	0 or 1
$\frac{\Delta P}{\rho u_{ref}^2}$	Pressure drop coefficient	1

2.4. Data interpretation between the model and the original system

The final object of the simulating experiment is to predict the temperature of the original system. Here, a normalized temperature difference is introduced for the explanation. The normalized temperature difference θ was defined in the equation (2-28). It is the temperature difference between the arbitrary point in the experimental facility and the boundary, divided by the reference temperature difference. As previously mentioned, the reference parameter is the representative magnitude of a certain parameter. In other words, the temperature can be expressed by multiplying the reference parameter and normalized temperature difference as in equations (2-29) and (2-30). It had basically the same meaning to the T* in equation (2-16), however, θ has a specific temperature point for calculation of the temperature difference, as boundary temperature.

$$\theta = \frac{T - T_{boundary}}{\Delta T_{ref}} \tag{2-28}$$

$$\Delta T_{original} = \Delta T_{reference,original} \times \theta_{original} \tag{2-29}$$

$$\Delta T_{model} = \Delta T_{reference,model} \times \theta_{model} \tag{2-30}$$

From the similarity law, two systems: the original system and the model, could have the same θ by matching the Bo' between the two systems. It is the similarity the author wanted to secure. In this regard, the temperature of the original system could be predicted by the model. Therefore, $\theta_{original}$ could be replaced by the θ_{model} because the two θ have the same value. Re-arrange equation (2-30) as an expression of the θ_{model} and substitute $\theta_{original}$ to the expression, ($\Delta T_{model}/\Delta_{reference}, T_{model}$), equation (2-31) could be derived. Equation (2-31) is the equation for the data interpretation from the model to the original system.

$$\Delta T_{original} = \frac{\Delta T_{reference,original}}{\Delta T_{reference,model}} \times \Delta T_{model} \tag{2-31}$$

Chapter 3. Similarity validation experiment: SINCRO-V

3.1. Experimental design

In this section, the SINCRO-V experiment would be briefly introduced including its objective and reason for the facilities and the experimental design. As mentioned before, the SINCRO-V is the abbreviation of the simulating natural circulation of reactor pool under the RVACS operation – validation of the similarity law.

3.1.1. Objective of the experiment

Research related to the similarity and simulating experiment briefly introduced in the section 2.1. There were several research related to validation of the similarity law, however, the similarity law has not been sufficiently validated with strict experiment. At first sight, it seems absurd to simulate liquid metal, which has an extremely low Prandtl number (Pr), using water which has high Pr. To clarify this issue, there has been some research on the validation of the similarity law. Some researchers compared the data from the simulating experiment and the data of the actual plant[43,46]. They focused on the qualitative phenomena and indirect parameters such as temperature gradient or drop rate. Direct and quantitative comparison between the simulating experiment and the original reactor was achieved by comparing the water data and the numerical sodium data[41]. The data were quantitatively compared, however, the sodium data were obtained by numerical methods, they had inherent limitations and uncertainties for strict validation. Moreover, these discussions on the similarity law were conducted under the DHX operation conditions. Therefore, the similarity law should be fully validated in the experimental way for the RVACS operation condition. In the present study, the similarity law between liquid metal and other fluids with relatively high Pr was validated in terms of temperature distribution. The temperature obtained by the liquid metal experiment and the liquid metal temperature obtained by water experiment were directly compared at the same points.

3.1.2. Selection of the working fluid and simulant

The basic concept of the SINCRO-V experiment is direct comparison of the temperature at the same position in the two facilities. In prior to the design, working fluid determines the scale ratio between the two facilities, whose working fluid is liquid metal and non-metallic fluid, respectively. The key similarity parameter is the Bo', which is the ratio of amount of heat transferred by natural circulation to that by the conduction. To make the Bo' identical between the two facilities, the

volumetric heat generation rate and the length scale could be manipulated. However, as discussed in section 2.3.2, it is fair to fix the volumetric heat generation rate. Therefore, the Bo' becomes a function of length scale solely.

Determining a specific liquid metal for the working fluid, the scaling ratio could make scale down the original system to the reasonable size, however, too large scale down could distort the flow or the geometry itself. Too small scale down also makes the advantages of the simulating experiment meaningless in terms of the economy and the flexibility of the experiment. To reduce distortion by scale, the difference of the length scale between two fluids should be properly determined. Among liquid metals, the mercury has the smallest difference of the length scale with nonmetallic fluid. However, the mercury is toxic to the human body and the environment. The field's metal was also excluded owing to an economic issue, because the Field's metal includes indium, which is one of the expensive rare metals. Then, Cerrolow136 and Wood's metal are left among the candidates. The composition and the properties of the two materials are quite similar. Between these two metals, which have similar values of the length scale, Wood's metal was selected because of previous operation experience.

For the simulant of the Wood's metal, to minimize the distortion of the flow or the geometry of the facility, length scale should be properly determined, not too large or not too small. With respect to Wood's metal, whose relative length scale for the identical Bo is large, the water has the smallest scale reduction ratio as 14.1 : 1. In this kind of scale difference, 1.41 m of the Wood's metal facility is reduced to 10 cm in the water facility. This kind of scale reduction is the minimum limit to reflect detailed structures in the Wood's metal facility. If the simulant is changed from water to other fluids, scale would be more reduced and correspondingly the flow and geometry would be more distorted. Meanwhile, other fluids do not have any advantages compared to water. They are expensive than the water and has improper melting point or boiling point for the experiment at the atmospheric condition. In terms of the material handling, economy, and clearness of the properties, water is the best simulant for the liquid metal.

Regard to properties of the Wood's metal, there could be some argument. For the water, which is the most well-known fluid, there is no argue. However, in case of the Wood's metal, it was not. Variance range of the Wood's metal properties was not negligible. The author investigated properties of Wood's metal and the results were summarized in table 3-1. Density had relatively narrower range than the other parameters. Excluding values with large levitation, it was determined as 9500 kg/m^3. Thermal conductivity, specific heat, and dynamic viscosity was determined by the same process as 13.5 W/m.K, 190 J/kg.K, and 4.0 mPa.s, respectively. However, volumetric thermal expansion coefficient was the parameter having the widest range. However, all the values have problems. In some reseaerches[57,59], 2.2×10^{-5} /K was reported, however, they were not from the direct measurement.

In fact, the author could not find background data of this value and guessed that that value was from the statement “solid field's metal has a thermal expansion coefficient that is very close to Aluminum (22 x 10^-6)” from wiki. Son et al.[61] and Kazandzhan et al.[62] reported relatively larger value than others. Son et al. also did not refer any reference about properties. Even Kazandzhan reported properties based on the experiment, however, there was another problem. Name “Wood’s metal” had been widely used for the Bismuth based alloy and it could be noticed by another literature[64]. Therefore, it could not be confidently used without suspicion. Therefore, for this parameter, author used properties of the similar material Cerrolow 117, which has 47.2°C of melting point and mostly composed with bismuth and lead. Therefore, final volumetric thermal expansion coefficient was determined as 2.5×10^{-5} /K. Finally, parameters values used in the present study were summarized in table 3-2.

The relationship between the working fluid and the simulant is summarized in figure 3-1. The length scale ratio between the Wood’s metal and the water is 14.1 : 1. Based on this length scale difference, a set of SINCRO-V experimental facility was designed. It would be discussed in the following section in detail.

3.1.3. Experimental facility design

As written its name, the objective of the SINCRO-V facility is validation of the similarity law, under RVACS operation condition, whose cooling is achieved by the RV wall. The reactor pool is heated by the decay heat from the core, as a power. It could be easily achieved by the power controlling of the cartridge heaters. The cooling condition should be given as a temperature boundary condition and their distribution should be similar.

First, the overall shape of the SINCRO-V was designed based on the characteristics of the RVACS. The natural circulation of the reactor pool under RVACS operation must pass the IHX, which is the only flow path between the hot pool and the cold pool. In other words, the natural circulation flow of the RVACS could be simplified as two-dimensional phenomena because there is only one flow path. Some previous research conducted experiment in 2-D slab facility[48,50]. In this study, the SINCRO-V facilities were designed in two-dimensional, slab model. Both Wood’s metal and water facility had the geometrically scaled cross section with 14.1 : 1 of the length ratio. This process is graphically summarized in figure 3-2.

However, it was not reduced in the isometric manner. The Wood’s metal facility and the water facility had the same thickness, which is the distance between two slabs in the slab model. It did not make sense in the aspect of the isotropic scale reduction, which was assumed in the derivation process of the similarity law. Here is some example to understand thickness scaling in the two-dimensional

facility. Because it is two-dimensional facility, along thickness direction, changes of the phenomena could be neglected. In other words, in the two-dimensional facility, change of the thickness could be neglected. If the thickness of the SINCRO-V water facility was reduced to half or increased double, it is certain that the results were the same because it was two-dimensional facility. Therefore, the facilities were treated as an isotropic scale reduction.

According to the characteristics of the RVACS and isotropy assumption, the SINCRO-V facilities were designed in two-dimensional, slab model. Both Wood's metal and water facility had the geometrically scaled cross section with 14.1 : 1 of the length ratio, while the distance between slabs have 1 : 1. The specifications of each facility are summarized in table 3-3. The radius of the pool was 1128 mm and 80 mm, each with 14.1:1 of length ratio. Because they were two-dimensional facility, the radius was the main parameter. The width was fixed at 100 mm. Pressure drop coefficient was assumed identical for both facility because the design of a pair of SINCRO-V was quite similar and simple. Because volumetric heat generation rate was maintained, the power of each pair was proportional to their volume so that their ratio is the squared length ratio. Under isotropic scaling assumption, power of the Wood's metal facility corresponded to 280 kW(~ 100 W x 14.1^3). It was reasonable to be treated as isotropic scaling. Because it is two-dimensional facility, along thickness direction, change of the phenomena could be neglected. In other words, in the two-dimensional facility, change of the thickness could be neglected. If the thickness of the SINCRO-V water facility was reduced to half or increased double, the author certain that the results were the same because it was two-dimensional facility. Following parameter were calculated under isotropic scaling assumption. In this scale difference, two Bo' were almost identical at a ratio of 1.06:1. In this scale difference, two Bo' were almost identical, as a ratio of 1.06 : 1. The corresponding reference temperature differences were 3.776 ℃ and 0.442℃ in the Wood's metal and water facility, respectively, with ratio of 8.55:1. The power and average cooling heat flux showed good accordance in both facility in the aspect of the non-dimensional heat source and sink, which were described in the equation (9). To fill the natural circulation pool of the SINCRO-V Wood's metal facility, 970 kg of the Wood's metal was required, while the water facility required only 0.5 kg. Frankly saying, 970 kg of the Wood's metal is huge amount, the author spent three days for its flooding into the SINCRO-V pool and wanted to leave some pictures for the hard work, like figure 3-3. The actual picture for the SINCRO-V water facility is in figure 3-4.

3.1.4. Test matrix

Although the SINCRO-V facilities had different shape with the reference reactor PGSFR, the fraction of the heating region and the volumetric heat generation rate were preserved to make a guide

for the power level of the SINCRO-V. Objective of the RVACS is decay heat removal, which is a function of time after shutdown. Considering long-term cooling and capacity of RVACS in the PGSFR, a maximum of 1% of the total power is assumed as decay heat. The decay heat level at the certain time after shutdown in the PGSFR and corresponding power in the SINCRO-V Wood's metal and water facilities are summarized in table 3-4. The time after shutdown and corresponding decay heat were obtained from the decay heat under the loss of flow accident condition of PGSFR.

The heating condition was clearly determined by the reference reactor. However, the cooling boundary condition was not easy to be determined. There has been no literature about the cooling boundary condition of the inner reactor pool. In other words, there is no research to study both the inner reactor pool and the outer air simultaneously under the RVACS operation. Therefore, realistic boundary condition could not be given. To avoid the validity of the cooling boundary condition of the RVACS pool natural circulation, the author determined to apply constant temperature boundary condition, which is the most basic and rigorous. In both facilities, the authors focused on providing almost constant temperature cooling. Especially in the Wood's metal facility, to cover the large heat flux variations along the cooling wall, boiling was selected as a cooling method. Boiling has the highest heat transfer coefficient, which increases as heat flux increases. Owing to the characteristics of boiling heat transfer, temperature variations along the cooling boundary were less than 5 ℃ in the experiment. Temperature at the inner side of the cooling wall was estimated approximately 16.7^{o}C higher than the outer temperature. However, only 110.59^{o}C was the maximum temperature among 16 thermocouples (every 6 degree) sheathed near the pool-side surface of the cooling wall, so that author used this value for the boundary temperature calculation. Temperature variation with the change of the angular position could be negligible due to characteristics of the boiling. In the water facility, a high flow-rate water jacket covered the cooling wall so that there was less than 5℃ of temperature variations along the boundary, which was observed at the three point at mid-plane of the cooling wall (10, 45, 80 degree). Considering the magnitude of the heat flux and observing point, temperature inside of the cooling wall could be treated as identical so that the maximum temperature (24.6^{o}C) was used as boundary temperature. These boundary temperature values were used in the data interpretation and prediction process.

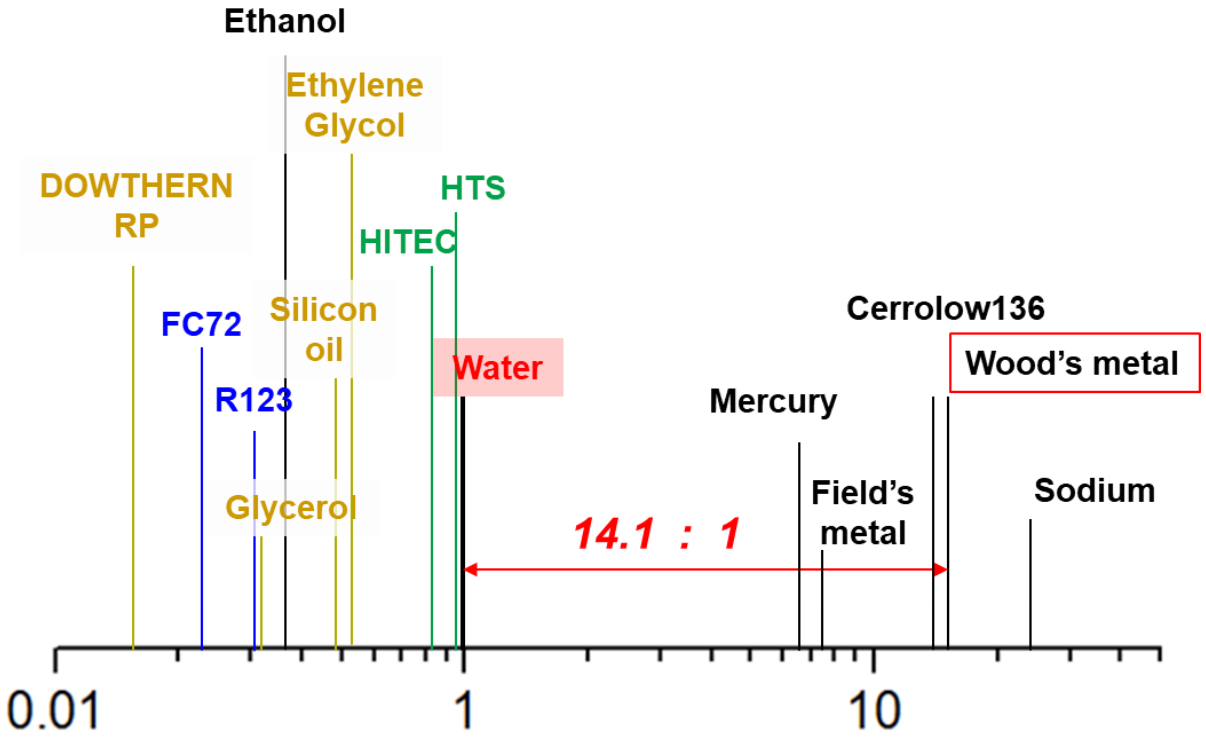

Figure 3-1. Length scale difference between the Wood's metal and the water

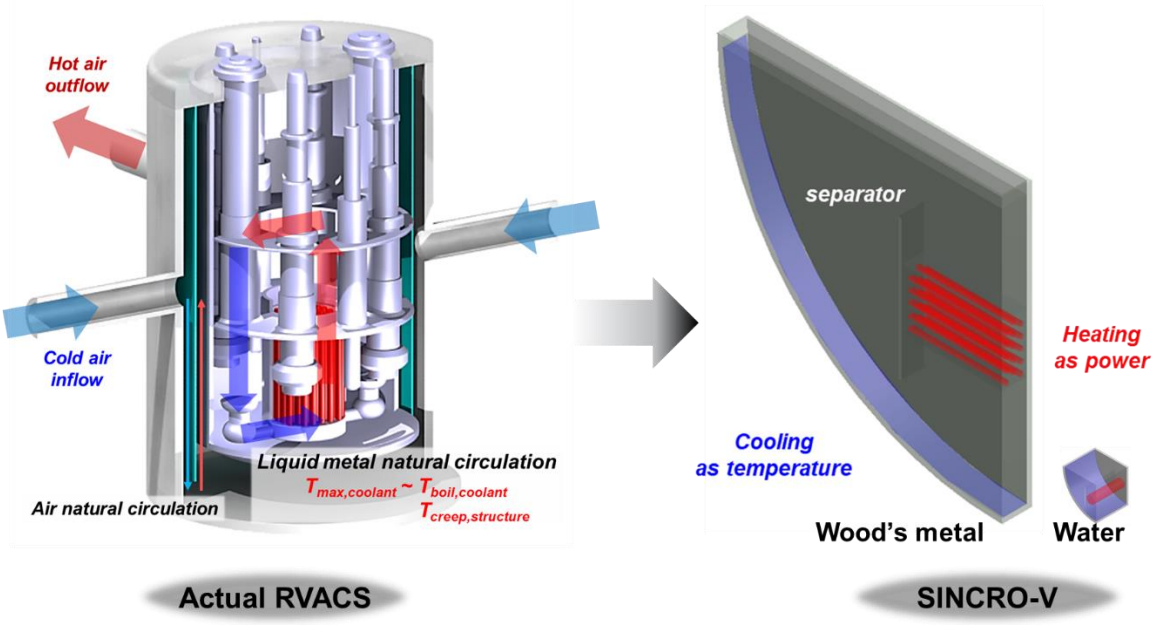

Figure 3-2. Schematic of the SINCRO-V

Figure 3-3. SINCRO-V Wood's metal facility and the author

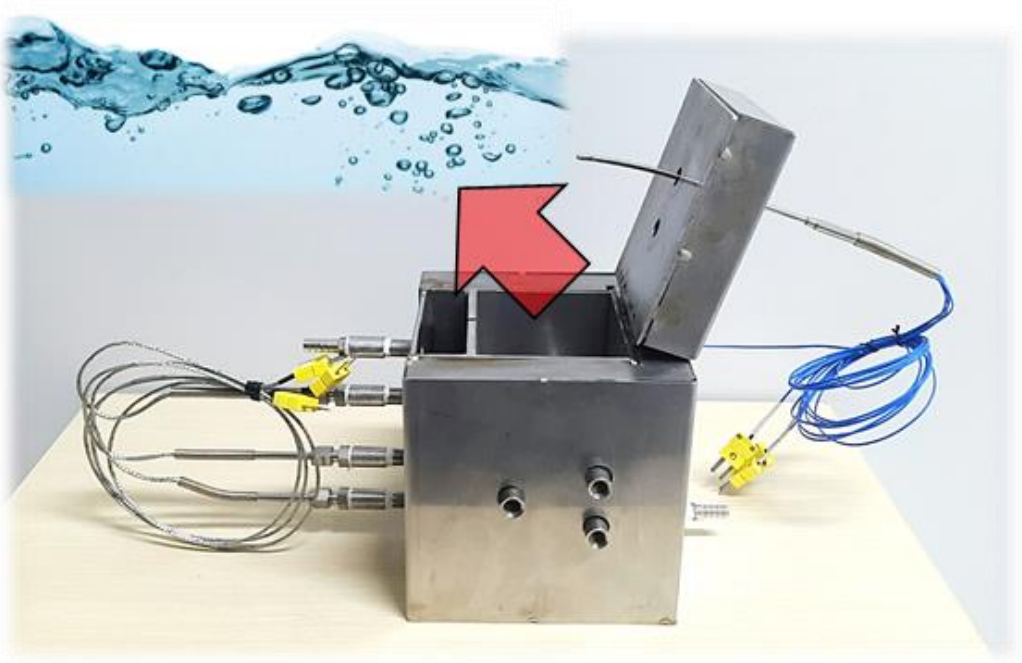

Figure 3-4. SINCRO-V Water facility

Table. 3-1 Summary of variance of the properties of Wood's metal

Literature	**Density [kg/m^3]**	**Volumetric thermal expansion coefficient [1/K]**	**Thermal conductivity [W/m.K]**	**Specific heat [J/kg.K]**	**Dynamic viscosity [mPa.s]**	**Notes**
[55]	9500 – 9530	-	2.00 – 4.15	150 - 261	5.1 – 7.0	@ 90 – 180^{o}C
[56]	9490	-	13.5	-	4.00	
[57]	8100	2.2 x 10^{-5}	11.1	150	1.62	
[58]	8528	-	12.8	190	2.4	
[59]	9383	2.2 x 10^{-5}	18.8	168	1.87	
[60]	9700	-	13.5	-	4.00	
[61]	8370	10.0 x 10^{-5}	14.05		2.3	
[62]	9870	12.1 x 10^{-5}	-	-	-	@ 400 – 1000 K
[63]	-	2.5 x 10^{-5}	-	-	-	
The present study	9500	2.5 x 10^{-5}	13.5	190	4	

Table. 3-2 Properties of the material in the present study

Parameter	**Water**	**Wood's metal**
Melting point	0°C	80°C
Density	998 kg/m^3	9500 kg/m^3
Volumetric thermal expansion coefficient	0.000207 /K	0.000025 /K
Thermal conductivity	0.598 W/m.K	13.5 W/m.K
Specific heat	4184.8 J/kg.K	190 J/kg.K
Dynamic viscosity	1.002 mPa.s	4.0 mPa.s

Table. 3-3 Specifications of a pair of SINCRO-V

Parameter	**Wood's metal**	**Water**
Radius	1128 mm	80 mm
	14.1 : 1	
Width	100 mm	100 mm
	1 : 1	
Power	20 kW	100 W
	14.1^2 : 1	
Bo'	1.394×10^8	1.398×10^8
	1.06 : 1	
ΔT_{ref}	3.776℃	0.442℃
	8.55 : 1	
$q''_{average}$ at cooling wall	112.9 kW/m^2	7.96 kW/m^2
	14.1 : 1	

Table. 3-4 Summary of the test conditions

Decay heat in the PGSFR (time after shutdown)	**Power in the SINCRO-V**	
	Wood's metal	**Water**
0.2% (90 days)	4 kW	20 W
0.4% (6.8 days)	8 kW	40 W
0.6% (1.5 days)	12 kW	60 W
0.8% (12.6 hrs)	16 kW	80 W
1.0% (5.5 hrs)	20 kW	100 W

3.2. Qualitative comparison

Before comparing predicted temperature by the water experiment and the actual Wood's metal temperature, the temperature distribution of the two experimental facility was quantitively compared. For the clear comparison, the maximum power condition in the experiment was employed. In figure 3-5, the temperature distribution of the Wood's metal and the water facility is shown under 1.0% of the decay heat condition, which corresponds to the 20 kW in the Wood's metal facility and 100 W in the water facility.

For the Wood's metal facility, the Wood's metal rose at the heating zone and descend at the cooling wall, which is an arc. Anticipated natural circulation flow was drawn as grey arrows, which was inferred by the temperature profile and preliminary CFD analysis. The thermal stratification of the pool could be observed in the whole pool. There were some distortions of the stratification layer in the aspect of the whole pool, however, for locally, there was no inversion of the temperature. The thermal stratification could be clearly observed by the temperature of a group of vertically arranged thermocouples. The bottom of the hot region in the top of the pool was near to the top of the separator, which was illustrated thick black vertical line in the (a) of figure 3-5. Below and above the heating zone, there were three thermocouples each. Temperature values from the upper three thermocouple were quite similar and it was same to the lower three thermocouples. It suggested that upward flow in the heating region was relatively uniform. Upward flow from the heating region went to the cooling wall through the top of the pool, and thickness of this flow could be inferred from the temperature data. At the top three thermocouple showed almost same temperature and it could be used as an index of the thickness of the hot upper region. At the cooling wall, the downward flow was generated, and it could be recognized by the temperature. Without natural circulation flow, temperature from two thermocouples at the same height should be the same. However, if natural circulation flow exists, temperature field is affected and distorted. This kind of distortion of the stratified temperature distribution could be observed near the cooling wall. Except for the one point from the top, temperature near the wall was always higher than that of the vertically arranged thermocouple. The downward flow at the cooling wall entrained stratified temperature field and consequently, temperature distribution was shifted downward. The temperature distribution at the wall suggested the point of the flow detachment. To circulate in the pool, the downward at the wall should be detached from the wall and re-enter to the heating zone. The lowest point of the vertically arranged thermocouple and the lowest point of the wall thermocouple were the same point. At this point, significant lower temperature was observed compared to the surrounding points and the surrounding temperature difference between a point and the next point. Therefore, it could be inferred that the downward flow was detached from the wall just above this point. Additionally, temperature from the

inlet if the heating region could give another reason for the determination of the flow detachment from the cooling wall. The temperature at the inlet of the heating zone was about 180°C. If the downward flow detached after the lowest point of the vertically arranged thermocouples, the heating zone inlet temperature should be similar, or lower than approximately 140°C, which is the temperature at the lowest point of the vertically arranged thermocouples. Therefore, it could be certified that detachment point of the downward flow at the cooling wall was about the second lowest point of the vertically arranged thermocouple. Regard to the horizontal flow of the natural circulation flow, both from the heating zone to the cooling wall, and the reverse case, they were related to the separator. In (a) of figure 3-5, the leftward flow was observed from the top to just above the separator, and the rightward flow was observed from the detachment point, and it was just below the separator. From this, it was revealed that the formation of the natural circulation flow is affected by obstacles between the heating and cooling region.

In case of the water facility, similar phenomena were observed, however, detailed phenomena could not be observed. Different to the Wood's metal facility, which has 1128 mm of the radius, the water facility has only 80 mm of the diameter, which is reduced from the 1128 mm with the scaling ratio of 14.1 : 1. Therefore, the observation point of thermocouple could not be much detailed and fine like the Wood's metal facility. The observation points in the two facility was not matched one to one. For example, for the vertically arranged thermocouple in the water facility was installed at the one for every three points from the top. In the water facility, temperature points near the wall were installed at the same height with the vertically arranged thermocouples. The inlet and outlet of the heating zone had one observation point, respectively. For the thermal stratification, the same tendency was observed. The water pool was thermally stratified. There were additional thermocouples between the vertically arranged thermocouples and near wall thermocouples. They were for the observation of the distortion of the temperature stratification, however, it was not observed clearly. For the top of the vertically arranged thermocouples, the thickness of the leftward flow could not be observed due to lack of resolution of the observation point. At the cooling wall, the downward flow was commonly developed. This downward flow could be observed from the temperature data. Similar to the Wood's metal facility, between two temperature point at the same height, one was in the near wall region and the other was vertically arranged, temperature at the cooling wall is higher than that of the vertically arranged thermocouple. As explained in the Wood's metal facility part, it was the downward shift of the stratified temperature distribution by the entrainment effect of the natural circulation flow. For the detachment of the flow, a clear observation of the detachment point was not possible because of the relatively coarser observation points. The one thing could be inferred from the temperature of the inlet of the heating zone and temperature of the cooling wall, the detachment of the downward flow occurred below the temperature observation point. The temperature at the inlet of the heating zone

was only 31.6ºC, however, the temperature at the lowest points of the pool was 35.86ºC and 34.26ºC, respectively. Therefore, there should be additional cooling below the lowest point and it could be suggested that flow detachment from the cooling wall occurred at the lower point than the lowest temperature observation point.

We discussed about the phenomena in the 1.0% of the decay heat condition for both facilities. Here, effect of the decay heat was observed in figure 3-6. It seemed that all the aforementioned phenomena, were commonly observed regardless to the decay heat level. Detailed temperature will be discussed in the further section for the quantitative analysis, and only qualitative phenomena would be discussed in this section. For all conditions, the overall thermal stratification, and the temperature distortion by the downward flow at the cooling wall were commonly observed. Relative magnitude of the temperature distribution by its color showed quite same tendency. Therefore, the decay heat level had insignificant effect in the aspect of the overall temperature distribution tendency. Only magnitude of the temperature changed along the decay heat level. In the following section, all the phenomena were discussed in detail with exact temperature.

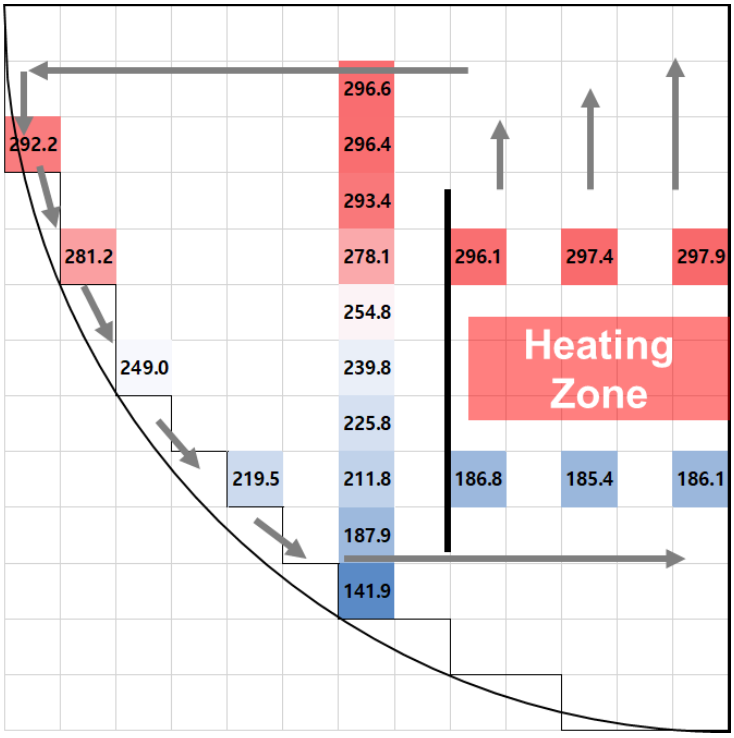

(a) Temperature distribution in the Wood's metal facility

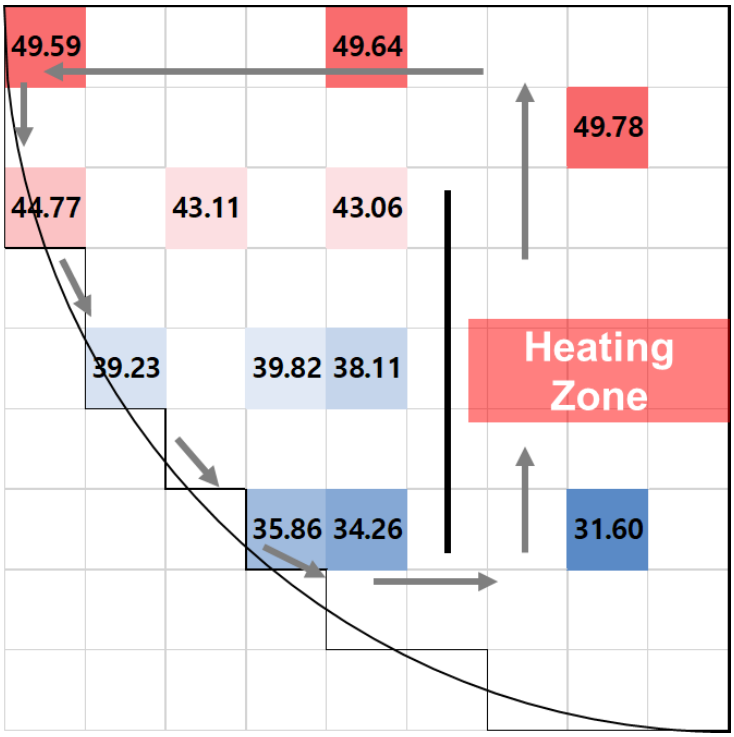

(b) Temperature distribution in the water facility

Figure 3-5. Temperature distribution of the two SINCRO-V facilities – 1.0 % of the decay heat

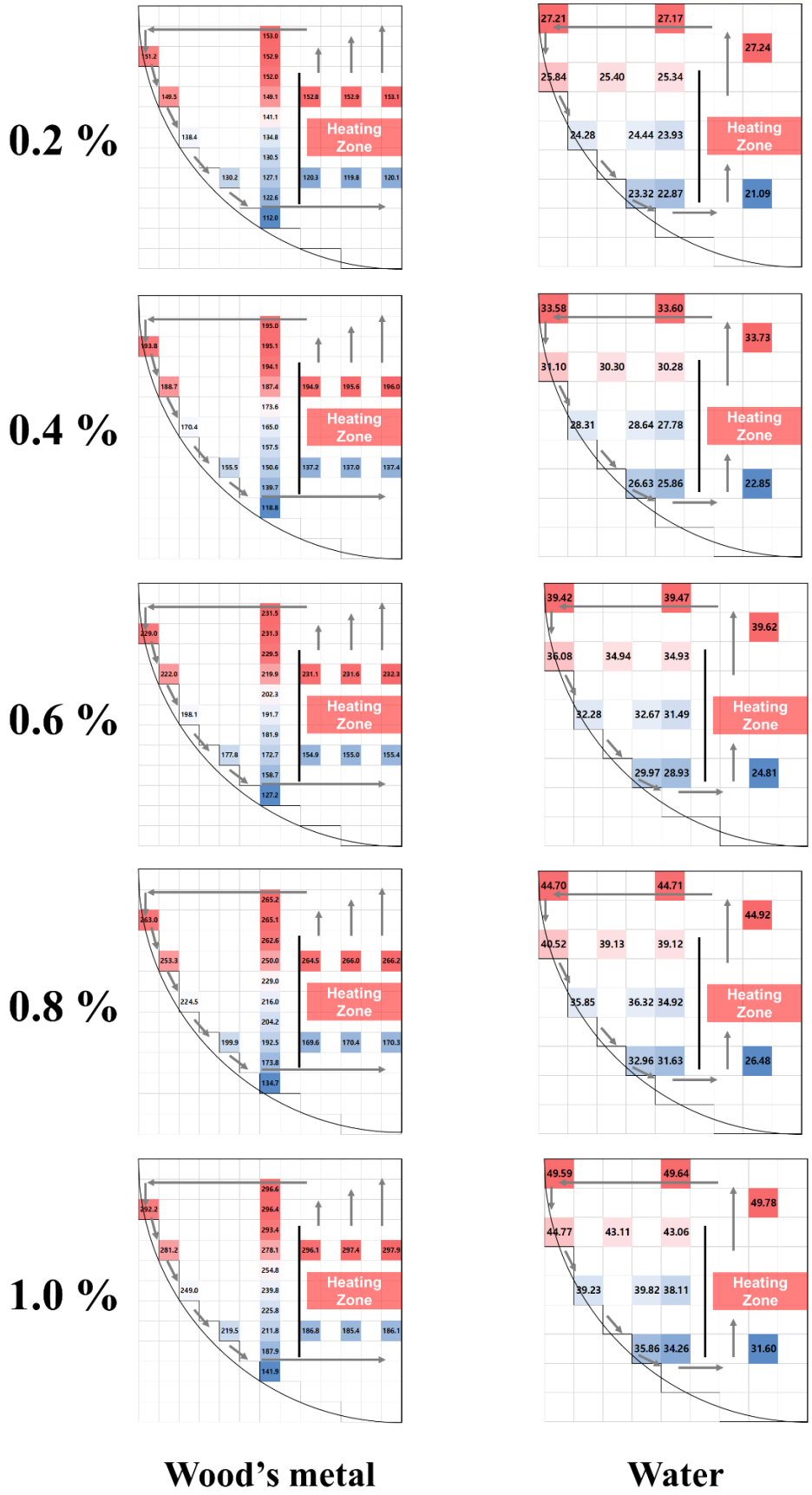

Figure 3-6. Temperature distribution of the two SINCRO-V facilities – decay heat effect

3.3. Quantitative comparison

We analyze the natural circulation phenomena in the SINCRO-V facilities in the qualitative manner to get the physical insight of the phenomena itself. The phenomena in the Wood's metal facility were observed in the water facility in common. In this section, actual Wood's metal temperature and the predicted temperature by the water experiment would be compared by point to point. The effect of the decay heat on the temperature distribution would be discussed in the quantitative manner. And finally, rough calculation about the flow rate of the natural circulation would be discussed based on the temperature of the inlet and the outlet.

3.3.1. Point to point temperature comparison

Considering their scale difference, the SINCRO-V Wood's metal and water facility could not have the same number and location of the temperature observing points. However, observing points in the two facilities could be matched by one to one according to their characteristics. Figure 3-7 shows the location of the temperature observing points. Based on this position, the temperature data were compared in the form of following graphs.

As introduced in chapter 2, the temperature data from the water experiment could be translated to the Wood's metal data using reference temperature of each system and boundary temperature for the calculation of the temperature difference. Because the Bo' based similarity law is simulating the temperature difference in the system, the temperature interpretation could be expressed in the form of the temperature difference. Exact formula to predict Wood's metal temperature by water temperature is equation (3-1) and its derivation process was summarized in chapter 2.

$$\Delta T_{Wood's\,metal} = \frac{\Delta T_{reference,Wood's\,metal}}{\Delta T_{reference,water}} \times \Delta T_{water} \tag{3-1}$$

$$\Delta T_{system} = T_{arbitrary,system} - T_{boundary} \tag{3-2}$$

The temperature difference term in equation (3-1) represent the temperature difference between the arbitrary point in the pool and the cooling boundary like equation (3-2). Therefore, proper estimation of the boundary condition is crucial for the reliability of the predicted data. To remove effect of the temperature distribution on the boundary, the author made an effort to provide the constant temperature boundary condition as possible. Especially in the Wood's metal facility, boiling was selected as cooling method to provide minimum temperature gradient along the cooling

wall.Boiling has the highest heat transfer coefficient, which increases as heat flux increases. Owing to the characteristics of boiling heat transfer, temperature variations along the cooling boundary were less than 5 ℃ in the experiment. Temperature at the inner side of the cooling wall was estimated approximately 16.7^{o}C higher than the outer temperature. However, only 110.59^{o}C was the maximum temperature among 16 thermocouples (every 6 degree) sheathed near the pool-side surface of the cooling wall, so that author used this value for the boundary temperature calculation. Considering the order temperature difference in the Wood's metal pool, the temperature variation with the change of the angular position could be negligible due to characteristics of the boiling. In the water facility, a high flow-rate water jacket covered the cooling wall so that there was less than 5℃ of temperature variations along the boundary, which was observed at the three point at mid-plane of the cooling wall (10, 45, 80 degree). Considering the magnitude of the heat flux and observing point, temperature inside of the cooling wall could be treated as identical so that the maximum temperature (24.6^{o}C) was used as boundary temperature for the maximum power case. Based on these boundary temperatures, the temperature of the Wood's metal was predicted.

Figure 3-8 shows the temperature distribution in the pool of both facilities. As discussed in previous section, similar tendency was commonly observed, and it could be recognized in figure 3-8. The effect of the decay heat could be clearly observed in the figure. For the Wood's metal, there was no sudden change in the tendency of the temperature distribution in the pool along the power level. From the 1.0% of the power level to the 0.2% of the power level, same tendency was maintained and only magnitude of the overall temperature changed. In conclusion, there was no power level effect in the given test matrix, which corresponded to the 0.2% to the 1.0% of the decay heat. Although geometry of the SINCRO-V was different to PGSFR, it could be concluded that there was no significant change of the temperature distribution characteristics under the operation condition of the RVACS. (b) of figure 3-8 shows the temperature distribution of the water facility with corresponding conditions. Similar to the Wood's metal cases, there was no significant change of the temperature distribution characteristics in the given power level.

For the validation of the similarity law, direct point to point comparison was conducted and summarized in figure 3-9. The black line represents the actual Wood's metal temperature, and the red line represents the predicted Wood's metal temperature by the water experiment, which was obtained by using equation (3-1) and corresponding water data. The maximum temperature, which was observed at the core outlet, was 297.1 ℃ in the Wood's metal experiment, while the water experiment predicted 325.6 ℃, an overestimation of 14.4%. The minimum temperatures observed at the core inlet were 186.1 ℃ and 170.2 ℃ in the Wood's metal experiment and water simulating experiment, respectively. This is an underestimation of 18.5%, and this point had the largest error. There was overestimation for the maximum temperature, and underestimation for the minimum temperature. In

other words, overall magnitude of the temperature difference was slightly overestimated in the water experiment.

In the middle of the pool, temperature was stratified and showed stabilized profile. Point 1 in the middle of the pool showed similar temperature with the core outlet. In this region, the temperature decreased as the point went down. In the Wood's metal experiment, the temperature at points 1 and 2 in the middle of the pool was similar. However, in the water facility, temperature greatly decreased at the point 2 compared with point 1. This means that hot flow from above the core to the cooling wall was shallower in the water experiment. In other words, the thickness of the hot region in the upper plenum was underestimated in the water experiment. This underestimation was related to the exact location of the temperature observation point. For the water facility, because of its small size, small error in the location could cause large error in the corresponding position in the Wood's metal facility. Point 2 in the middle of the pool was located near the top of the separator, which was a kind of lower boundary for the hot, horizontal flow. Thus, there was drastic change of the temperature near the point 2, and large disagreement at the point 2 could be explained as an error contributed from the location. There was no data about the exact thickness of the hot horizontal flow due to limited the number of the observing point. Therefore, the error contribution from the location of the observing point could not be quantified, however, it still could be suggested as one contributor of the error. At points 3 and 4, the predicted temperature showed good agreement with the Wood's metal data. The temperature gradient was smaller in the water experiment; however, considering the overestimated upper plenum temperature and underestimated thickness of the hot region, the temperature in the middle of the pool at point 4 showed good agreement with the actual Wood's metal temperature.

In the cooling wall, there was relatively good accordance between the actual Wood's metal temperature and the predicted Wood's metal by the water experiment. Point 1 in the cooling wall was in the hot region in the upper plenum; hence, it showed overestimated temperature like the core outlet and point 1 in the middle of the pool, which were in the domain of the horizontal hot flow from the core to the cooling wall. The temperature change at the points along the cooling wall indicates the cooling rate along the cooling wall. The rate of temperature decrease along the wall was overestimated in the water experiment such that the temperature at point 4 was underestimated, while point 1 was overestimated. This overestimated cooling rate corresponds to the overestimated overall magnitude of the temperature difference in the water experiment. The reason for the overall error in the simulating experiment would be discuss in the latter part.

In conclusion, there were few local errors in prediction: overestimation of the maximum temperature by 14.4% and underestimation of the minimum temperature by 18.5%. Despite these local errors, it can be concluded that the overall temperature was accurately predicted, and the tendency of temperature distribution was accurately reproduced. The Bo' based similarity law could

give theoretical base for the simulating experiment of liquid metal by water, and it was validated by the SINCRO-V experiment.

However, there were some errors in the predicted temperature in the SINCRO-V. Figure 3-10 shows summarization of the errors of the predicted temperature along the power level. For the overall tendency, the decay heat did not affect the characteristics of natural circulation, which was confirmed by the error graph. The tendency of the error distribution was not changed along the power level. In the hot region like core outlet and the top of the pool, there were always overestimation. Similarly, cold region like the bottom of the pool and the core inlet were always underestimated. Consequently, the overall magnitude of the temperature difference was slightly overestimated in the water experiment. This kind of relatively large temperature difference could be attributed to the difference in the Gr'. As shown in Figure 3-11, Gr' in the Wood's metal facility was larger than in the water facility. The pressure drop coefficient was larger in smaller Gr' system. Additionally, Gr' itself means degree of turbulency in natural circulation flow, like Reynolds number. Therefore, thermal mixing was also reduced in the smaller Gr' system. Theoretically, the pressure drop coefficient is inversely proportional to the Reynolds number, which can be translated as the Gr' in natural circulation in terms of flow inertia. For example, in laminar flow, the pressure drop coefficient could be expressed as in the form of 64/Re and it is similar for the turbulent flow. The SINCRO-V water facility had smaller Gr' than in the Wood's metal facility; thus, it can be said that the water facility had a larger pressure drop than the Wood's metal facility. Thus, the flow of the water facility flowed with relatively larger pressure drop, and the predicted temperature difference at the inlet and outlet by water experiment was slightly exaggerated.

The uncertainty of the material property could be suggested as a fundamental reason for the error in the water experiment. First, properties of the water were well-known. So that water properties at the 20^{o}C were used and corresponding value were summarized in the table. Luckily, change of the properties of the water along temperature was not significant except for viscosity, so that we could employ properties at 20^{o}C. However, as reviewed in section 3.1.2, properties of the Wood's metal had large range of uncertainties. Most of the values were based on the data from the Korea atomic energy research institute (KAERI). The author used a proper value between the minimum and the maximum. Therefore, the scaling law had inherent errors from the properties used in the design of the SINCRO-V experiment. In the definition of the Bo', as shown in equation (2-18), it contains a global constant like g, the system properties like L and Q, and the properties of the working fluid like β, c_p, and α. Therefore, uncertainties in the material properties had an influence on the Bo', and consequently, overall system design like scaling ratio was also affected. In addition, the reference temperature of the system was also affected, which contains material properties in its definition like equation (2-10). Therefore, the other contributor in the simulating experiment was uncertainties of the Wood's metal

properties.

In the discussion stage, there was some regret for using Wood's metal because of the uncertainties of their properties. However, as reviewed in the working fluid selection, the Wood's metal is the only materials for representing the liquid metals. The Cerrolow136 had similar degree of the suitability with the Wood's metal, however, properties of the Cerrolow136 is more uncertain than the Wood's metal. Based on this validation experiment SINCRO-V, in the further research for simulating the sodium, the material property issue is expected to be much relived because properties of the sodium are well-known.

3.3.2. Additional similarity for the flow

The SINCRO-V experiment was designed to validate the similarity law for the temperature distribution. As the author reviewed in the design of the experiment, the scaling ratio of the SINCRO-V facilities was determined only considering the Bo', which is related to the temperature distribution under natural circulation, while Gr' was neglected, which is related to the flow regime of the natural circulation.

Here, temperature distribution, in other words, temperature difference in the pool is the driving force of the natural circulation. In addition, for the flow similarity, it was discussed in chapter 2 that Gr' is less important than the pressure drop coefficient, while there were only 2 parameters could be manipulated in the equation. Regard to the pressure drop coefficient, the author considered that the difference of the pressure drop coefficients of the pair of the SINCRO-V facility could be treated identical because their geometry was quite similar. Therefore, based on these ideas, the author continued to the additional similarity validation for the velocity field, which is driven by reasonably simulated temperature distribution.

However, there was no apparatus for measuring the velocity in detail in the SINCRO-V facility. Therefore, the flow rate was selected as parameter for comparison. Here, the flow rate could have additional meaning in the similarity in terms of the safety. For the core and fuel assembly, under loss of flow accident, decay heat is only cooled by the natural circulation. The maximum temperature of the bulk sodium, which is related to the sodium bulk boiling and corresponding positive reactivity insertion, is determined by the natural circulation flow rate and decay heat. In addition, for the local maximum temperature of the sodium is also affected by the natural circulation flow. Therefore, the similarity of the flow rate is meaningful because the natural circulation flow rate is related to various safety parameters.

The basic idea of the similarity is summarized in the equation below. As shown in equation (3-3), the flow rate can be expressed in the multiplication of the density, velocity and the cross-sectional

area of the channel. Here, similar to the temperature difference and reference temperature, the velocity could be expressed as multiplication of the non-dimensionalized velocity u* and the reference velocity u_{ref} like equation (3-5). Here, the author assumed velocity fields has a significant degree of the similarity to that of the original, because the driving force is similar. Therefore, the non-dimensionalized velocity u* is quite similar between the Wood's metal and the water. From this relationship, an equation for the prediction of the flow rate through water simulating experiment could be derived like equation (3-5)

$$\dot{m} = \rho u A \tag{3-3}$$

$$u = u^{*} u_{ref} \tag{3-4}$$

$$\dot{m}_{Wood's\,metal} = \dot{m}_{Water} \frac{\left(\rho u_{ref} A\right)_{Wood's\,metal}}{\left(\rho u_{ref} A\right)_{Water}} \tag{3-5}$$

As mentioned before, the velocity measurement was not possible in the SINCRO-V facilities, even for the bulk phenomena like flow rate. Therefore, the author used indirect measurement of the flow rate using equation (3-6). There are four parameters in equation (3-6). Among these parameters, total power q is an experimental input, c_p is a specific heat of the working fluid, and the temperature difference could be measured in the experiment. For the Wood's metal facility, the maximum temperature was an average of the three thermocouples in the outlet of the core. Similarly, the minimum temperature was an average of the three thermocouples in the outlet of the core. Each three temperature for the average temperature showed almost same temperature, respectively. Therefore, the author could take an average of the three temperature. Among the observed temperature, the lowest thermocouple in the middle of the pool to observe the temperature stratification in the pool, showed the minimum temperature. However, this point was excluded because it was revealed that the Wood's metal at this point did not actively participate in the natural circulation from the previous analysis. In case of the water facility, there was each only one thermocouple at the inlet and the outlet of the core. Therefore, the temperatures at the inlet and the outlet of the core were used as the minimum and the maximum temperature. Using the other parameters, the only unknown parameter mass flow rate could be obtained. For the comparison, the 1% decay heat case was selected as a representative case.

$$q = \dot{m} c_p \Delta T \tag{3-6}$$

The value of each parameters and results were summarized in table 3-5. Using equation (3-6), calculated flow rate in the Wood's metal facility was 0.9477 kg/s, while only 1.315 x 10^{-3} kg/s was

calculated in the water facility. According to equation (3-5), the flow rate of the Wood's metal facility could be predicted by the water experiment. The predicted Wood's metal flow rate was 0.6739 kg/s, which was 28.89 % underestimation of the actual flow rate.

Regard to the prediction of the flow rate, there could be inescapable error. Regard to the temperature difference, the author used temperature of the inlet and the outlet of the core. Considering geometry of the SINCRO-V facilities, there should be significant error because flow path of the natural circulation was not confined like a loop. Although there were some errors, the predicted and the actual Wood's metal flow rate showed reasonable accordance. Therefore, it could be concluded that Bo' based similarity law could have similarity for the flow field and flow rate, while detailed flow could be differed from each other due to the discordance of the Gr'.

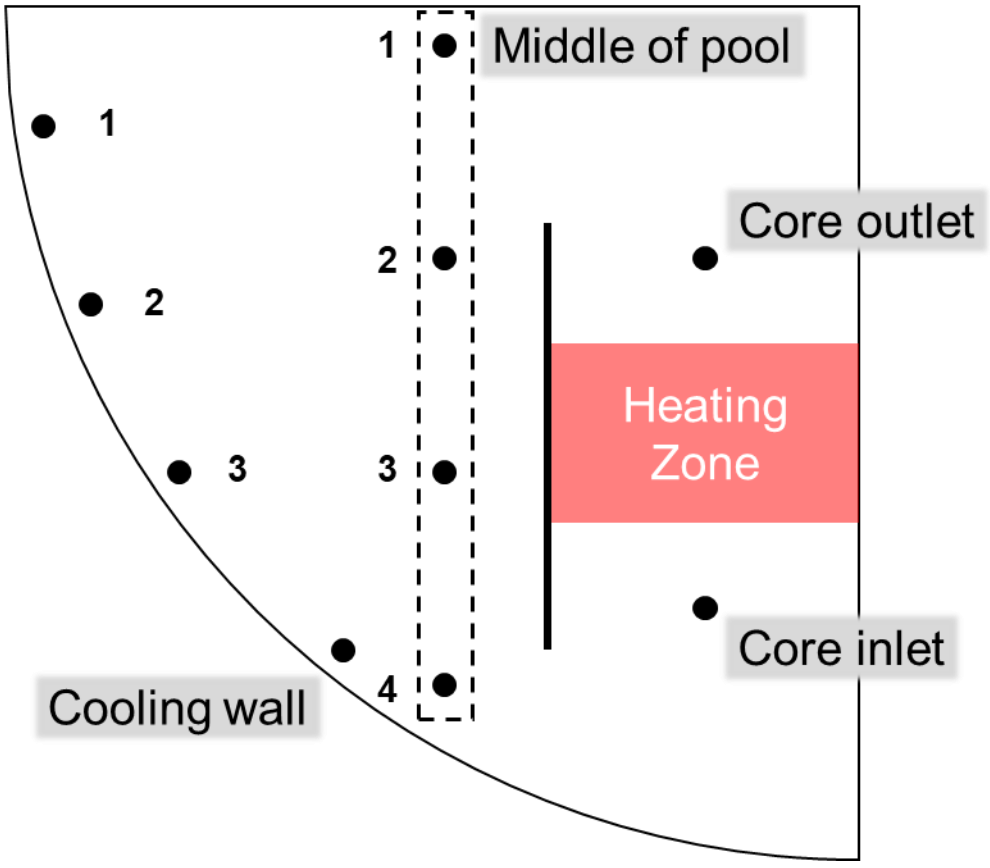

Figure 3-7. Point of the temperature observing in the following graphs

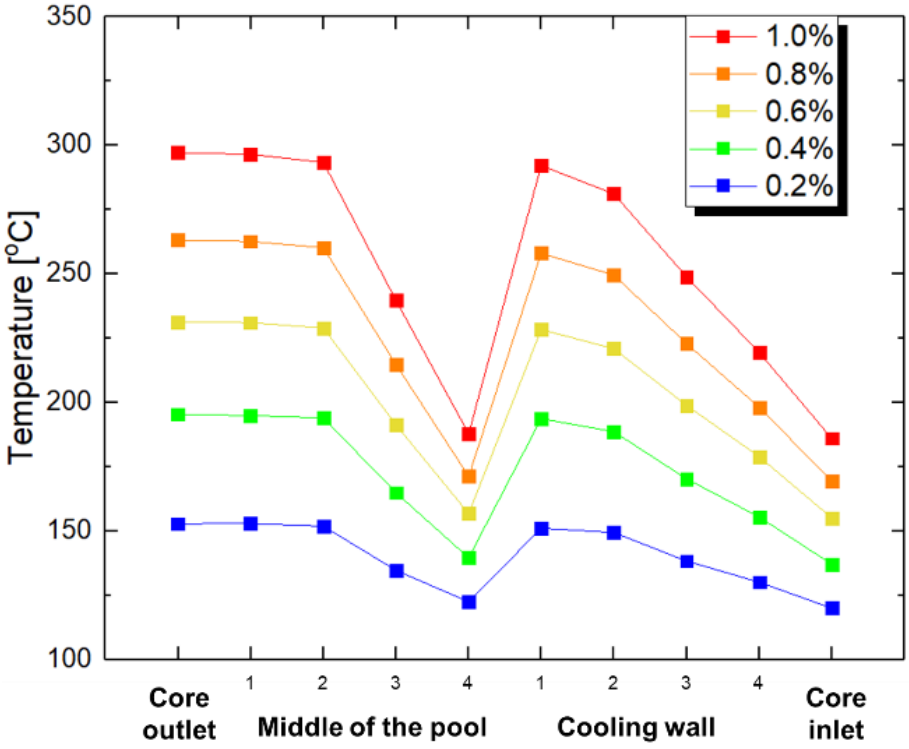

(a) Wood's metal

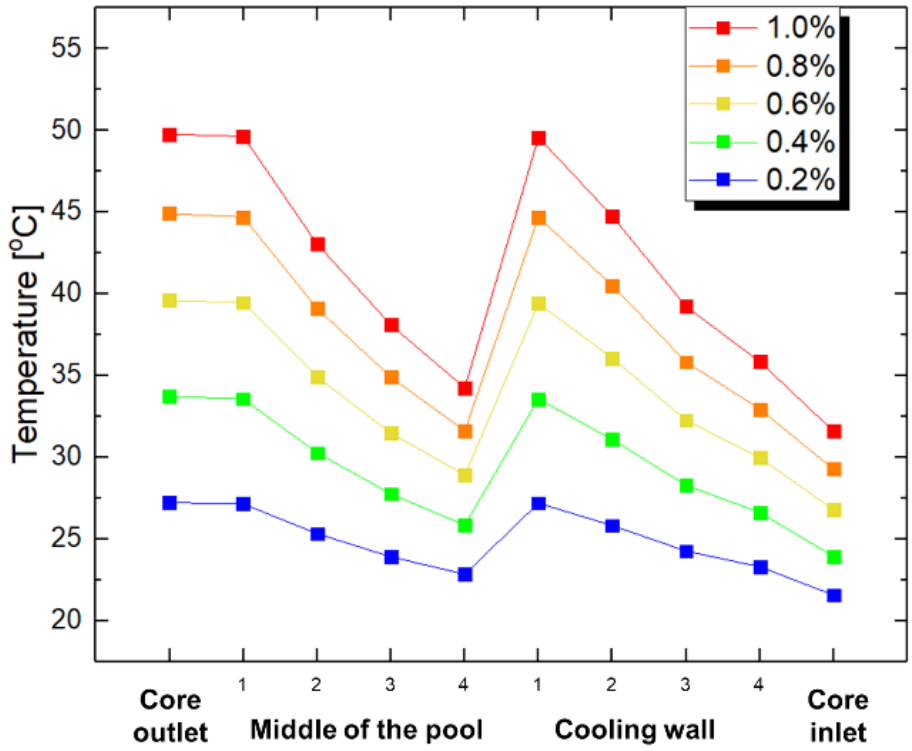

(b) Water

Figure 3-8. The temperature at the selected point with various decay heat

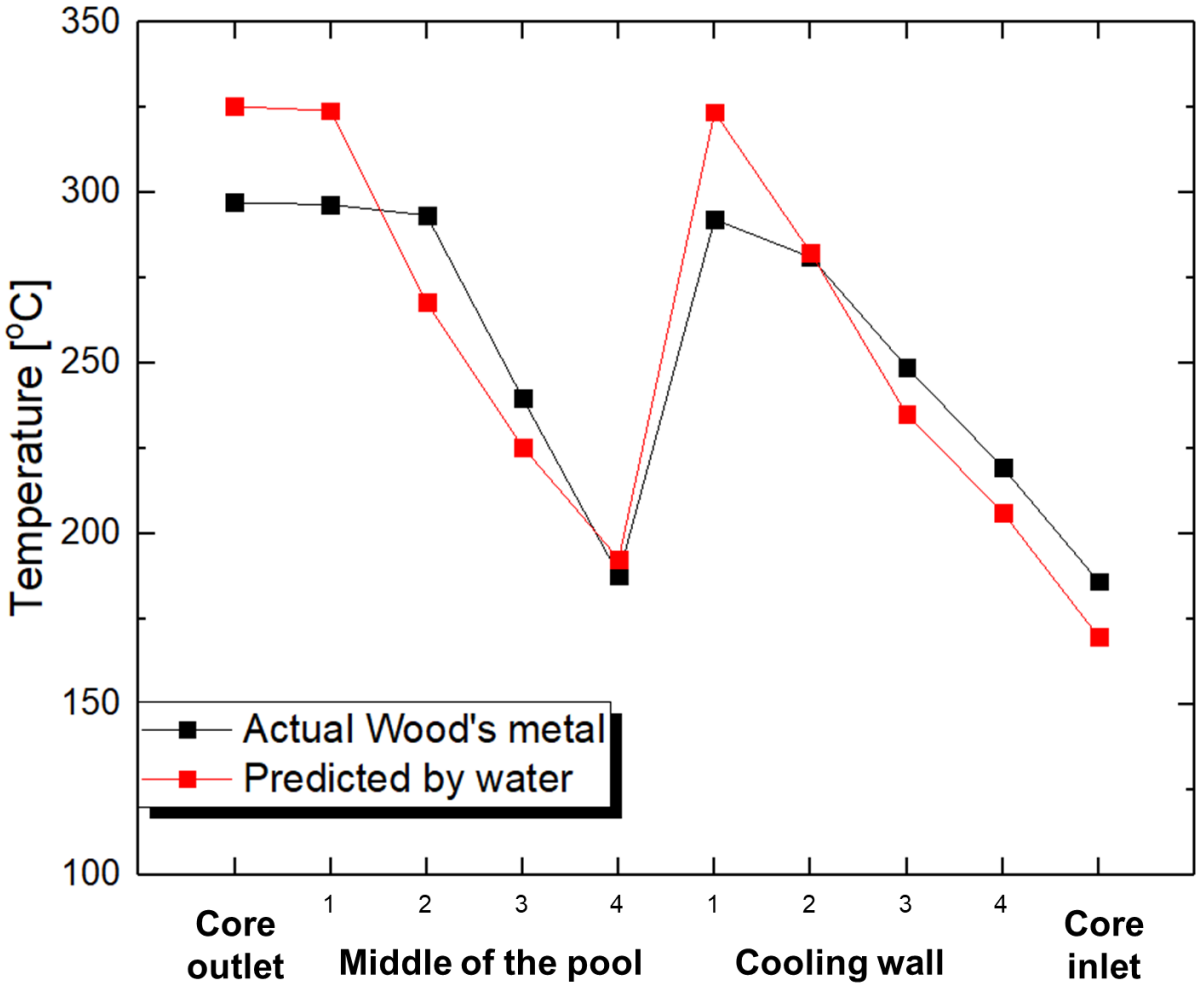

Figure 3-9. Actual and predicted Wood's metal temperature by water under 1.0% of decay heat

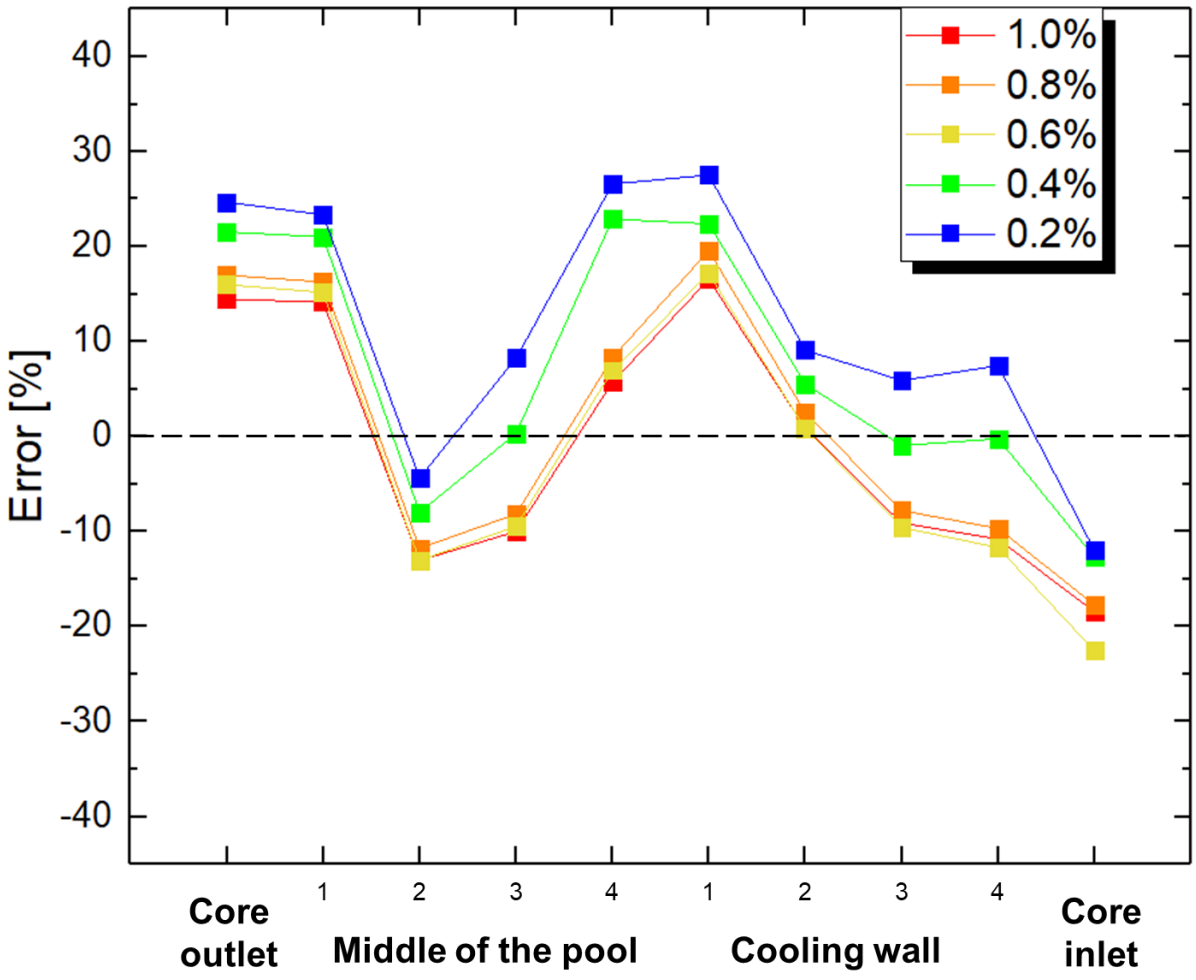

Figure 3-10. Error in the Wood's metal temperature predicted by water experiment

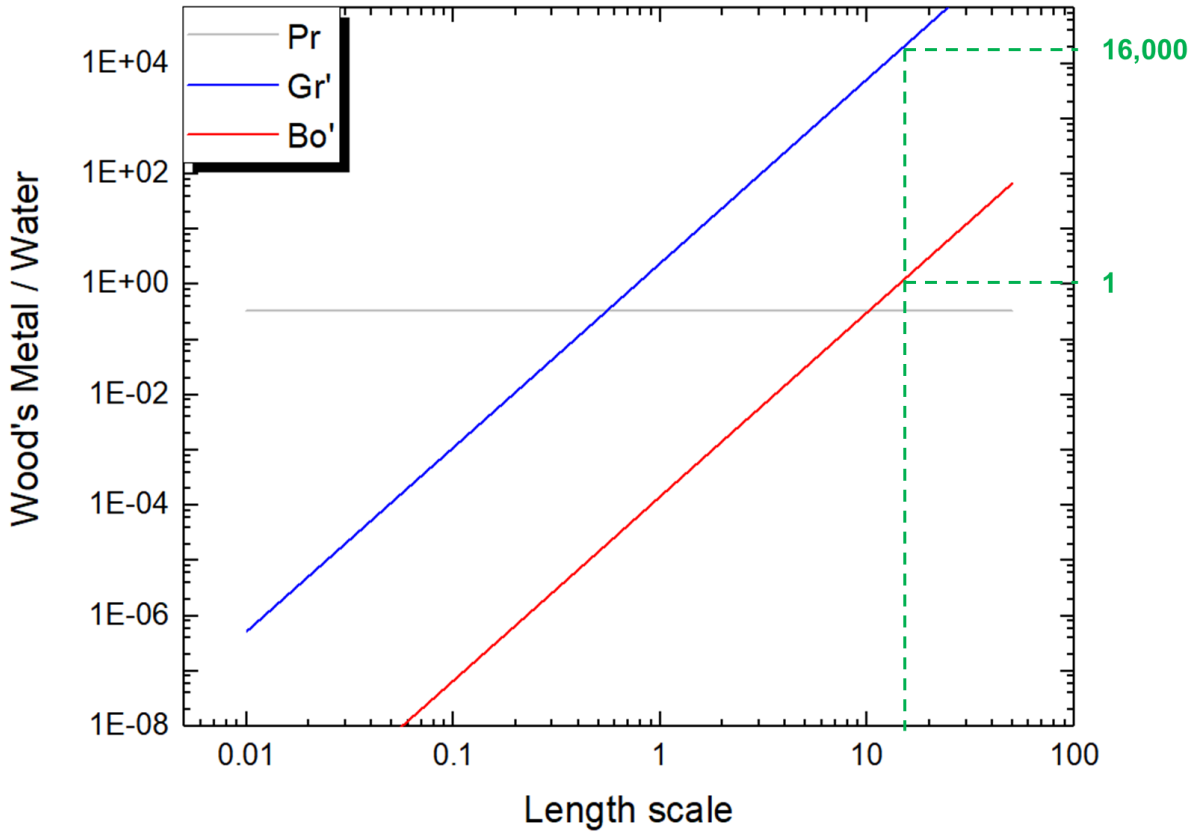

Figure 3-11. Behaviors of the Bo' and Gr' along the length scale

Table 3-5. Similarity of the flow rate

	Wood's metal facility	**Water facility**
Density [kg/m^3]	9500	990
Specific heat [J/kg.K]	190	4185
Power [W]	20000	100
Reference velocities [m/s]	24.57 x 10^{-3}	4.95 x 10^{-3}
Area of the channel [m^2]	0.0406	0.0029
Actual flow rate [kg/s]	**0.9477**	1.315 x 10^{-3}
Predicted flow rate by water [kg/s]	**0.6739**	-
Error	**- 28.89% underestimation**	

3.4. Summary and conclusion

Various LMRs employed the natural circulation for cooling of the decay heat. To evaluate the decay heat removal performance, liquid metal natural circulation should be analyzed based on its temperature. However, liquid metal itself has a lot of disadvantages for experiment, and the experiment should be conducted using a simulant. Here, the Bo' based similarity law was introduced, and current SINCRO-V experiment was conducted to validate the similarity law.

The Wood's metal and water was selected as representative fluids for the liquid metal and non-metallic fluid. Experiments were conducted in the experimental facility named SINCRO-V. The result showed good accordance in the qualitative analysis. Even in qualitative analysis, the prediction capability of the water experiment was proven. Despite some error, the water experiment predicted the Wood's metal temperature with an error of 27%. For the flow rate, the predicted Wood's metal flow rate by the water experiment showed 28.89 % of the difference with the actual Wood's metal flow rate.

Through the SINCRO-V experiment, the Bo' based similarity for the temperature distribution under the natural circulation was experimentally validated. The liquid metal natural circulation could be simulated by the non-metallic fluid.

Chapter 4. 2-D Simulating experiment : SINCRO-2D

4.1. Experimental design

Based on the Bo' based similarity law for the temperature distribution under natural circulation, SINCRO-2D experiment was designed to observe the natural circulation phenomena under the RVACS operation. The objectives and the design of the experimental facility, and corresponding similarity issues would be discussed in this section.

4.1.1. Objective of the experiment

As briefly discussed in chapter 1, the RVACS has unique characteristics compared to the DHX, which has been mainly researched. In case of the DHX, whose heat removal could be treated as the heat sink at the heat exchanger region, the heat removal of the RVACS is achieved at the reactor vessel (RV) wall. It means that the heat removal of the RVACS could not be simplified as volumetric heat sink like that of the DHXs. The heat sink term in the RVACS should be treated as heat flux distribution at the RV wall and its natural circulation phenomena itself is also important for the temperature distribution inside of the pool. Under the RVACS operation condition, the sodium is heated from the core and rises to the upper plenum. Then, it is slightly cooled by the narrow gap between the redan and the intermediate heat exchanger (IHX), and goes downward through the IHX. Then, the sodium is re-entered to the core through the pump and corresponding piping. It has the almost same flow with the normal operation, however, the driving force of the RVACS is natural circulation.

The objective of the SINCRO-2D experiment is to observe the natural circulation phenomena in the RVACS. For the simplified analysis for the fundamental parameters, the experimental facility was simplified as a 2-D slab model. Although the geometry was simplified into 2-D, two-dimensional phenomena could be observed in the SINCRO-V facility. In the SINCRO-2D experiment, effect of the level of the decay heat and the change of the external air cooling-condition were selected as our points of interests.

4.1.2. Experimental facility design

The prototype reactor for the SINCRO-2D was the PGSFR, and the coolant of the PGSFR is the sodium. For the design of the SINCRO-2D, scaling issue and corresponding system parameters should be determined first. To determine system parameters of the SINCRO-2D, a simulant for the sodium

and corresponding scale was calculated based on figure 4-1. As discussed in chapter 2 and 3, water is the best simulant for the liquid metal natural circulation. Too much scale reduction could cause another problem like too much simplification of the detailed geometry for manufacturing issue. Water is the best fluid in terms of the economy, proper scale, clearness of the properties, and operating condition. Final length scale difference between the original sodium system, the PGSFR, and our SINCRO-V was 1 : 25. It represents that the SINCRO-V is 25 times smaller than the PGSFR in the aspect of the length scale. According to this scale reduction ratio, several system parameters were automatically determined by the scaling ratio and working fluid. The reference temperature difference, total power, and the Bo' of the SINCRO-2D, and their ratio to that of the PGSFR were summarized in table 4-1. The radius and height were linearly reduced. The volumetric heat generation rate was maintained, thus, corresponding total power was reduced as cubic of the length ratio. The reference temperature was calculated based on equation (2-10).

SINCRO-2D was designed in two-dimensional shape, a 2-D slab model. Therefore, the original geometry of the PGSFR should be simplified as 2-D. Three-dimensional schematic of the PGSFR was illustrated in figure 4-2. However, essential components should be maintained and reflected into the design. Considering the natural circulation under the RVACS operation, it is the same with that under the normal operation, and includes the core, upper plenum, IHX, narrow gap between the IHX and the redan, lower plenum, and pump and corresponding inlet piping. Therefore, the SINCRO-2D facility should have aforementioned components.

Regard to the slab model, there is another issue for the cross section. Because the PGSFR has three-dimensional shape and could have various cross-sectional geometry depending on the angular position of the cross section. It could be easily recognized by figure 4-2. The IHXs were placed at the side of the figure, while the pump and corresponding piping were placed in the back of the figure. In addition, the top view of the redan is similar to the bow tie. In this regard, the cross section of the two-dimensional facility should be considered. Regard to the natural circulation path of the RVACS, it passes through the IHX and, and cooling would be dominant in that region. Therefore, cross section of the SINCRO-2D was determined as the cross section including the IHX. Position of the pump inlet and piping were neglected, while their effect on the natural circulation flow was considered as the pressure drop through the components.

The cross section containing IHX and the geometry of the SINCRO-2D was in figure 4-3. Left half of the assembly drawing was used for the design of the SINCRO-2D because it was symmetric. The cross section included the IHX. (a) represents the cross section of the PGSFR including IHX. Inside of the yellow line, which represents the redan, there is a hot pool. Under the normal operation, the hot pool is relatively hot than a cold pool because the heated coolant is discharged form the core. Outside of the yellow line, there is the cold pool. The coolant from the hot pool is cooled through the IHX, and

goes downward to the cold pool. The coolant flow from the cold pool to the core via pump and inlet piping, however it is not shown in (a) of figure 4-3 because it is not located in the IHX plane. The core is tall, however, only active core region, which generates heat, was considered. These components were reflected into the design of the SINCRO-2D. In (b), the redan and corresponding cold pool and hot pool, IHX, active core was modeled. Only for the pump and inlet piping, it was simplified and modeled as inlet orifice before the core. Based on the cross-sectional design, SINCRO-2D was designed like (c) in figure 4-3.

In addition to the overall geometry of the SINCRO-2D, the pressure drop should be designed. Table 4-2 shows the portion of the pressure drop of the PGSFR under the normal operation. Three components (the core, and inlet piping) were the main components for the total pressure drop. Among these components, the pressure drop of the core had ambiguousness in terms of the pressure drop analysis in the natural circulation due to characteristics of the CFD analysis. In the natural circulation, it was not easy to clearly distinguish between deriving force from the heating and pressure drop of the heating section. Therefore, for the other two components, the IHX and inlet piping, pressure drop analysis was conducted.

According to the similarity law, the pressure drop coefficient (ζ) should be identical. For the pressure drop, we assumed that 1% of the flow rate condition for the natural circulation. However, there was no reference value for the pressure drop under 1% of the flow rate. Therefore, extrapolated pressure drop values were used for the calculation and their process was graphically summarized in figure 4-4. The pressure drop coefficient could be calculated from the pressure drop and the velocity. Here, the reference velocity for the natural circulation in equation (2-8) was used for the velocity in the pressure drop calculation. Pressure drop coefficient in the SINCRO-V was obtained from the CFD analysis and its domain was shown in figure 4-5. Pressure drop coefficients were calculated based on the reference velocities and pressure drop from the reference, and CFD analysis using equation (4-1).

$$\zeta = \frac{2\Delta P}{\rho u_{ref}^2} \tag{4-1}$$

These values and results were summarized in table 4-3. In general, the pressure drop is modified by the orifice and the diameter of the flow channel. The values of SINCRO-2D in table 4-3 is the final values after modification of the flow channel area. Diameter of the flow channel of the IHX in the SINCRO-2D was 14 mm, which was 94 % of the linearly reduced value. In case of the inlet orifice, which corresponds to the pump and inlet piping, it had a diameter of the 12 mm. Regard to the error of the pressure drop coefficients, the pressure drop coefficients of the SINCRO-2D showed good accordance with that of the PGSFR, less than 5% of the error.

Finally, the SINCRO-2D facility was designed like figure 4-6 (a), and thermocouple installed points were summarized in (b). Red points represent the location of the thermocouples for observation of the core region. Considering the natural circulation flow path, it was anticipated that the maximum and the minimum temperature would be observed in the red points. Green thermocouples were installed near the IHX. There is a narrow gap between the IHX and the redan. Through the redan wall, significant of the cooling was anticipated and to observe this cooling phenomena and corresponding temperature distribution near the IHX, these thermocouples were installed. Blue thermocouples were installed in the lower plenum. The lowest thermocouple is to observe the minimum temperature of the pool, which is independent to the natural circulation. The other three blue thermocouple is installed to observe the temperature distribution of the lower plenum (in other words, the cold pool) like a thermal stratification. Through these temperature points, temperature distribution in the reactor pool in the experiment could be recognized and analyzed.

4.1.3. Test matrix

The SINCRO-2D facility is a 2-D slab model and all the phenomena would be simplified as 2-D and three-dimensional effect could not be appropriately observed in the SINCRO-2D facility. Therefore, the author focused on the effect of two dimensional, or scalar parameter, whose three-dimensional effect could be neglected. The parameters were the level of the decay heat and the distribution of the cooling along the RV wall.

Regard to the decay heat, it is the function of the time after shutdown. The decay heat removal rate of the RVACS in the PGSFR was analyzed as 2.5 MW in maximum[22,37,38], which is approximately than 0.65% of the total power of the PGSFR. It means that accidents without scram (unprotected) could not be mitigated by the RVACS only. Considering enhancement of the performance of the RVACS, the experimental range was determined up to 1.0 % of the decay heat. For the lower limit, the RVACS could perform as a long-term cooling system because it is fully passive. Therefore, 0.2% of the total power, which corresponds to the decay heat at 90 days after shutdown, was determined as lower limit of the test matrix. The interval was 0.2 %. Finally, the decay heat level, the time after shutdown, and the corresponding power in the SINCRO-2D were summarized in table 4-4. The time after shutdown and corresponding decay heat level was calculated based on the literature[21]. The meaning of the 60ΔT in the cooling boundary condition would be discussed in the following paragraph for the temperature gradient along the cooling wall.

Considering the mechanism of the RVACS, change of the external air-cooling condition has an influence on the cooling profile at the CV surface, and consequently, cooling at the RV in terms of the reactor pool. Assuming the decay heat is the same, if the external air flow rate is high, temperature

increment of the air flow would become lower. Consequently, the temperature distribution of the RV wall is changed. Considering the flow path of the external air, temperature of the RV is always higher in the upper part of the RV than the lower part, because hot air rises along the CV wall. Therefore, the temperature distribution along the RV wall is simplified as temperature difference between the top and the bottom of the RV.

For the natural circulation of the coolant, the temperature distribution along the RV wall corresponds with the cooling boundary condition. The validity of the temperature boundary condition was proven in the SINCRO-V experiments. In the practical point of view, the temperature boundary condition is much easier to control than the heat flux boundary condition in case of cooling. Although the heat flux boundary condition was described in equation (2-13), temperature boundary condition is more practical, and easier to reflect its change considering characteristics of the RVACS. External air flow rate and its velocity profile, which is related to the heat flux out from the CV surface, are not fixed and showed various values from approximately 10 to 15 kg/s, according to literatures[22,37,65]. However, the boundary temperature maintained almost constant while the external air flow rate was changed two times[66]. Therefore, it is valid that using the cooling boundary condition as a temperature distribution of the boundary.

Regard to the quantification of the boundary condition of the natural circulation, the temperature difference related to the natural circulation could be used, in other words, the reference temperature difference in equation (2-10). Boundary temperature is certainly related to the natural circulation phenomena, thus, the idea was suggested that the boundary temperature could be normalized using the reference temperature difference for the natural circulation. This idea was numerically validated in the literature[66]. Overall, the normalized temperature difference, by the reference temperature difference, between the top and the bottom of the RV was used for the cooling boundary condition for the SINCRO-2D experiment.

To determine the range of the temperature difference between the top and the bottom of the RV, temperature difference in various condition were summarized in table 4-6. From the second raw, he estimated temperature difference in the natural circulation represents is rough estimation of the temperature difference between the cold pool and hot pool under 1% of the flow rate with 0.6 % of the decay heat, which is heat removal rate of the RVACS. In terms of the reference temperature, the temperature difference is approximately 54 times of the reference temperature difference. Next natural circulation means the temperature difference between the hot pool and cold pool under the DHX operation in the loss of flow accident. It was approximately 40 times of the reference temperature difference, which was the smallest temperature difference among the conditions. Air inlet and outlet means the temperature increment of the external air through the RVACS, which was 82-97 times of the reference temperature difference. The normal operation was the temperature increment through the

core under the normal operation, approximately 95 times of the temperature difference. The largest temperature difference was approximately 107 times of the reference temperature difference, which was observed in the preliminary SINCRO-2D experiment under the 1% of the decay heat. Considering the range of the temperature difference, approximately 40 – 100 times of the reference temperature was determined for the test range, whose interval was 20.

Regard to the setting the temperature in the experiment, it could be manipulated by changing flow rate of the external water flow. It could be expressed with equations. As mentioned before, the temperature gradient was simplified as the temperature difference between the temperature at the top and the bottom of the RV, like equation (4-2).

$$T_{gradient} = T_{RV,top} - T_{RV,bottom} \tag{4-2}$$

The author calculated the temperature inside of the RV from the temperature of the coolant. For the temperature of the bottom, it could be assumed that temperature increment by the thermal resistance of the convection and the conduction of the wall because heat flux at the bottom of the wall could be neglected. From the preliminary experiment, there was less than 1°C of the temperature increment was observed between the thermocouple in the inlet of the water jacket and the thermocouple in the lowest part of the lower plenum. Therefore, temperature of the inside of the RV wall at the bottom could be expressed as equation (4-3), which is equivalent to the coolant inlet temperature.

$$T_{RV,bottom} = T_{coolant,inlet} + \Delta T_{cooling} + \Delta T_{wall} \tag{4-3}$$

For the RV top temperature, problem is more complicated because the heat transfer through the top of the RV was not negligible. Therefore, the temperature increment by the thermal resistance of the cooling channel, RV wall, and the pool natural circulation should be considered. They were summarized in equation (4-4) through (4-7).

$$T_{RV,top} = T_{coolant,outlet} + \Delta T_{cooling} + \Delta T_{wall} \tag{4-4}$$

$$\Delta T_{cooling} = \frac{q''}{h_{cooling}} \tag{4-5}$$

$$\Delta T_{wall} = \frac{q''\Delta x}{k} \tag{4-6}$$

$$T_{gradient} = \Delta T_{coolant\,in,out} + q''\left(\frac{1}{h_{cooling}} + \frac{\Delta x_{wall}}{k_{wall}}\right) \quad (4\text{-}7)$$

Using equations (4-2) through (4-6), temperature difference between the top and the bottom of the RV could be expressed as equation (4-7). It could be obtained by the temperature increment of the inlet and the outlet of the water jacket, and heat transfer coefficients. It was graphically summarized in figure 4-7.

Regard to the convective heat transfer coefficient of the cooling channel, $h_{cooling}$, it was evaluated using Dittus-Boelter equation like equation (4-8). The final value of the $h_{cooling}$ was evaluated as 475.4 W/m^2.K.

$$Nu = \frac{hL}{k} = 0.23Re^{0.8}Pr^{0.4} \quad (4\text{-}8)$$

For the conduction, the thermal resistance of the cooling wall could be directly evaluated from equation (4-6). It was 9333W/m^2.K, which was negligible compared to the magnitude of the other heat transfer coefficients and corresponding thermal resistance.

The RV inner wall temperature could be calculated from the above equations, however, we should compare the calculated value with the experimental value in the experiment to certificate validity of the correlations. The pool temperature could be a reference for the comparison. Therefore, in addition to equation (4-4) and (4-8), one term was added to evaluate pool temperature, like equation (4-9) and (4-10).

$$T_{RV,top} = T_{coolant,outlet} + \Delta T_{cooling} + \Delta T_{wall} + \Delta T_{pool} \quad (4\text{-}9)$$

$$T_{gradient} = \Delta T_{coolant\,in,out} + q''\left(\frac{1}{h_{cooling}} + \frac{\Delta x_{wall}}{k_{wall}} + \frac{1}{h_{pool}}\right) \quad (4\text{-}10)$$

The added term h_{pool} was evaluated using the general correlation for the natural circulation in the cavity, equation (4-11). It was evaluated as 542.6W/m^2.K.

$$Nu = \left[0.825 + \frac{0.387Ra^{1/6}}{\left\{1 + \left(0.492/Pr\right)^{9/16}\right\}^{8/27}}\right]^2 \quad (4\text{-}11)$$

Here, heat flux for the calculation of the temperature increment through the thermal resistance was not defined. It was evaluated 6000 W/m^2 in the preliminary CFD analysis. Therefore, the 6000 W/m^2 was used for calculation. After the experiment, using the temperature distribution in the narrow gap, it was calculated from approximately 5600 to 7480 W/m^2 in the experimental data. Therefore, it could be concluded that assumption for the heat flux was reasonable. Further analysis were discussed based on the this assumption.

Table 4-6 shows the comparison of the pool temperature. Based on the coolant temperature, temperature of the outer and inner surface of the cooling wall were obtained, and finally, bulk pool temperature was obtained and compared to the experimental results. By the correlations, 40.5^{o}C of the temperature was evaluated, while the experimental temperature was observed as 41.7^{o}C. From this result, the validity of the evaluation was confirmed, and the inner cooling wall temperature was considered as calculated results from the above evaluation method.

As discussed before, temperature difference along the cooling wall surface could be manipulated by changing the flow rate of the external water-cooling jacket. Test conditions, corresponding normalized temperature difference of the top and the bottom of the RV, and flow rate at that condition was summarized in table 4-7, which is the test matrix for the boundary temperature distribution.

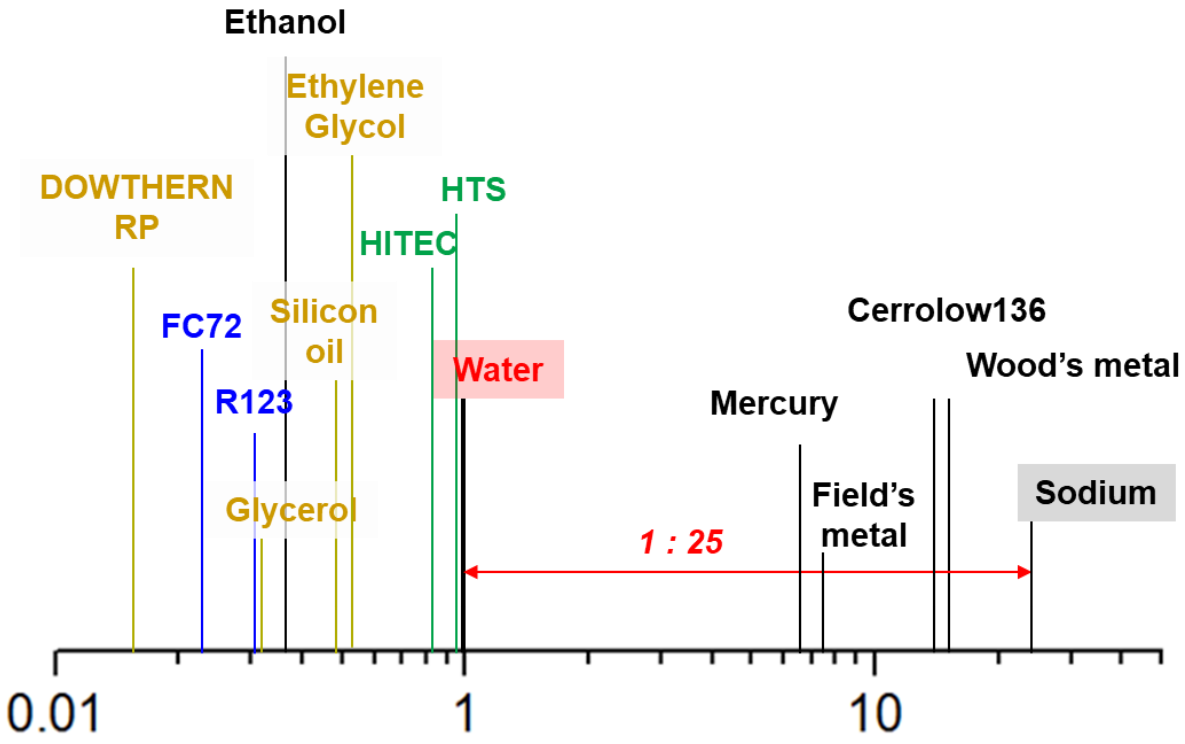

Figure 4-1. Length scale difference between the sodium and the water

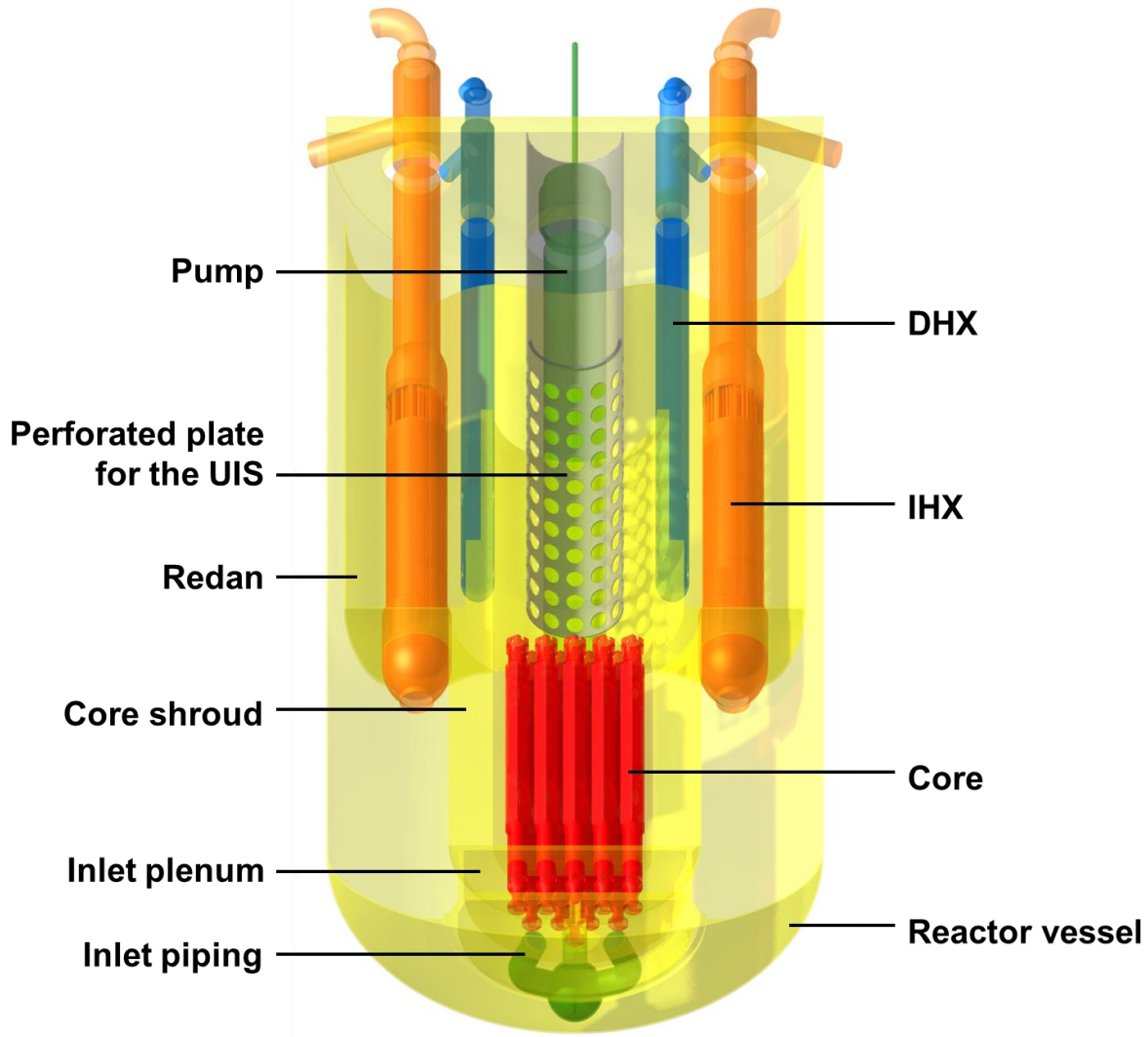

Figure 4-2. 3-D model of the PGSFR

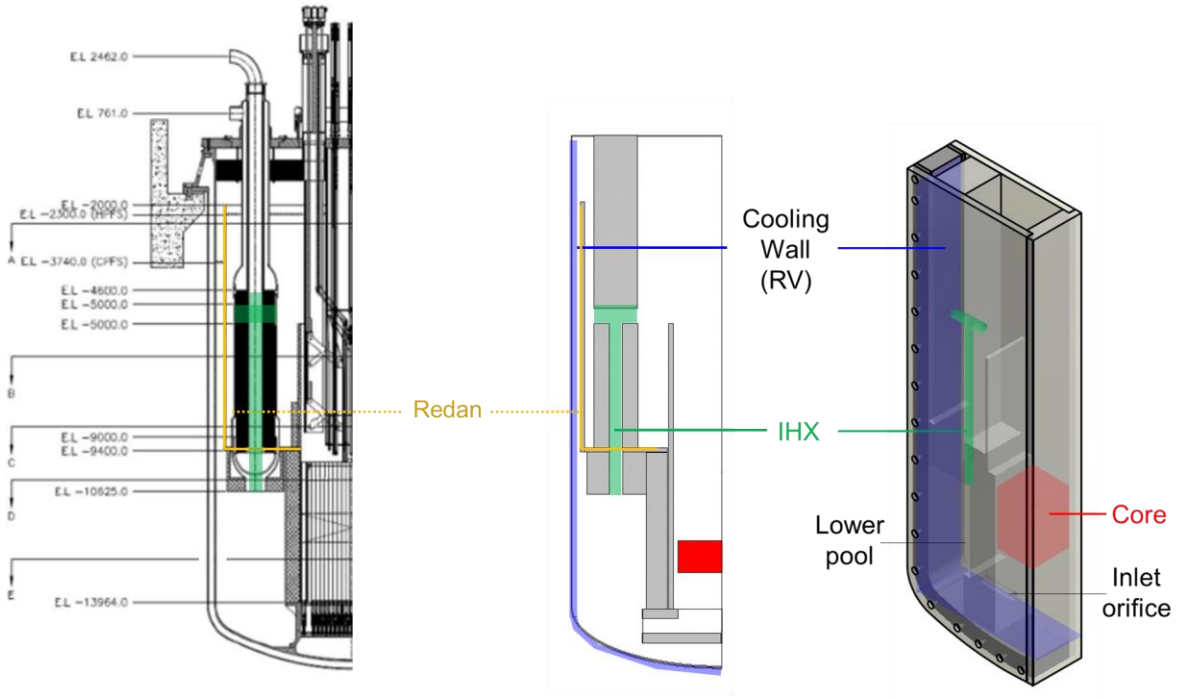

(a) PGSFR[65] (b) SINCRO-2D cross section (c) SINCRO-2D 3D modeling

Figure 4-3. 2-D cross section of the PGSFR and SINCRO-2D

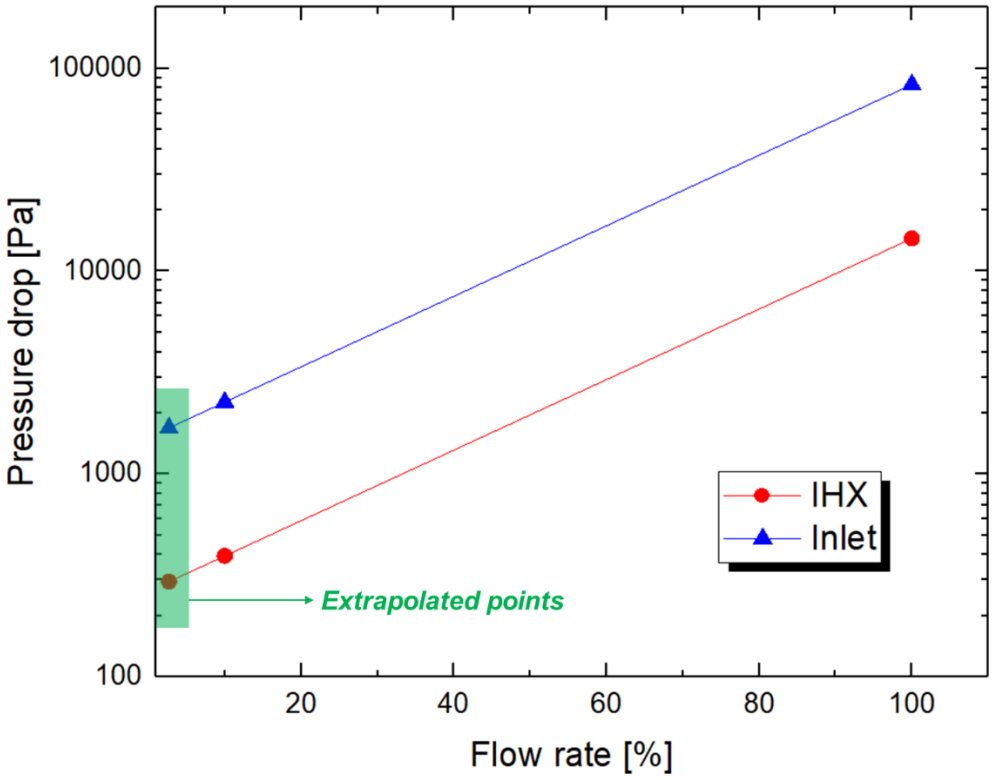

Figure 4-4. Pressure drop of the IHX and inlet piping of the PGSFR

Figure 4-5. Fluid domain of the pressure drop analysis

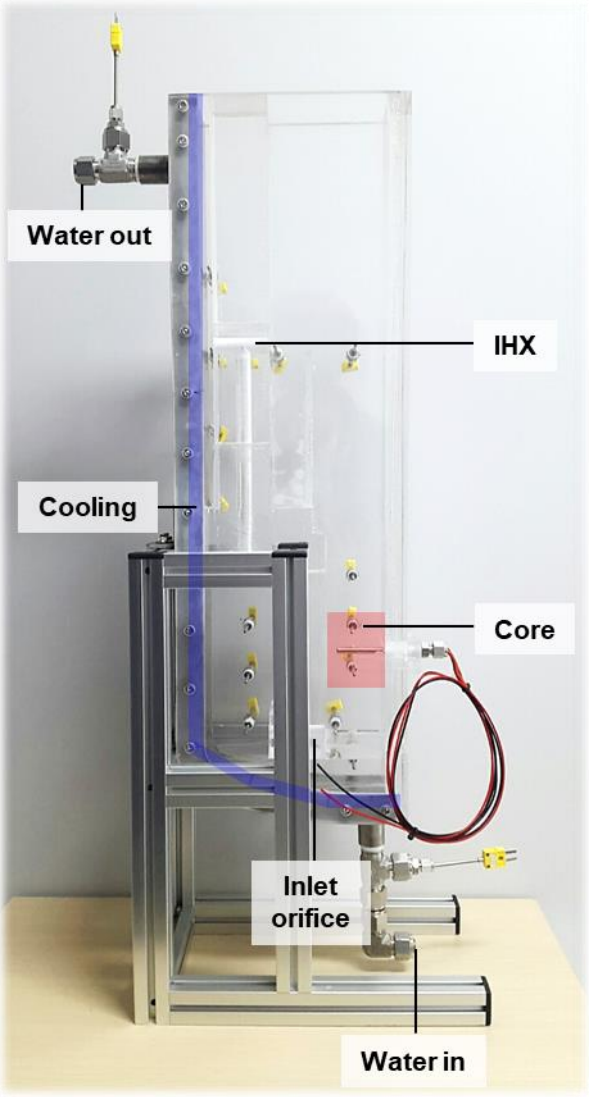

(a) A photo of the SINCRO-2D

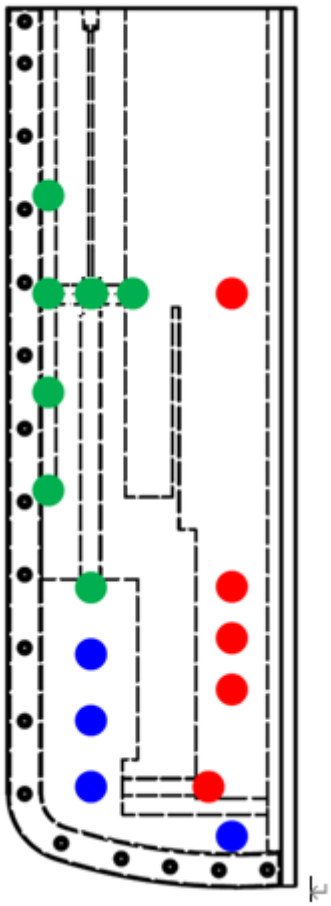

(b) Temperature observation points

Figure 4-6. SINCRO-2D and location of the thermocouples

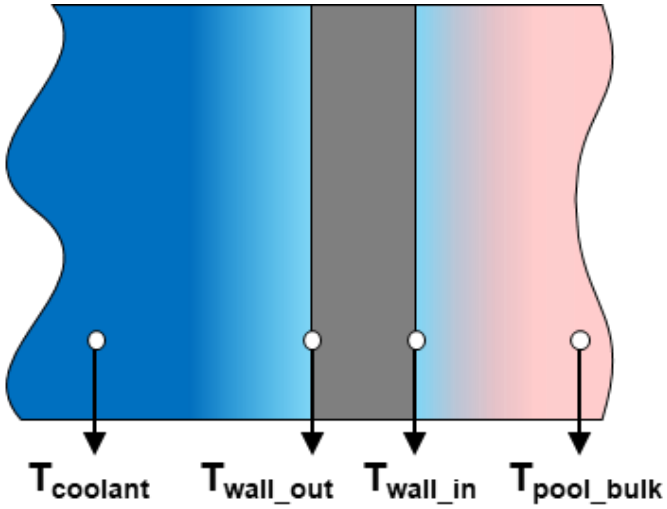

Figure 4-7. Schematic of the obtaining RV inner wall temperature

Table 4-1. Parameters of SINCRO-2D and their ratio

Parameter	**PGSFR**	**SINCRO-2D**	**Ratio**
Radius	4.3 m	173 mm	1/25
Height	15.3 m	540 mm	1/25
Q’’’	213.4 W/cm^3	213.4 W/cm^3	1
Q_{total}	392 MW	200 W	1/25^3
ΔT_{ref}	1.637 ºC	0.248 ºC	0.15

Table 4-2. Parameters of SINCRO-2D and their ratio

Component	**Pressure drop**	**Contribution**
Inlet plenum	3.5 kPa	0.6 %
Core	429.0 kPa	76.0 %
Upper plenum	0.0 kPa	0.0 %
IHX	14.5 kPa	2.6 %
Lower plenum	34.1 kPa	6.0 %
Inlet piping	83.2 kPa	14.7 %
Total	564.3 kPa	100.0 %

Table 4-3. Parameters of SINCRO-2D and their ratio under 1% of the flow rate condition

Component	**IHX**	**Inlet piping**	**Note**
Pressure drop under natural circulation	394.14 Pa	2261.55 Pa	
ζ in the PGSFR (pressure drop coefficient)	32014	183697	u_{ref} = 0.136 m/s
ζ in the PGSFR (pressure drop coefficient)	30562	178733	u_{ref} = 0.009 m/s
Error	- 4.5 %	- 2.7 %	

Table 4-4. Summary of the test matrix for the decay heat level

		PGSFR	**SINCRO-2D**
Power	90 days	0.78 MW *(0.2%)*	40 W
	6.8 days	1.57 MW *(0.4%)*	80 W
	1.5 days	2.35 MW *(0.6%)*	120 W
	12.6 hrs	3.14 MW *(0.8%)*	160 W
	5.5 hrs	3.92 MW *(1.0%)*	200 W
Cooling		Simplified	
		??	60ΔT
Bo'		25 % differ	
		0.86×10^{8}	1.07×10^{8}

Table 4-5. Possible range of the temperature difference of the top and the bottom of the RV

Condition	**ΔT_PGSFR**	**ΔT_SINCRO**	**θ by ΔT_{ref}**
Natural circulation[67]	65℃	9.8℃	39.7 times
Natural circulation (estimated)[65]	88℃	13.3℃	53.8 times
Air inlet & outlet[37]	135 - 160℃	20.4-24.2℃	82-97 times
Normal operation[19]	155.0℃	23.48℃	94.7 times
Max ΔT in the experiment	174.8℃	26.49℃	106.8 times

Table 4-6. Comparison between evaluated and experimental pool temperature

Position	**$T_{evaluated}$**	**$T_{experiment}$**
Coolant	16.2℃	
Wall_out	28.8℃	Unknown
Wall_in	29.5℃	We want to know
Pool_bulk **Comparing parameter**	**40.5℃**	**41.7℃**

Table 4-7. Test matrix of the parametric study on the boundary condition

Case	**Normalized to ΔT_{ref}**	**$\Delta T_{top,bottom}$**	**Flowrate**
1	40 times	9.92℃	9.2 lpm
2	60 times	14.88℃	5.4 lpm
3	80 times	19.84℃	3.8 lpm
4	100 times	24.79℃	2.8 lpm

4.2. Discussion on the base case

The natural circulation characteristics of the reactor pool under RVACS operation was analyzed in this part. 1.0 % of the decay heat, and 60 times of the reference temperature difference was selected as a representative case. Temperature distribution, flow field estimated by the temperature distribution, natural circulation flow rate, and the cooling fraction would be discussed. For this case, numerical validation with the CFD, ANSYS-CFX, and the system code, MARS-KS were conducted.

4.2.1. Overall natural circulation behavior.

Figure 4-8 shows the represent temperature distribution of the SINCRO-2D experiment under 1% of the decay heat, with $60\Delta T_{ref}$ boundary condition. It was certificated by figure 4-9 that steady state was achieved without fluctuation or instability of the natural circulation. Because it was a natural circulation system, overall thermal stratification was observed. As shown in the figure 4-8, temperature was higher in the upper region in general. The narrow gap and the other parts of the pool showed separated profile because they were almost separated and connected at the small IHX inlet. The effect of the natural circulation on the temperature distribution could be clearly observed by the temperature stratification. If the temperature pool is fully stratified, the temperature points at the same height should show the same value. However, as shown in the figure, it was not. The temperature distribution was strongly affected by the natural circulation flow. After the heating zone, water was heated and went upward to the end of the liquid volume. Until entering IHX, natural circulation flow was not cooled and maintained similar temperature to temperature at just after the heater. At the T-junction of the IHX, flow temperature decreased to 52.0℃ and finally decreased to 47.6℃ at the outlet of the IHX. Along the observation points in the lower plenum, the temperature was not significantly decreased until the third points from the top. However, sharply decreased to 36.1℃ at the lowest points at the nest point below. Considering the minimum temperature of the natural circulation path, which is the 26.9℃ of the inlet piping, significant cooling was achieved in the lower plenum. It represents that the strong downward flow from the IHX outlet affected to the third points from the top. The points 36.1℃ and 26.9℃ were located at the same height, however, temperature was quite different. It was another evidence of the effect of natural circulation on the stratified temperature profile.

From the previous paragraphs, the effect of the natural circulation on the temperature distribution was discussed. The temperature distribution was strongly depended on the flow. Here, a limitation of the SINCRO-2D facility could be suggested. It is two-dimensional facility, which neglect three-dimensional phenomena like flow. However, in the actual reactor PGSFR, the natural circulation flow

should be generated in three-dimensional space, especially, in the lower plenum between the IHX outlet and the pump inlet. As discussed in the experimental apparatus design, the pump inlet is located at the different angular position with the IHX, in case of top view. In figure 4-2, it is located behind of the core structure, while IHXs (orange) are located at the left and right side of the figure. In the lower plenum, the natural circulation flow under RVACS operation is discharged from the IHX outlet, and enters to the pump inlet, which has fully three-dimensional shape. Considering the effect of flow on the temperature distribution and the characteristics of the flow, three-dimensional effects by the flow could not fully observed in the SINCRO-2D facility. Therefore, three-dimensional facility is required for the observation of the temperature distribution in the lower plenum.

The narrow gap, which is the space between the redan and the IHX, also showed stratified temperature distribution. Before the experiment, the author presumed that conduction is dominant heat transfer mechanism in the hot pool cooling because the width of the narrow gap was is relatively smaller than others. To evaluate heat transfer mechanism in the narrow gap, simple 1-D calculation was conducted. Equation (4-12) represents the simple 1-D conduction equation under steady state. Heat transferred amount by the conduction was evaluated and it would be compared to the total power, temperature decrement after the IHX, and calculated heat removal fraction at the narrow gap, which would be calculated later.

$$q = -k \frac{\Delta T}{\Delta x} A \tag{4-12}$$

Among the thermocouples, a thermocouple at the T-junction of the IHX and thermocouple in the narrow gap having same height with the T-junction of the IHX were selected to calculated the amount of conductive heat transfer, which have temperature as 52.0℃ and 35.2℃, respectively. The distance between these two points were 30 mm. Thermal conductivity of the water was assumed as 0.6 W/m.K. The area of the IHX channel was 176.7 mm^2. From these values, only 0.06 W of the heat was transferred by solely conduction in this interval. Considering the temperature decrement through the IHX, from 52.8℃ at the IHX inlet to the 47.6℃ at the IHX outlet, 0.06 W is too small amount of the heat transfer rate to make such a significant temperature difference. Comparing to the total power, 0.06 W is negligible to the 200 W. However, significant temperature change was observed through IHX. It means that cooling at the narrow gap was meaningful. Therefore, it can be inferred that even in narrow gap, natural circulation is the dominant heat transfer mechanism. For the whole part of the reactor pool, natural circulation was the dominant heat mechanism.

Next, considering the temperature change along the natural circulation flow and corresponding cooling fraction at each part. It was certain that the maximum temperature was observed just after the

heating region, having 53.3℃ of the temperature. The minimum temperature was observed at the inlet piping, and it was 26.9℃. It means that total 26.4℃ of the temperature increased in the core, and decreased through the other parts of the natural circulation flow path. Here, the temperature at the outlet of the IHX was 47.6℃. It means that the hot flow from the core was cooled down by the cooling at the narrow gap, from 53.3℃ to 47.6℃. In other words, 5.7℃ of the temperature was decreased by the narrow gap cooling. In the viewpoint of the lower plenum, 47.6℃ of the coolant was entered to the lower plenum and went out to the inlet piping with the temperature of the 26.9℃. It means that 20.7℃ of the temperature was cooled down in the lower plenum. From the temperature change history along the natural circulation path, cooling fraction could be calculated, and consequent cooling rate. Because the SINCRO-2D facility was almost insulated, (see appendix), the cooling rate could be calculated using the total power and the cooling fraction. It could be expressed like equation (4-13) and (4-14).

$$Cooling\ fraction = \frac{\left(T_{inlet} - T_{outlet}\right)_{component}}{\left(T_{max} - T_{min}\right)_{system}} \tag{4-13}$$

$$Cooling\ rate = Cooling\ fraction \times Total\ power \tag{4-14}$$

Consequently, 20.8 % of the heat was removed at the narrow gap, and it corresponds to 41.6 W of the heat was cooled at the narrow gap. The other 79.2 % of the heat, which is 158.4 W was cooled at the lower plenum. This cooling fraction can suggest importance of the internal structure in the natural circulation. In general, higher part of the pool has the higher temperature than the lower part of the pool. Under constant temperature boundary condition, and, if there is no internal structure disturbing natural circulation flow in the pool, cooling heat flux is higher in the higher region because the heat flux is proportional to the temperature difference between the pool and the boundary. However, in the SINCRO-2D experiment, most of the heat was removed in the lower part of the pool, the lower plenum. Decrease of the upper cooling fraction was caused by the internal structures which disturb the flow to the upper cooling wall, in this experiment, the IHX.

In case of the PGSFR, there is a structure which was not considered in the SINCRO-2D. It is clearly shown in figure 4-2. Between the redan and RV, there is a small space, which is a part of the cold pool (lower plenum). This small space could act as an additional thermal resistance in terms of the top cooling. Therefore, the cooling fraction of the narrow gap would be overestimated in the SINCRO-2D experiment. Additionally, this thin space is a part of the lower plenum. Therefore, complex natural circulation phenomena are expected in this region, which could not be analyzed in the SINCRO-2D experiment. Consequently, cooling fraction of the lower plenum would be increased in the PGSFR.

Finally, it was revealed that the Bo' based similarity law could estimate flow field, except for the flow regime. Therefore, flow rate could be reasonably reproduced by the Bo' based, simulating experiment. However, there is no flowmeter in the SINCRO-2D facility. Therefore, the flow rate was calculated based on the simple equation (4-15) using temperature difference. It is reasonable because the SINCRO-2D facility had almost insulated condition (see appendix).

$$\dot{m} = \frac{q}{c_p \left(T_{max} - T_{min}\right)_{natural\ circulation}} \tag{4-15}$$

Total power was 200 W in this case, and specific of the water was used as 4181 J/kg.K. The calculated flow rate was 1.8 g/s, which corresponds to the 2.4 % of the flow rate of the normal operation condition, using equation (3-5).

For the direct data interpretation between the results of the SINCRO-2D and the PGSFR, there were some points which should be considered. First, the SINCRO-2D was simplified as 2-D. 1% of the decay heat was removed by the cooling wall. The volume of the core was considered as cross-sectional area in the SINCRO-2D, however, it was half of the volume was neglected because it was symmetric. In addition, there are four IHXs in the PGSFR, however, only one IHX was reflected into the SINCRO-2D design. It means that the pressure drop related of the IHX were not strictly simulated. To simplify this situation, let's think about pizza with big pepperoni in the center. To have exact symmetry, it should be cut like a piece of a pizza, a circular sector. However, SINCRO-2D was 2-D slab model. In other words, pepperoni was overestimated and cornicione of the pizza was underestimated, which correspond to the core and the cooling wall in the PGSFR. The pressure drop through the core was not properly modeled in the SINCRO-2D. Therefore, the results of the SINCRO-2D experiment could not be directly interpreted to the that of the PGSFR. However, the SINCRO-2D experiment could give enough physical insights for the natural circulation phenomena under the RVACS operation condition.

4.2.2. Numerical validation by CFD

The numerical validation was conducted by CFD to validate the experiment and to find a proper turbulence model for the natural circulation under RVACS operation. For the turbulence model, there were six models were considered and their characteristics and the reason for selection were summarized in table 4-8. The laminar model was applied because most of the flow regime was considered as laminar. The k-ε model is the most common turbulence model. The k-ω model showed better accordance at the wall than the k-ε model. The SST model is combination of the k-ε and k-ω

model. The eddy viscosity model is based on the transportation of the viscosity with suppression of the viscosity generation near the wall. The RSM Reynolds stress model is the 2nd order turbulence model. These models were applied, and the result would be discussed.

The commercial software ANSYS-CFX was used. Approximately 373 thousand of the mesh was applied with inflation on the wall of the flow domain. Heating was applied as volumetric heat generation of the cartridge heater, which is same to the experiment. The cooling boundary condition was simplified as 20°C. Because the SINCRO-2D facility was almost perfectly insulated except for the cooling wall, an adiabatic condition was applied to the all the external surfaces. There were three kinds of the material in the domain and the same material with the experiment was used for the domain. First, stainless steel was applied to the cooling wall because the cooling through the cooling channel was simplified as a constant temperature cooling at the cooling wall. Second, acrylic resub was applied to the front panel, back panel, and the internal structure surrounding water. Last, water was applied to the working fluid inside of the acrylic resin. The thermal conductivity of the acrylic resin was 0.1 W/m.K.

Figure 4-10 shows the results of the CFD analysis with different turbulence model. For the laminar model (a) and the k-ω model (c) showed similar temperature distribution. Stratified temperature in the pool and the narrow gap was properly describe by the CFD analysis. The magnitude of the temperature also showed good accordance with the experimental result. The difference between the laminar and the k-ω model was mixing characteristics in the downward channel of the IHX. However, in the k-ε model (b), significant overestimation of the temperature was observed. Not limited to the certain region, but overall overestimation of the temperature was observed. In particular, the overestimation at the bottom of the pool showed more than approximately 40°C of the temperature. In this region, there no natural circulation flow. As the thermal conductivity of the acrylic resin between the core region and the lower plenum was commonly applied as 0.1 W/m.K, the temperature overestimation of the bottom of the pool was not caused by the conduction through the structure. This difference was caused by the turbulence model and corresponding thermal diffusivity.

$$\frac{\partial \rho T}{\partial t} + \nabla\left(\rho u T\right) = \nabla\left(\left(\rho\alpha + \frac{\mu_t}{Pr_t}\right)\nabla T\right) \tag{4-16}$$

As shown in equation (4-16), the diffusion coefficient of the temperature gradient includes μ_T, which is the turbulent viscosity. It is determined by the turbulent model. That is the reason that the turbulence model has an influence on the heat transfer even in the flow-free region. In case of the k-ε model, there is an additional turbulent viscosity generation term by cross diffusion, while it is not in the k-ω model. In addition, in the k-ω model, there is a suppression of the turbulent viscosity

generation and wall effect is considered as more dissipation near the wall. Thus, overestimation in the k-ε model was caused by the overestimation of the production of the turbulent viscosity, and the underestimation of the dissipation of the turbulent viscosity near the wall. Based on this fact, the temperature distribution of the other turbulence model could be explained. The SST model (d) is the combination of the k-ε and k-ω model, therefore, the characteristics of the k-ω model was properly reveled in the wall region. It showed good accordance with the actual temperature distribution. This trend is same in the RSM Reynolds stress model (e), which considers pressure strain term in addition. Because the Reynolds stress model has the higher order of turbulence closure, it was anticipated that this model showed the best accordance with the experiment. In case of the eddy viscosity model (f), there is a consideration of the wall effect, however, it is limited to the suppression of the turbulent viscosity production. The increase of the dissipation near the wall is not considered, therefore, it showed similar temperature distribution characteristics with the k-ε model.

Figure 4-11 shows above discussions in more quantified manner. The position of the temperature observation points was labeled as number, which corresponds to the location in the graph. For example, number 3 means the T-junction of the IHX. The effect of the turbulence model was discussed in the following paragraph. Overall, CFD analysis showed very good accordance with the experimental results, like the core inlet, outlet, IHX outlet and the lower plenum. Common for all CFD results, large discrepancy at the T junction of the IHX between the CFD results and the experimental result was remarkable. All CFD results significantly underestimated the temperature than the experiments. In the experiment, temperature of the T junction showed similar temperature with the core outlet and the IHX outlet. However, in the CFD results, temperature of the T junction was significantly lower than adjacent points. It could be explained by the temperature distribution in figure 4-10. Hot water from the core, and the cooled water from the narrow gap were mixed together at the T junction in the IHX, and went downward through the downward pipe of the IHX. Complex mixing phenomena occurred at the T junction and corresponding temperature gradient was very sharp. It could be easily recognized in figure 4-10. The large temperature gradient at the T junction was commonly observed in all turbulence model. Therefore, discordance at the T junction was not severe as shown in the graph, figure 4-11. Additionally, there could be an error in the position of the thermocouple at the T junction. As described above, the large temperature gradient causes a large temperature change with small error in the position. Thus, large discordance at the T junction between the experiment and CFD could be acceptable. There is an additional large discordance between the experiment and CFD in the bottom of the lower plenum, which was labeled in figure 4-11, as the inlet piping, and the pool bottom. The discordance in the inlet piping and pool bottom was caused by the simplified cooling boundary condition. In the experiment, cooling was achieved by the cooling water, which enters at the bottom of the facility and exit at the top of the facility. This made temperature

difference along the cooling wall and cooling boundary condition for the pool was applied as the temperature gradient of the wall. However, in case of the CFD, the cooling boundary condition was simplified as constant temperature cooling at the cooling wall, and cooling channel was omitted. The boundary temperature of the experiment was approximately 17°C, while 20°C was applied for the whole cooling wall in the CFD. For the inlet piping, it showed significantly lower temperature than the lower plenum in the experiment, while the CFD results were similar in the two points. It represents that between the lower plenum point and the inlet piping, there was additional cooling or the inflow of the cooled water. Both could be possible. Considering the flow in the lower plenum, flow was entered from the IHX outlet and went to the inlet piping. The entered flow from the IHX outlet was went downward and changed to the horizontal direction as entering the inlet piping. Between the downward flow and the horizontal flow, there was strong driving force at the cooling wall. Falling of the colder water was natural and could be observed in figure 4-10 by the entrained temperature distribution near the cooling wall. This downward flow would be detached from a certain point of the cooling wall, and entered to the inlet piping, as mixing with the bulk fluid in the lower plenum. Regard to this process, cooling in the lower plenum was stronger in the experiment. According to the simple relationship between the heat transfer and temperature difference between the media, the temperature of the wall and its distribution were important. More cooling could be achieved with the cooling wall of the lower temperature. In terms of the average temperature, an average cooling wall in the lower plenum was lower than that in the narrow gap. However, it was simplified as the same in the CFD analysis. Therefore, overall cooling in the lower plenum was underestimated in the CFD. For the detailed temperature distribution, if the temperature of the cooling wall was not constant, it was certain that more cooling is achieved at the lower temperature cooling wall. It could influence the detachment of the downward flow on the cooling wall. In summary, the total cooling in the lower plenum could be regarded as a temperature difference between the IHX outlet and the inlet piping, and it was underestimated in the CFD because of the underestimated cooling boundary temperature. One of the clues for the cooling phenomena in the lower plenum was temperature difference between the lower plenum point and inlet piping point. The cooling and mixing phenomena in the lower plenum was not realistically evaluated in the CFD analysis because of the simplified, constant boundary temperature.

The CFD results could be categorized into two groups; one includes the laminar, k-ω, SST, and BSL Reynolds stress model, while the other includes the k-ε and eddy viscosity transport model. The first group evaluated almost same value along all points, and showed good accordance with the experimental results. Especially, the core inlet, core outlet, IHX outlet and the lower plenum showed very good accordance with the experimental results. The reasons for the discordance at the T junction of the IHX, inlet piping, and pool bottom were discussed in the previous paragraph. These models

showed good accordance with the experimental results by properly modeled turbulent viscosity. As discussed with equation (4-16), the turbulent viscosity has an effect on the heat transfer. The models in the first group have a turbulent viscosity damping term near the wall. Both suppression of the production of the turbulent viscosity and increase of the dissipation were considered in the near wall region. This suggests us that under confined geometry like SINCRO-2D, the wall effect should be considered like the model in the first group, which considers both suppressed generation and increased dissipation of the turbulent viscosity near the wall. For the laminar case, it was natural that the lowest temperature was estimated because the laminar model is not considered about the turbulent viscosity and corresponding enhancement of the heat transfer. The laminar model showed good accordance with the experimental results and proper turbulent models in the first group. This suggests that the flow regime in the SINCRO-2D was dominated by the laminar flow. The second group includes the k-ε and the eddy viscosity transport model. The k-ε model did not considered both suppressed generation and increased dissipation of the turbulent viscosity near the wall, while the eddy viscosity model took the suppression of the generation into consideration. Therefore, the k-ε model predicted higher temperature than the eddy viscosity transport model. Due to the overestimated heat transfer in the pool, the magnitude temperature difference in the pool was smaller than that of the first group. The overestimation of the temperature was significant at the inlet piping and the pool bottom. Because the thermal conductivity of the acrylic resin was only 0.1 W/m.K, the effect of the conduction through the acrylic structure could be negligible. It could be concluded that the overestimation at these two points was caused by solely the overestimated turbulent viscosity. The discussions about the turbulence model in so far, were summarized in table 4-8.

4.2.3. Numerical validation by MARS-KS

The system code is necessary to evaluate performance of the RVACS, which has inherently transient characteristics. To check the applicability of the system code to the natural circulation, numerical analysis with MARS-KS code was conducted, which is the abbreviation of the Multi-dimensional Analysis of Reactor Safety - KINS Standard. The nodalization of the SINCRO-2D in the MARS-KS code was summarized in figure 4-12 with temperature observation points. Compared to the points in figure 4-11, the temperature observation points were in the basically same position with that of the experiment and CFD analysis. The water domain was modeled as a combination of the various pipe and multi-dimensional component. Regard to the T junction, there were complex mixing phenomena. To reflect complex flow structure at the T junction, the horizontal channel of the T junction was modeled as combination of the two pipes and multi junctions. One pipe is for the flow to the narrow gap, and the other pipe is for the flow from the narrow gap. There was natural circulation

in the narrow gap, which was the key heat transfer mechanism. To reflect this natural circulation, the narrow gap was modeled by a combination of the two pipes and multi junctions, which allows both upward and downward flow. In the lower plenum, two-dimensional phenomena were dominant, like natural circulation and horizontal temperature gradient, which was perpendicular to the flow direction. Therefore, to consider two-dimensional phenomena should be into consideration, and the lower plenum was modeled by multi-dimensional component in the MARS. Other regions could be easily simplified as one-dimensional pipe. The cooling channel was modeled as a single pipe out of the water domain, with the inlet volume and outlet volume for the cooling flow control. The cartridge heater was modeled as a heat structure, which was attached to the pipe number 100. There was an additional heat structure for the cooling wall, which was attached to the cooling channel and the water domain. Inlet temperature of the cooling water was assumed as 20^{o}C.

Figure 4-13 shows the results of the MARS-KS code and comparison with the experimental data, and numerical analysis by ANSYS-CFS with the SST model. Point by point, at the core inlet, there was a significant underestimation of the temperature in the MARS. The exact location of the point 1 in the MARS was just below the volume attached to the heat structure. In the actual situation, there should be conductive heat transfer between each volume of the pipe, however, it was not modeled in the MARS, especially, there was no backward heat transfer. A kind of backward heat transfer in the MARS only exists in the heat structure, which is used under back flooding of the accident transient. Absence of the backward heat transfer model in the MARS caused the underestimation of the temperature at the core inlet. The maximum temperature was shown at the core outlet, and showed good accordance with the other methods. The temperature at the T junction showed a similar value with the experiment because observation point in the MARS was located in the upper pipe of the modeled T junction. At the IHX outlet, the results by the MARS showed reasonable accordance with the other methods. Here, the temperature at the IHX outlet was mixing of the temperature of the upper and the lower pipe of the modeled T-junction, and also represented the cooling through the narrow gap. The significantly lower temperature at the IHX outlet represents cooling through the IHX was overestimated. Temperature at the lower plenum and inlet piping showed almost similar temperature. The lower plenum was modeled as a multi-dimensional component, therefore, two-dimensional phenomena could be considered. Effect of the multi-dimensional component could be recognized by the temperature difference between the lower plenum and inlet piping. There was temperature difference between the lower plenum and inlet piping. It means that there was horizontal temperature gradient in the new modeling of the lower plenum, and effect of the natural circulation inside the lower plenum was considered.

The MARS-KS results could be divided into three regions; well-predicted regions, poor predicted regions, and regions could be modeled. The well predicted region includes the core outlet, inlet piping,

and pool bottom, where one-dimensional simplification could be applied without calculation of the backward conduction through the fluid. The core inlet could be easily simplified as one-dimensional pipe, however, there was significant backward conduction through the fluid. The poor predicted regions include the T junction of the IHX. There were complex mixing phenomena in the T junction, and the value in figure 4-11 did not properly represents the value of the T junction. Regard to the outlet of the IHX, it was a result of the cooling through the narrow gap. The lower plenum was the region where could be modeled. It could be simplified as two-dimensional pool for the SINCRO-2D facility and could be simplified as three-dimensional, wide pool in the prototype reactor PGSFR. The lower plenum was simplified as two-dimensional pool, and there were complex phenomena like penetration of the downward flow from the IHX, mixing of the fluids, and detachment of the downward flow at the cooling wall. These phenomena were reasonably modeled in the system code and results showed good accordance with experimental temperature. In summary the system code well predicted natural circulation phenomena in the region where could be easily simplified as one-dimensional pipe, while did not showed satisfactory prediction in the region with complex mixing phenomena. Wide, multi-dimensional pool could be simplified as a multi-dimensional component and natural circulation inside of the pool could be reasonably predicted.

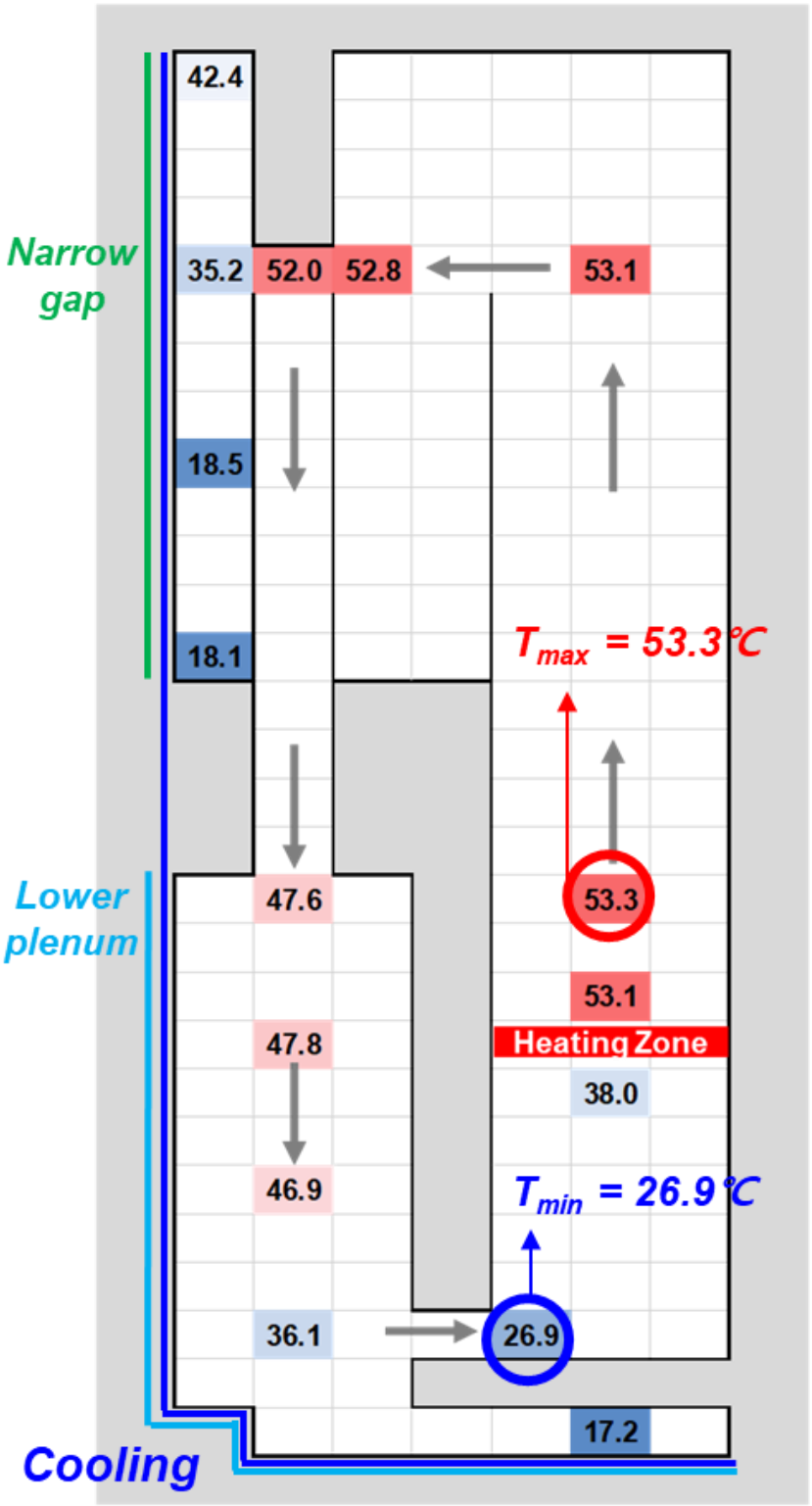

Figure 4-8. Representative temperature distribution of the SINCRO-2D (1%, $60\Delta T_{ref}$ condition)

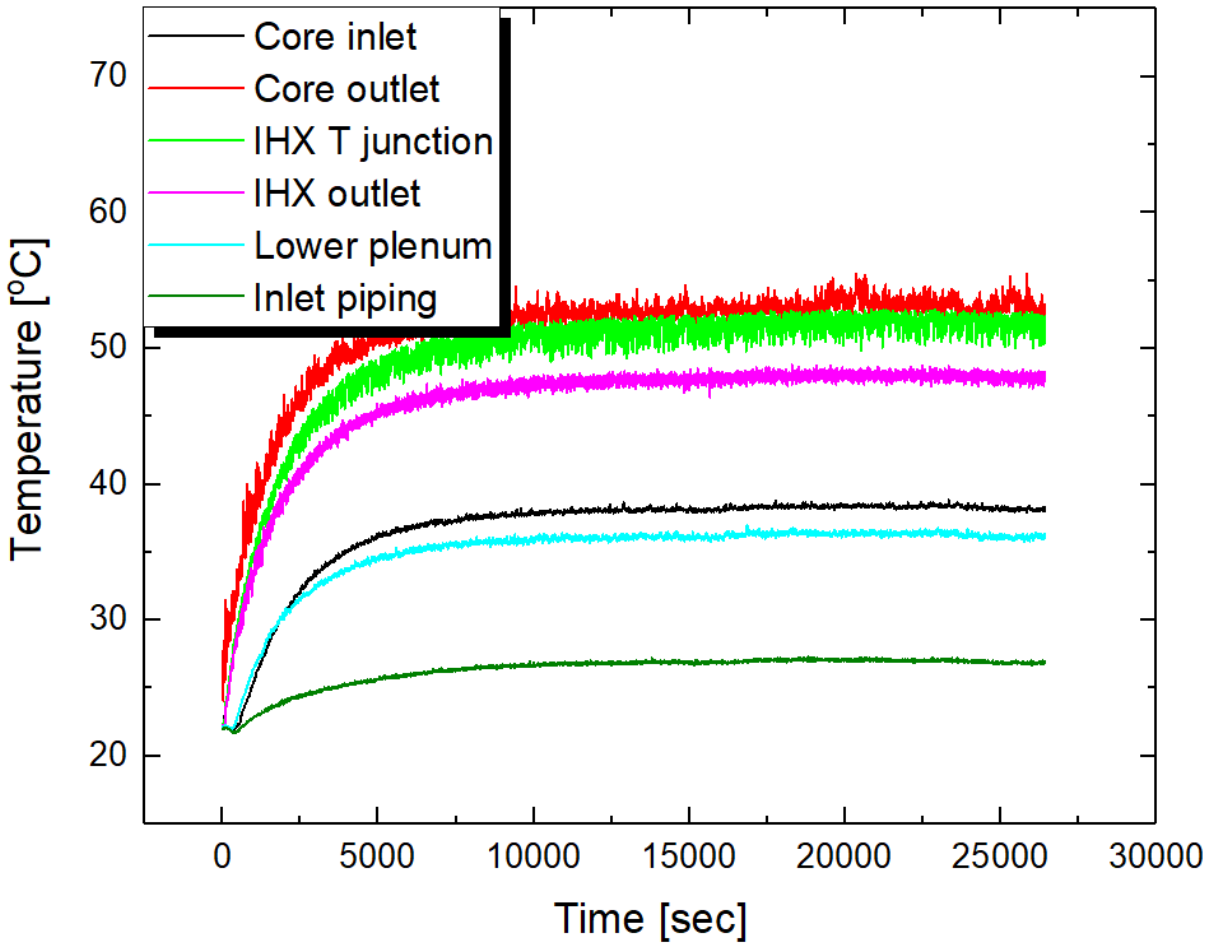

Figure 4-9. Temperature change along time in the SINCRO-2D experiment (1%, $60\Delta T_{ref}$ condition)

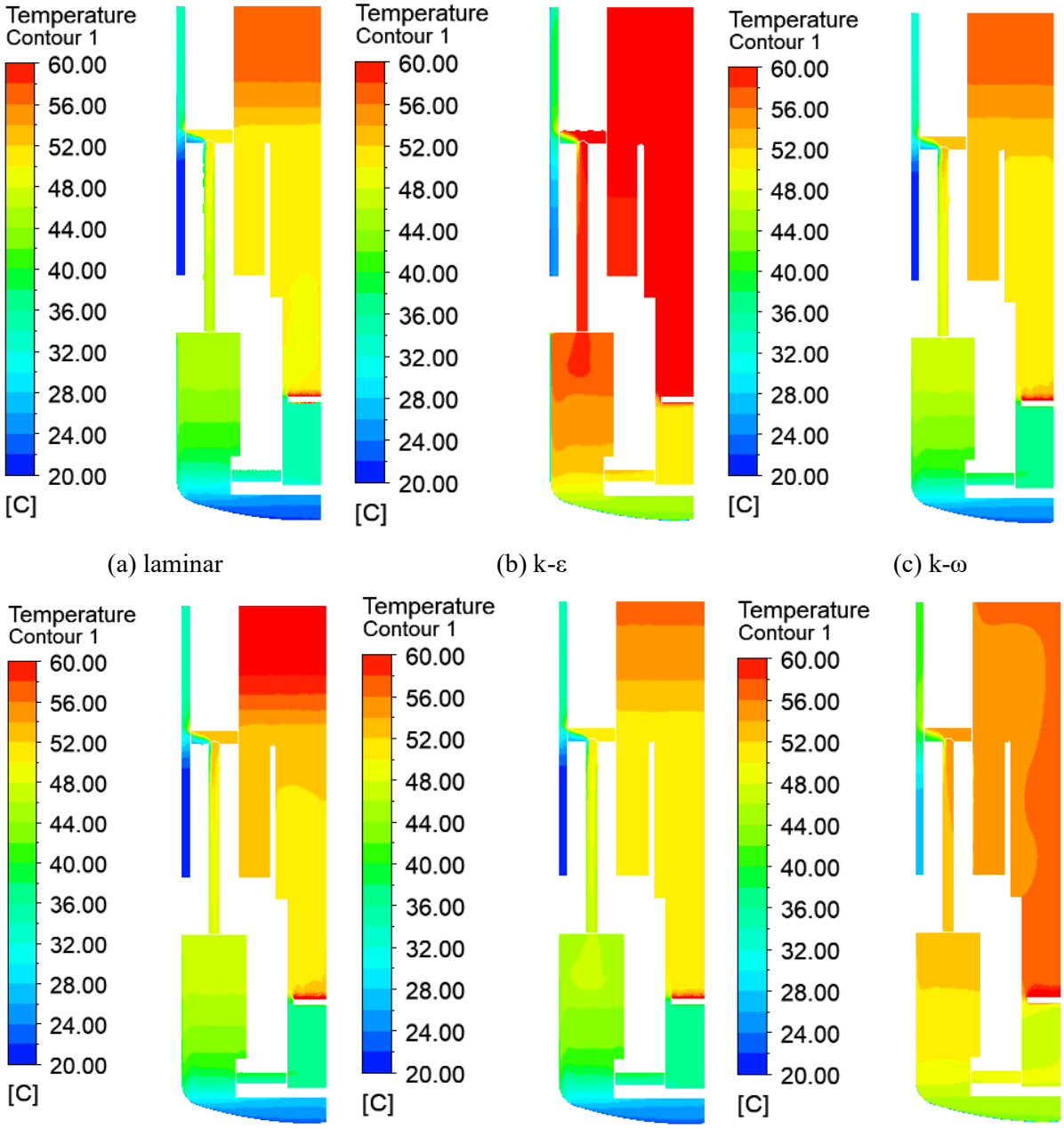

(a) laminar (b) k-ε (c) k-ω

(d) SST (e) Reynolds stress (f) Eddy viscosity transport

Figure 4-10. Temperature distribution of the SINCRO-2D by CFD with various turbulence model

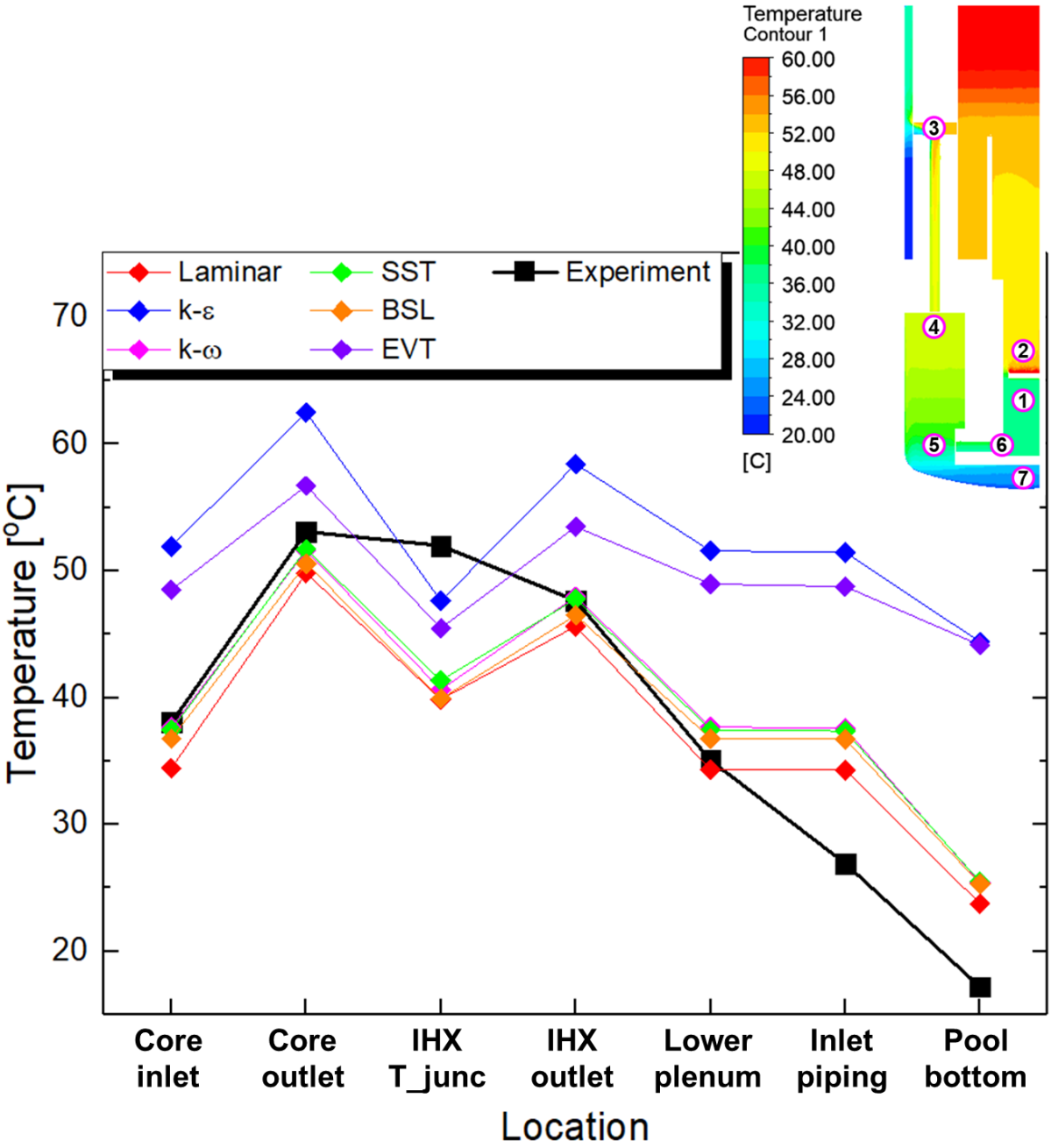

Figure 4-11. Temperature at the selected points in the SINCRO-2D by various methods

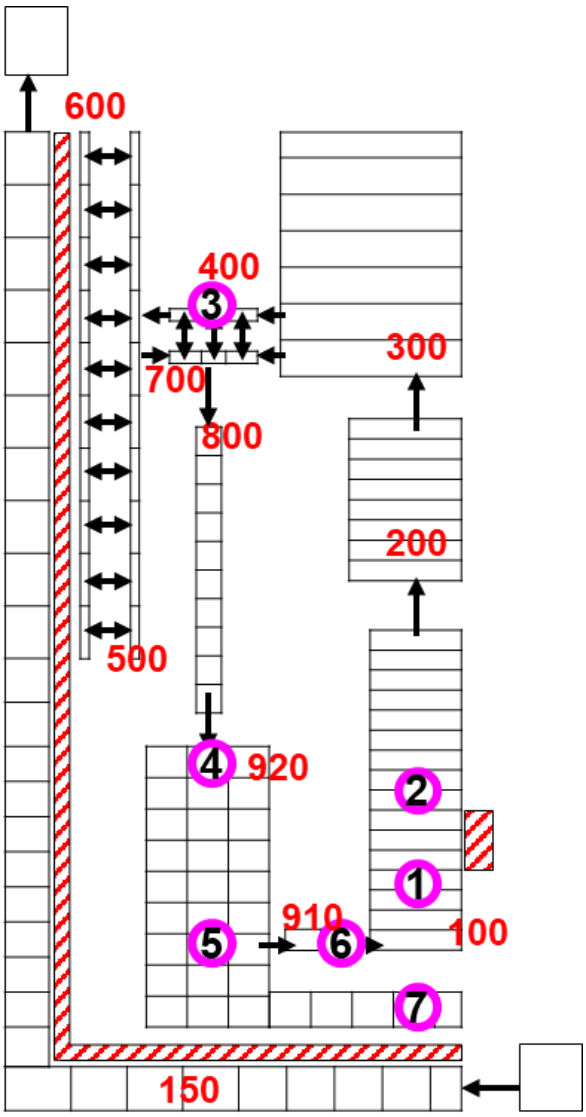

Figure 4-12. Nodalization of the SINCRO-2D in the MARS-KS code

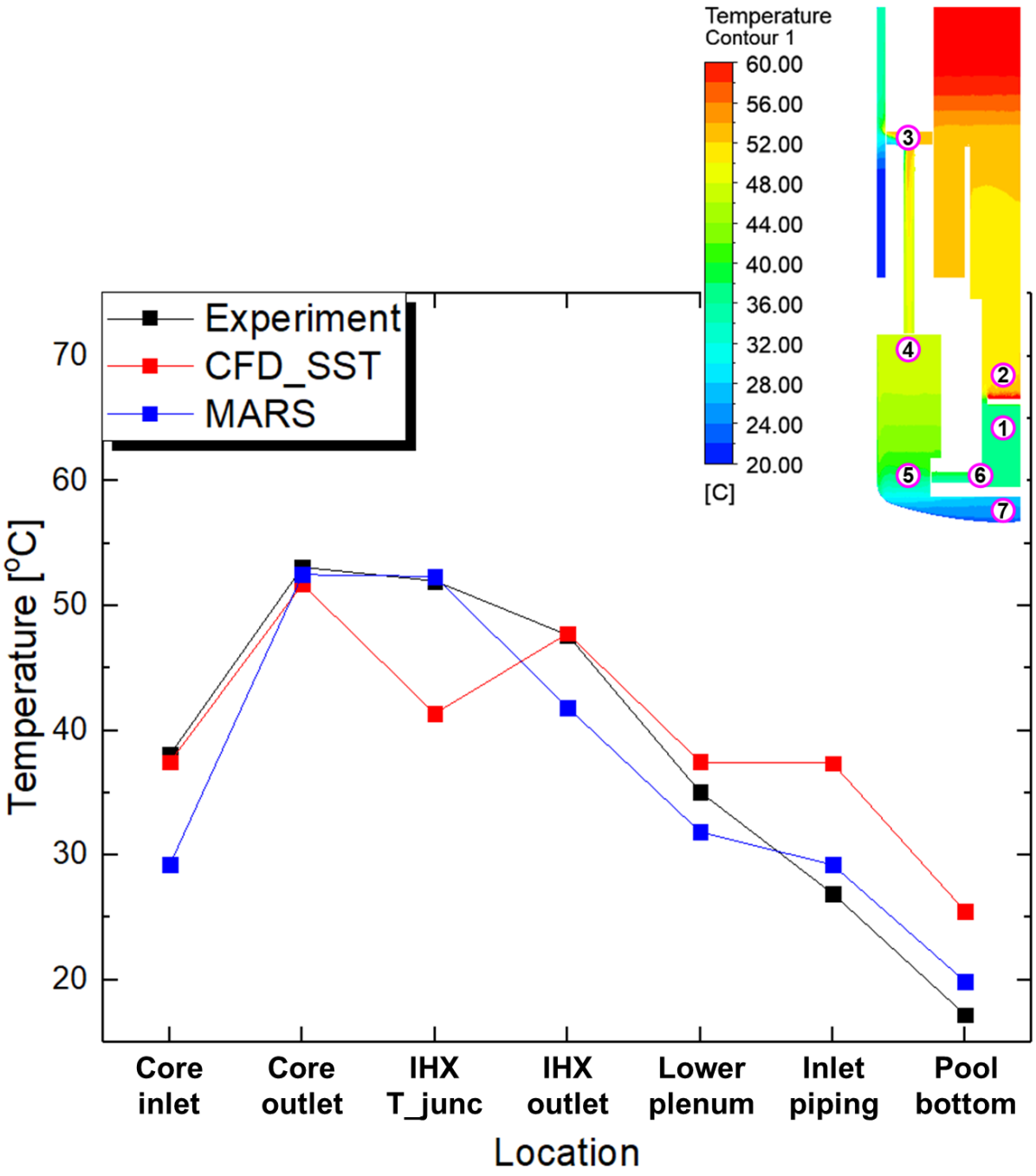

Figure 4-13. Temperature distribution in the SINCRO-2D by MARS-KS

Table 4-8. Summary of the results applying different turbulence model

Model	General characteristics	Discussions
Laminar	- Ignoring turbulence effect (less mixing, lower pressure drop)	- Lowest temperature was estimated - **Well predicted** the experiment → current experiment was mainly in the laminar region
k-ε	- Proper for free shear layer and small pressure gradient	- Overestimation of the turbulent viscosity at the near wall region → **overestimation** of the heat transfer in the confined flow
k-ω	- Considering wall effect to the k-e model and not considering cross diffusion (kind of production)	- **Well predicted** by considering wall effect → Wall dominant case, k-w is better than k-e model
SST	- Combination of the k-e and k-w by blending factor based on the distance from the wall	- **Well predicted** and similar to k-w → Current case had small hydraulic diameter so that k-w was dominant during calculation
Reynolds stress	- 2nd order closure - Good at phenomena related to second moment (heat transfer)	- Theoretically, it was the most complex and advanced one among the current model - Similar to the other **well predicting** models (laminar, k-w, SST)
Eddy viscosity transport	- Wall effect was considered as suppression of the production near wall, not more dissipation	- Eddy viscosity was overestimated near wall → **overestimation** of the heat transfer in the confined flow

4.3. Effect of decay heat

The maximum heat removal capacity of the RVACS is about 0.65 % of the total power of the PGSFR. Considering enhancement of the heat removal capacity, upper boundary of the test matrix was determined as 1.0% of the total power. The objective of the RVACS includes long term cooling, lower boundary of the test matrix was 0.2%, and the interval was 0.2%. It was summarized in the table 4-7. Boundary condition was fixed as 60 time of the reference temperature difference at each power level.

Figure 4-14 shows temperature distribution along various decay heat level. Legends of each contour in figure 4-14 were determined based on each case, thus, color distribution of each figure represents a relative temperature distribution. All phenomena observed in the base case (1.0 % condition) were commonly observed in the other cases. The overall thermal stratification was commonly observed in all cases in both main pool and narrow gap. The effect of natural circulation flow on the stratified temperature was observed. The cooling through the narrow gap was achieved by the natural circulation, considering temperature difference between the T junction of the IHX and the left point.

To more quantitatively analyze temperature distribution, temperature at some points were summarized in figure 4-15. Similar to figure 4-14, regard to the temperature distribution characteristics, there was no significant difference between different power levels. The graph showed lines with similar tendency and different magnitude. Certainly, the magnitude of the temperature showed the highest in the 1.0% power case. Because there was no significant change of the temperature distribution characteristics, a normalized temperature (θ) was introduced to observe change of the temperature distribution characteristics in more detail. The definition of the normalized temperature difference is in equation (4-16). It is the temperature difference between the boundary and an arbitrary point over the reference temperature. It was the same with equation (2-28). The difference between the SINCRO-V experiment is assumption related to the boundary temperature. It would be discussed in more detail in the following section.

$$\theta = \frac{T_{arbitrary} - T_{boundary}}{\Delta T_{ref}} \tag{4-17}$$

The trend of the θ along difference power level was summarized in figure 4-16. Similar to figure 4-15, there was no significant difference along the power level. Especially, the θ distribution under 0.6, 0.8 and 1.0 % of the total power showed almost the same values. With small power level like 0.2 and 0.4 %, the θ was slightly polarized compared to the other cases. In the low temperature regions like

the core inlet, lower plenum, and inlet piping, θ was lower in the lower power case. On the contrary, high temperature regions like the core outlet, IHX T junction, and IHX outlet, θ was higher in the lower power case. However, the polarization of the θ was not significant. In the aspect of the maximum θ, at the core outlet, θ of 0.2% is approximately 15 % higher than that of the 1.0 % condition, while the power level changes five times. Therefore, it was concluded as a mild polarization of the θ. The reason for the θ polarization could be increase of the pressure drop. The geometry of the SINCRO-2D was not changed, however, property change of water could affect the increase of the pressure drop. The water has higher viscosity in the lower temperature, and the overall temperature was lower in the low power case. Therefore, it could be inferred that the pressure drop was larger in the low power case due to higher viscosity, and consequently, temperature distribution was slightly polarized.

Based on the temperature data, the flow rate, cooling fraction of the narrow gap and lower plenum, and a new parameter, equivalent area was obtained. They were summarized in table 4-9. The flow rate and the cooling fractions were calculated by the same methods with that of the base case, using equation (4-13) and (4-15). Here, a new parameter, equivalent area was introduced to evaluate validity of the reference velocity for evaluating flow rate. Its concept and derivation were summarized in equation (4-17) and (4-18).

$$\dot{m} = \rho u_{ref} A_{eq} \tag{4-17}$$

$$\left(A_{eq}\right)_{1.0\%} = \left(\frac{\dot{m}}{\rho u_{ref}}\right)_{1.0\%} \tag{4-18}$$

As described in equation (4-17), the flow rate could be calculated by the density, velocity and area. Regard to these parameters, the density is material property, thus, it is clearly substitute by its value. For the velocity, the reference velocity is the parameter which could represent the overall magnitude of the velocity under natural circulation. Therefore, the velocity could be expressed as the reference velocity. However, there is no reference for the area. Because the reference velocity is not an actual value at the specific region of the facility, corresponding area could not be specified in the actual area in the facility. Therefore, the equivalent area was introduced. It is an area at the arbitrary region which has velocity as e reference velocity. If the reference velocity of the system really represents the overall magnitude of the system, the flow rate would be linearly proportional to the reference velocity, because the density and the area were already fixed. In this analysis, the value for an equivalent area was assumed as that of the 1.0 % of the decay heat condition. In addition, the equivalent area could be an index for evaluating total pressure drop of the natural circulating system. There is no term for

considering the pressure drop in the definition of the reference velocity, equation (2-8). Therefore, in the two systems having same design parameters, only except for the pressure drop, the flow rate would be smaller in the system having larger pressure drop. Consequently, the equivalent area of the larger pressure drop system is smaller than that of the smaller pressure drop system. It could be more intuitive index for natural circulation flow rate of the system.

As summarized in table 4-9, cooling fraction at the narrow gap and lower plenum did not showed significant change along the power level. Approximately 26.4 % of the heat was removed at the narrow gap in 0.2% of the total power condition, while it was 21.6 % in the 1.0 % condition. The change of the cooling fraction at the narrow gap was only 4.8 %, while power level increased 5 times. Correspondingly, the cooling fraction at the lower plenum showed the same tendency. From these results, it could be concluded that the cooling fraction of the narrow gap and lower plenum did not change significantly change within 0.2 % to 1.0 % of decay heat condition.

The flow rate was calculated based on equation (4-15), and the reference velocity was calculated by equation (2-8). The equivalent area was obtained from the result of the 1.0 % case. Then, by using the obtained equivalent area of 1.0 % condition, reference velocity of each condition, and density, the flowrate of each condition was predicted. It showed interesting results. As described in the chapter 3, the natural circulation flow rate could have similarity using Bo' based similarity law. It was indirectly validated from these results. The flow rate from the temperature distribution and predicted flow rate using the equivalent area of 1.0% condition showed good accordance. Error was negligible in 0.6, and 0.8 % case, less than 2 %, while 0.2 and 0.4 % showed 17.1 % and 7.1 % of the overprediction, respectively. The overestimation of the flow rate by using the equivalent area of 1.0 % suggests another evidence for the increase of the relative pressure drop in the low power case. Considering equation (4-17), the overprediction means that the equivalent area at that condition was overestimated. As mentioned before, equivalent area of the larger pressure drop is smaller than that of the smaller pressure drop system. Therefore, the fact that smaller equivalent area was required for better prediction represents that the pressure drop was larger than the reference system.

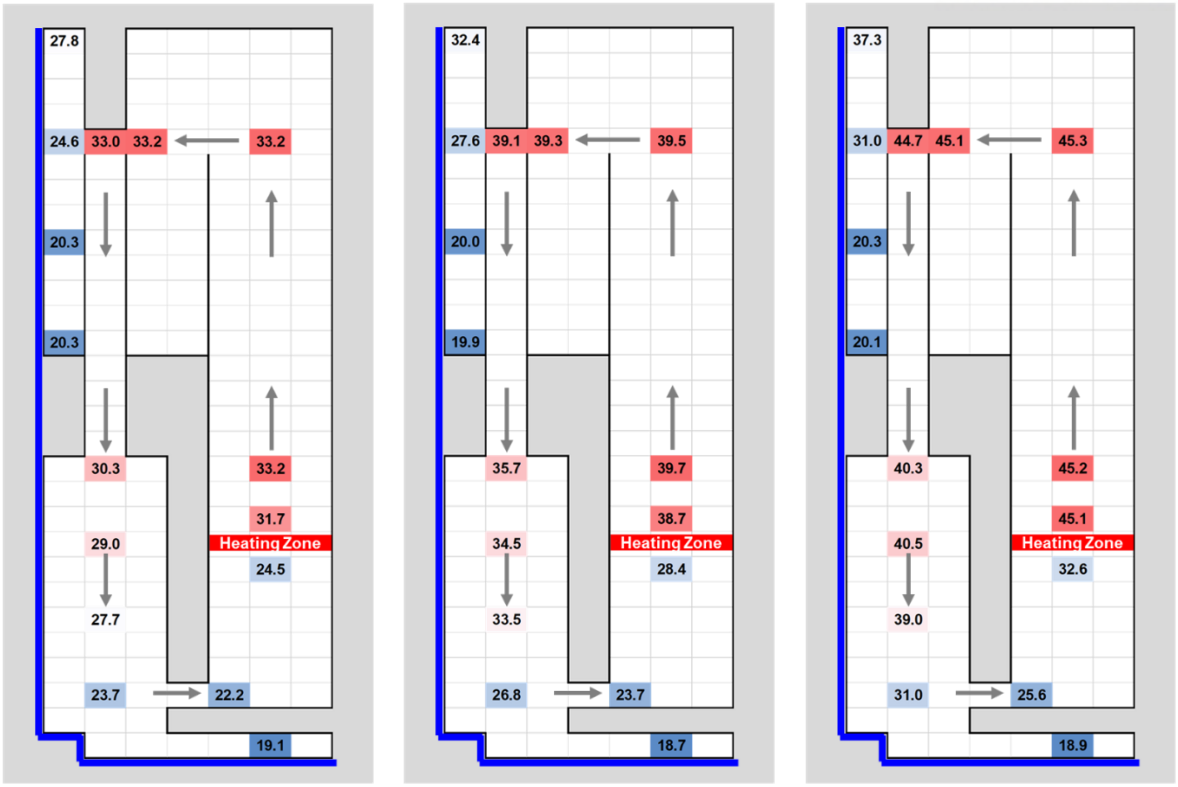

(a) 0.2 % (b) 0.4 % (c) 0.6 %

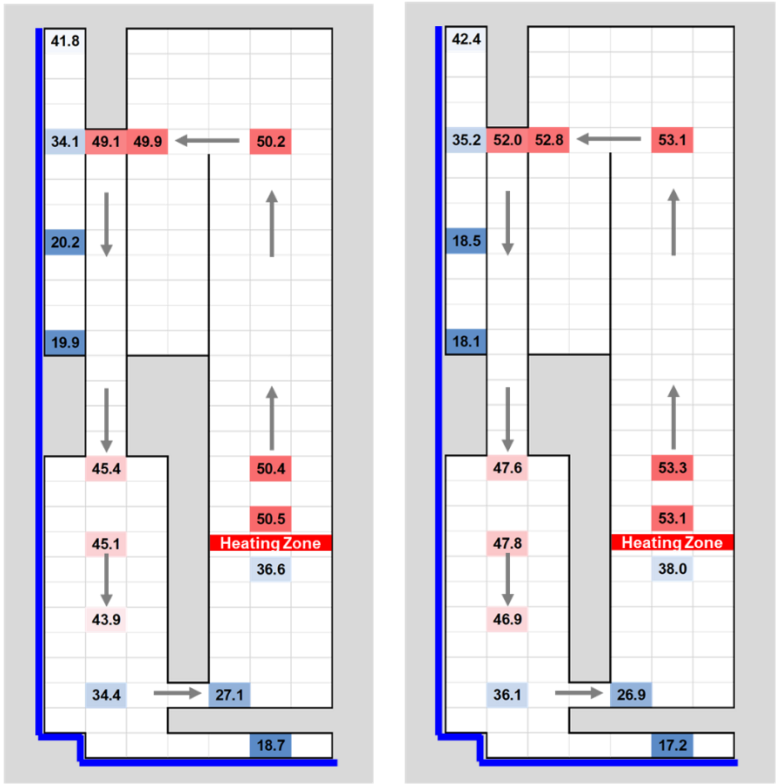

(d) 0.8 % (e) 1.0 %

Figure 4-14. Effect of the decay heat on the temperature distribution of the SINCRO-2D

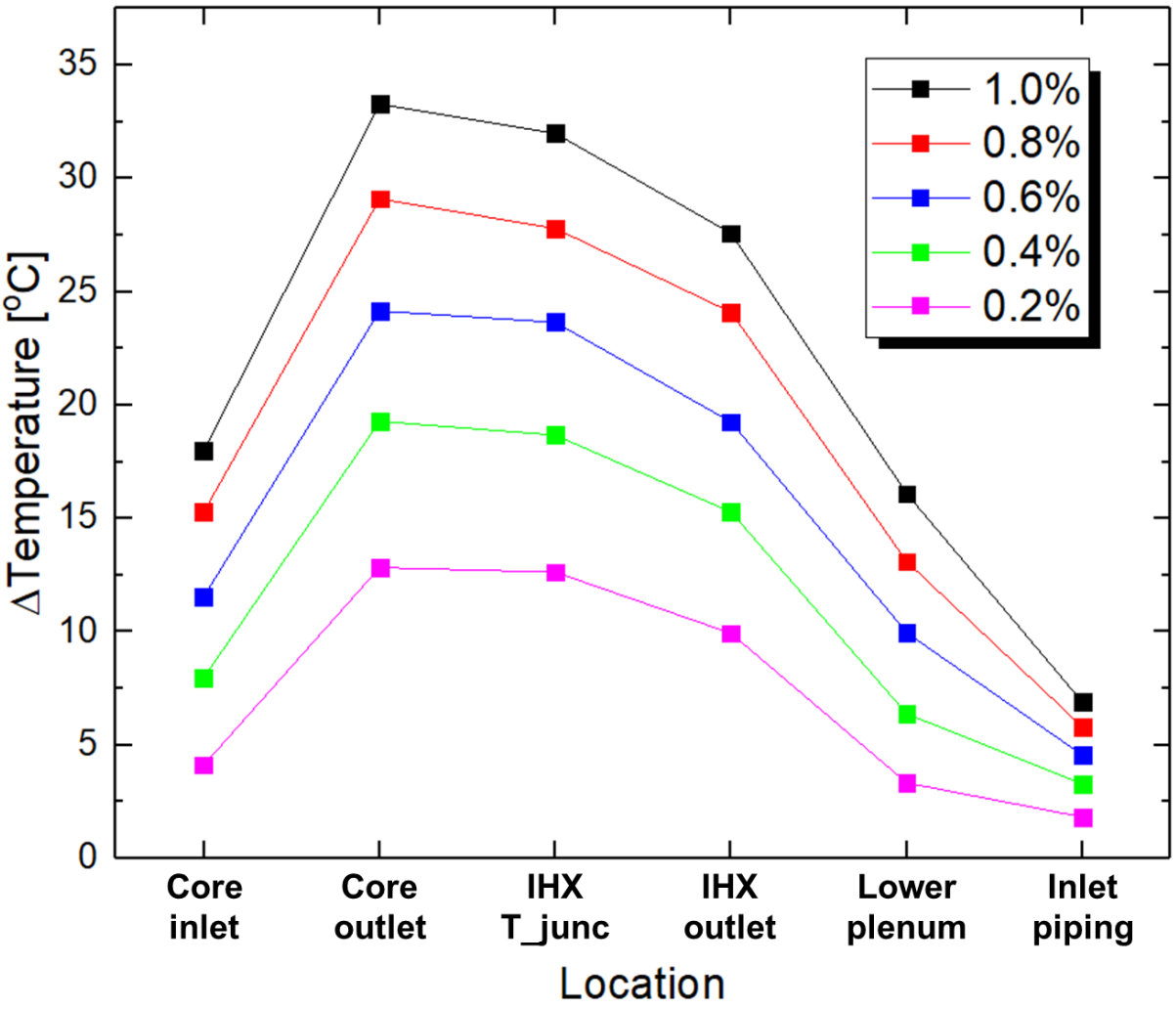

Figure 4-15. Temperature distribution of the SINCRO-V with different power level

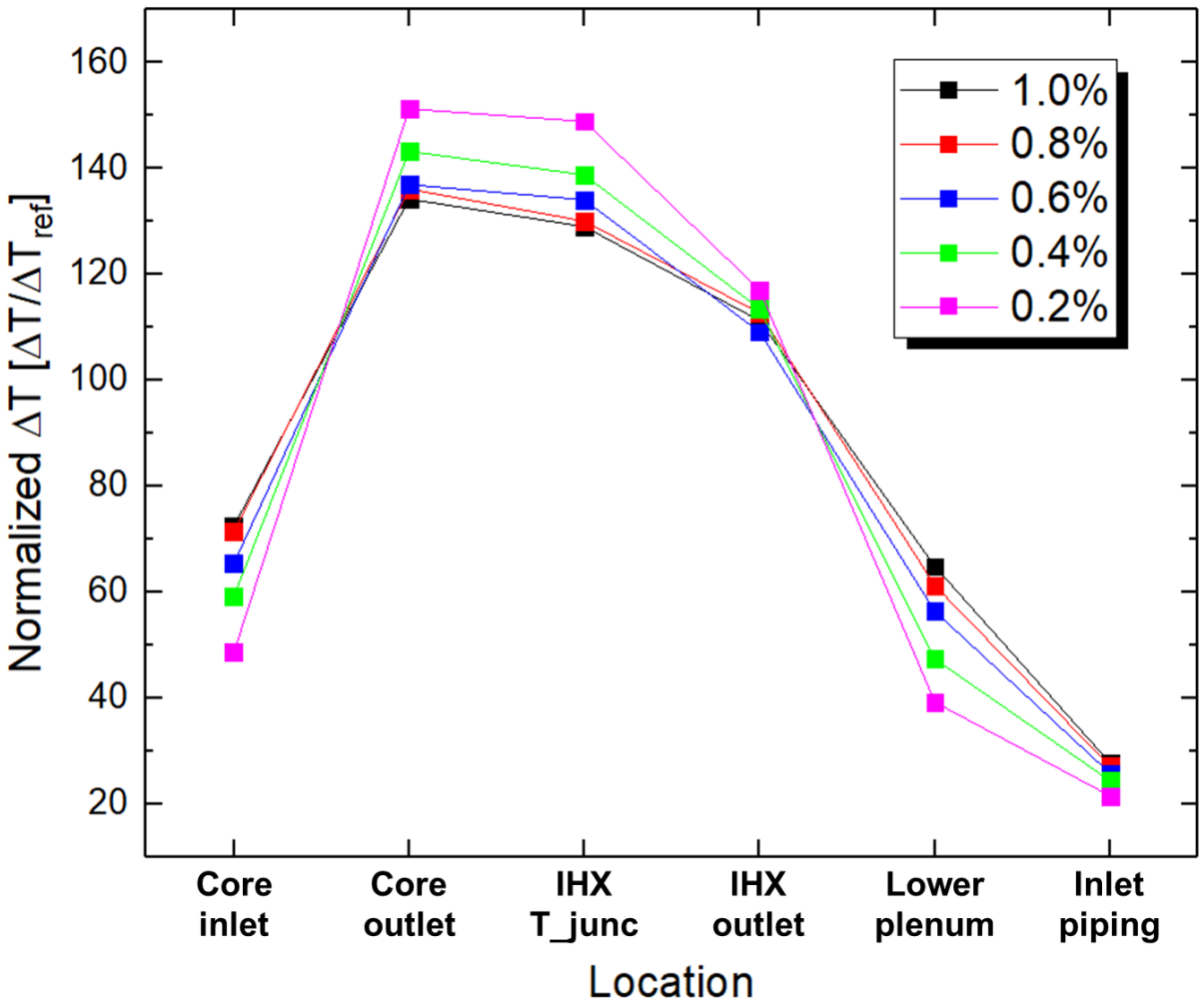

Figure 4-16. Normalized temperature distribution of the SINCRO-V with different power level

Table 4-9. Summary of the effect of decay heat in the SINCRO-2D experiment

	0.2 %	**0.4 %**	**0.6 %**	**0.8 %**	**1.0 % (base case)**
T_{max}	33.2℃	39.7℃	45.2℃	50.4℃	53.3℃
$T_{IHXoutlet}$	30.3℃	35.7℃	40.3℃	45.4℃	47.6℃
T_{min}	22.2℃	23.7℃	25.6℃	27.1℃	26.9℃
Cooling at narrow gap	**26.4 %**	**25.0 %**	**25.0 %**	**21.5 %**	**21.6 %**
Cooling at lower plenum	**73.6 %**	**75.0 %**	**75.0 %**	**78.5 %**	**78.4 %**
Flow rate by temperature	**0.87 g/s**	**1.20 g/s**	**1.46 g/s**	**1.64 g/s**	**1.81 g/s**
u_{ref}	**5.31 mm/s**	**6.68 mm/s**	**7.65 mm/s**	**8.42 mm/s**	**9.45 mm/s**
A_{eq}	-	-	-	-	**192.7 mm^2**
Flow rate by prediction	**1.02 g/s**	**1.28 g/s**	**1.47 g/s**	**1.61 g/s**	-
Error	**+17.1 %**	**+7.1 %**	**+0.2 %**	**-1.7 %**	-

4.4. Effect of boundary condition

The effect of boundary condition, in other words, temperature distribution on the cooling boundary, was analyzed with the same power condition as 1.0% of total power. Change of the temperature distribution was summarized in figure 4-17, as a graph. Because the power level was same as 1.0 %, the overall magnitude of the temperature was similar in all cases. In short, regardless to the cooling boundary condition, the characteristics of the temperature distribution did not change. There was only one thing changed; the line of the graph was shifted vertically. With a larger temperature gradient, overall temperature was upwardly shifted. Only offset without change of the distribution means that the heat transfer characteristics, cooling fraction of each part, and flow rate did not change. Therefore, no change in the temperature distribution characteristics could be enlarged to no change in the overall natural circulation characteristics, and effect of the boundary temperature distribution could be simplified as a global offset of the temperature inside of the pool.

$$T_{coolant} = T_{Rv,ref} + \Delta T_{decay\ heat} + \Delta T_{B.C.} \quad (4\text{-}19)$$

$$T_{coolant} - T_{Rv,ref} - \Delta T_{B.C.} = \Delta T_{decay\ heat} \quad (4\text{-}20)$$

The temperature of the coolant could be expressed like equation (4-19). Here, to apply effect of boundary condition as a global offset, the reference RV temperature, which is $T_{RV,ref}$ in equation (4-19), should be maintained without change as the boundary condition changes. By doing so, the effect of boundary condition is solely expressed as a term $\Delta T_{B.C.}$. The coolant temperature change by the boundary condition, and the effect of the boundary condition were varied along the boundary condition, while the effect of decay heat and RV reference temperature remained the same. To find proper reference of RV temperature with consideration of boundary condition effect, a relationship among the aforementioned terms could be expressed like (4-20), whose right-hand side is constant. To find proper RV temperature with consideration of the boundary effect, candidates for the term ($T_{RV,ref}$ + $\Delta T_{B.C.}$) were summarized in table 4-10. The temperature of the coolant was designated as the maximum temperature of the coolant. First, the maximum temperature of the cooling wall, which corresponds to the RV, was considered as reference RV temperature including the boundary effect. However, the result in the table showed change of the calculation results with different boundary condition. It means that the effect of the boundary condition was not properly expressed as one term solely, and the reference RV temperature was not assumed properly. The situation became better in the average RV temperature case. The variance of the calculation results reduced from the reduced, however, it did not show satisfying accordance. In case of the minimum temperature of the RV, the trend was reversed; the calculation results increased as the boundary temperature difference increases.

Therefore, it could be inferred that the proper value of the term ($T_{RV,ref} + \Delta T_{B.C.}$) existed between the average and minimum temperature of the RV. The minimum temperature was more relative to the boundary temperature of the lower plenum, than that of the narrow gap. Similarly, the maximum temperature was more related to the boundary temperature of the narrow gap. To obtain the proper boundary temperature, it is important to reflect boundary temperature with their influence, in other words, cooling contribution. Therefore, the author took the value between the maximum and minimum temperature as ($0.2\ T_{RVmax} + 0.8\ T_{RVmin}$), by considering cooling fraction of the near components. The maximum temperature was related to the cooling by the narrow gap, and the minimum temperature was related to the cooling by the lower plenum. Their cooling fraction was approximately 20% and 80%, respectively. Therefore, the author suggests that kind of interpolation between the maximum and minimum, and it showed almost same results, which represents that effect of the boundary condition was nicely reflected into the term.

This boundary temperature was used as a boundary temperature in equation (4-17) during calculation of the normalized temperature difference. The validity of assumption that ($T_{RV,ref} + \Delta T_{B.C.}$) is ($0.2\ T_{RVmax} + 0.8\ T_{RVmin}$), was indirectly confirmed in figure 4-16. Due to the properly assumed boundary temperature, normalized temperature could have small vertical offset even with different power level.

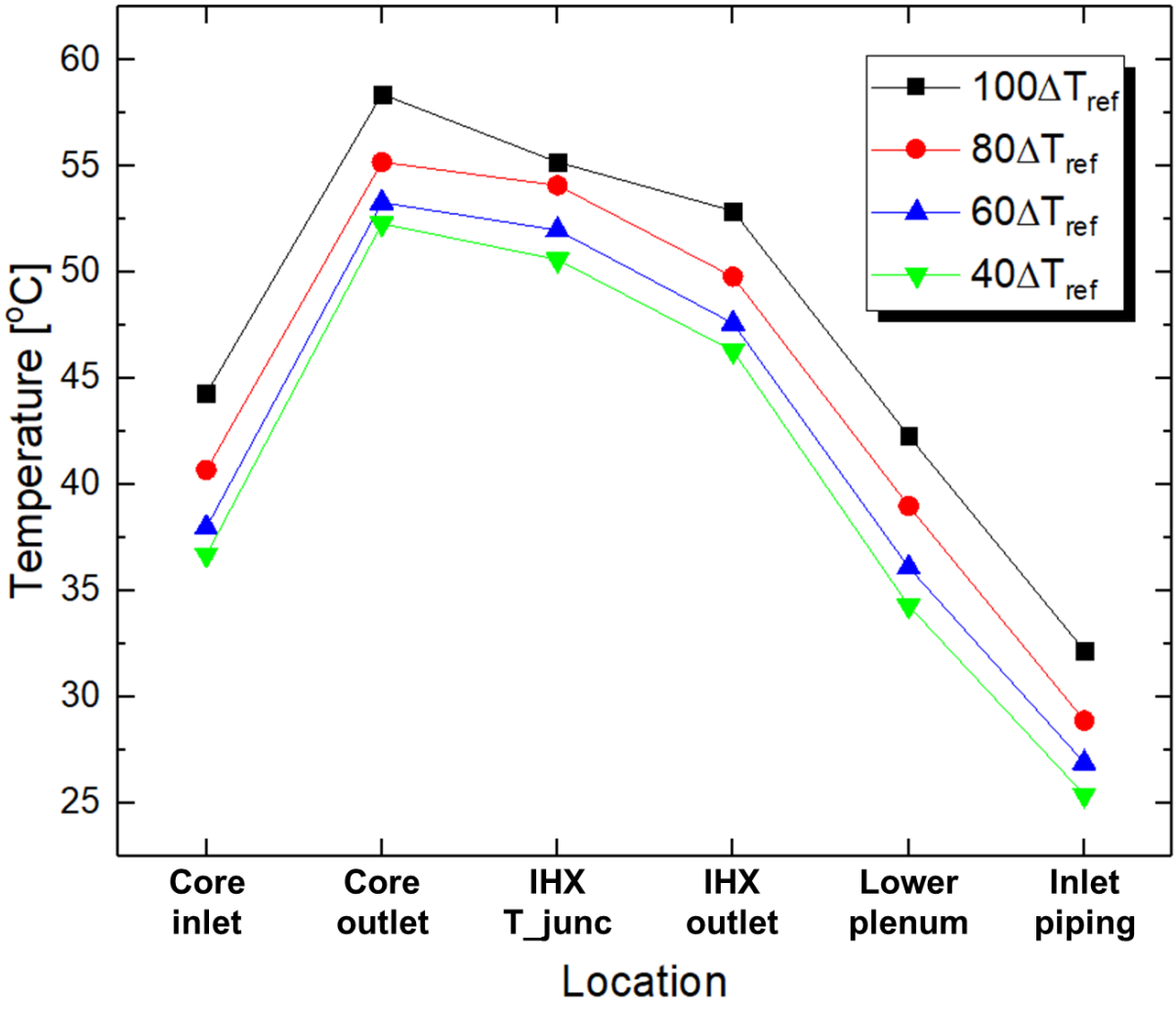

Figure 4-17. Temperature distribution of the SINCRO-V with different boundary condition

Table 4-10. Candidates of ($T_{RV,ref}$ + $\Delta T_{B.C.}$) and its results

Case	$\mathbf{T_{max} - T_{RVmax}}$	$\mathbf{T_{max} - T_{RVavg}}$	$\mathbf{T_{max} - T_{RVmin}}$	$\mathbf{T_{max} - T_{RVref}}$ ($\mathbf{0.2\ T_{RVmax} + 0.8\ T_{RVmin}}$)
$40\Delta T_{ref}$	26.23℃	31.22℃	36.20℃	**34.21**℃
$60\Delta T_{ref}$	22.15℃	29.60℃	37.05℃	**34.07**℃
$80\Delta T_{ref}$	18.49℃	28.43℃	38.36℃	**34.39**℃
$100\Delta T_{ref}$	14.81℃	27.22℃	39.62℃	**34.66**℃

4.5. Summary and conclusion

To observe the natural circulation phenomena under the RVACS operation, the SINCRO-2D experimental facility was designed based on the PGSFR, using the water as a simulant of the sodium, having 1 : 25 of the scaling reduction. 1.0% of total power and 60 times of the reference temperature case was selected as a base case, and various phenomena were observed: the overall thermal stratification, effect of the natural circulation flow on the stratified temperature, cooling fraction, and dominant heat transfer mechanism – natural circulation.

And the experimental result of the base case was compared to the numerical results obtained by ANSYS-CFX, and MARS-KS. The commercial CFD code showed good accordance with the experimental result, and it was concluded that dissipation and suppression of the turbulent viscosity is the key for proper turbulence model for natural circulation heat transfer. Thus, k-ω, SST, and Reynolds stress model were revealed as proper models. Among these models, SST model was the best considering the computation cost and time. The MARS-KS result showed good accordance for the region like the core outlet, and inlet pipe, where could be easily and properly simplified as 1-D. However, it showed bad accordance for the region like lower plenum and T junction of the IHX, where has complex 3-D phenomena like mixing, because it was the 1-D system code.

Effect of the decay heat and cooling boundary temperature distribution was experimentally studied. Regard to the decay heat, it did not have influence on the characteristics of the temperature distribution, while the magnitude of the temperature was changed. Consequent parameters like flow rate and cooling fraction showed negligible change with change of the decay heat. It was indirectly confirmed that the flow rate of the system could be simulated by the Bo' based similarity law, by predicting flow rate of the other condition with the equivalent area of 1.0 % case. The boundary temperature distribution also did not show significant change of the temperature distribution, only global upward and downward shift of the temperature was observed. Therefore, the boundary condition effect could be simplified as one term as form of the ($T_{RV,ref} + \Delta T_{B.C.}$), the RV reference temperature plus the effect of the boundary condition. The proper term for the RV reference temperature including boundary condition effect was ($0.2\ T_{RVmax} + 0.8\ T_{RVmin}$), which was determined based on the cooling fraction of the relevant temperature.

5. Conclusion and recommendation

5.1. Overall summary and conclusion

The RVACS is the important decay heat removal system having different natural circulation characteristics with the DHX, which has been commonly researched. To analyze natural circulation phenomena under RVACS operation, the experimental study was conducted using simulant.

The similarity law was focused on the reproduction of the temperature field under natural circulation, and modified Boussinesq number (Bo') was the key parameter for the similarity, which represents the ratio of natural circulation heat transfer to conductive heat transfer.

Regard to the similarity issue, the Bo' based similarity was experimentally validated through SINCRO-V experiment. Wood's metal and water was selected as representative fluids for the liquid metal and non-metallic fluid. The result showed that the water experiment could predict Wood's metal temperature with reasonable error, approximately 16.4% of the overprediction in the 1.0% of the decay heat level.

Based on the similarity law, SINCRO-2D was designed to observe the natural circulation phenomena under the RVACS operation, whose based on the PGSFR with 1 : 25 of the scaling reduction. Following phenomena were revealed as characteristics of the natural circulation under RVACS: the stratified temperature, cooling fraction, and natural circulation dominated heat transfer. Numerical analysis was conducted compared to the base case in the experiment. The commercial CFD code showed good accordance with the experimental result, and the SST model revealed as the best turbulence model for this case. MARS-KS results showed good accordance in the region where could easily and properly simplified as 1-D, however, it showed bad accordance for the region with 3-D phenomena like mixing and pool thermal hydraulics. Regard to both decay heat and boundary temperature distribution, both parameters did not have a great influence on the temperature distribution characteristics under natural circulation. For the decay heat level, only the magnitude of the temperature distribution was changed, while global offset of the temperature was observed for the boundary condition change.

As shown in figure 1-3, this research could be utilized in the validation of the code for the performance evaluation of the RVACS, which is necessary for the safety analysis of PGSFR. The result of the system code could be validated to the data of the sodium system, which was interpreted by the data from the water experiment, especially for the steady state. And the experimental validation of the natural circulation similarity law could be adopted in the design of the other experimental facility for simulating natural circulation. Currently, various research related to the natural circulation

of the LFR are under progress. I hope this experimental validation could give a confidence and criteria to their facility design.

Regard to the contribution of the present study, effect of the cooling boundary condition was one of the most unique point in the study. The fact that distribution of the temperature of the cooling wall could be simplified as global temperature increase of the natural circulation pool, could provide experimental basis for the simplified consideration of the effect of the boundary condition for safety analysis. Most important contribution is validation of the similarity law. Based on this validation, other natural circulation experiments could be designed using simulant.

5.2. Recommendation

Regard to present research scope in figure 1-3, there are some parts required to be researched further. For the minor incompletion, research related to the flow rate was based on the calculation results, not by direct measurement of the flow rate. Although the validity of the calculation method was indirectly confirmed, a strict validation was required. Three-dimensional parameters could not be discussed in the research because SINCRO-2D was limited as two-dimensional slab model. For the major incompletion, although theoretical base was discussed in chapter 2, research related to transient phenomena were not conducted in the present research due to initial condition. However, corresponding validation on the experiment could give some quantitative discussions about transient similarity. It was discussed in the appendix, part C. Because of difficulties for making identical initial conditions between the prototype and water model, it was not strictly discussed especially for the initial transient. Regard to the transient analysis tool, system code, it is required to adopt proper model for conduction between fluid elements.

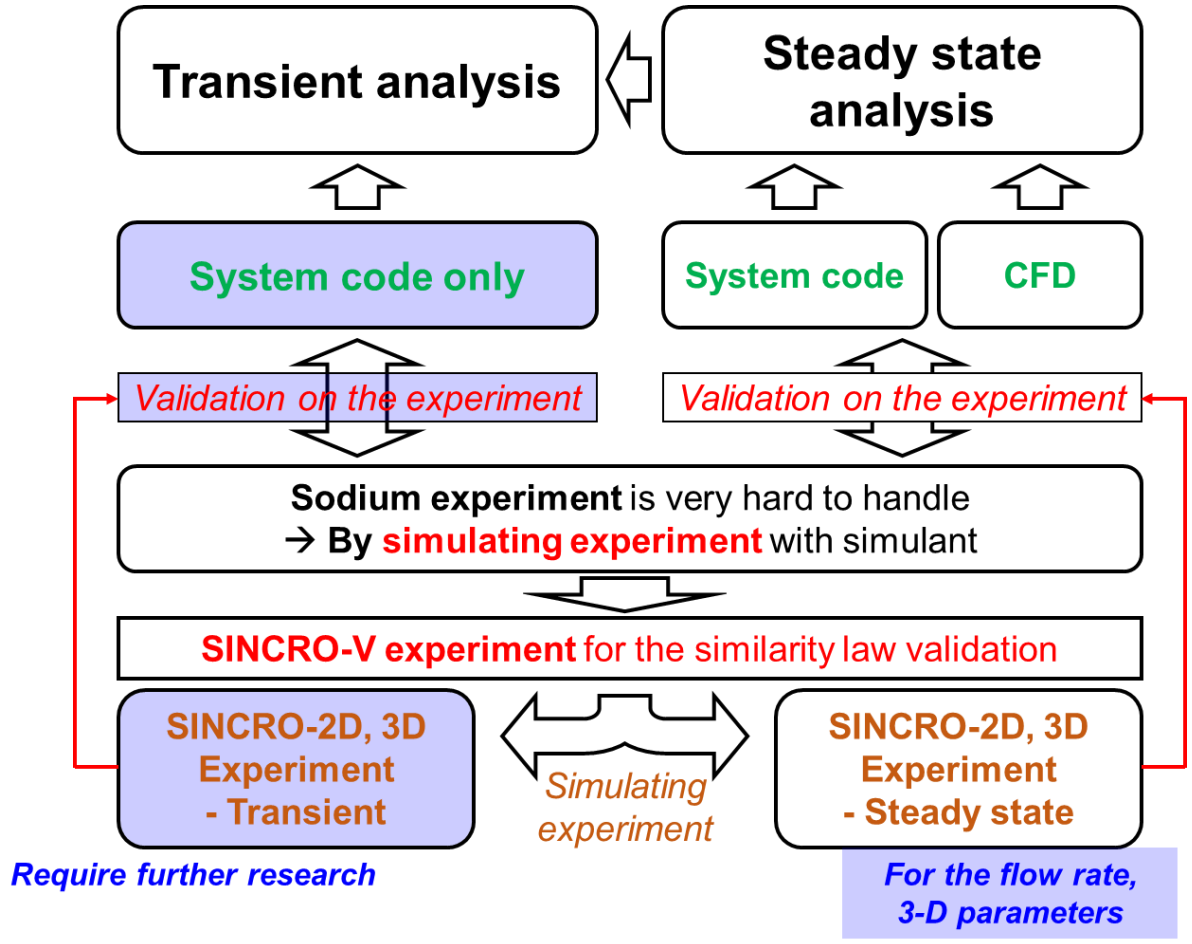

Figure 5-1. Summary of the research scope of the present study and further research area

Appendix

A. Uncertainty analysis of the experimental facility

For the present study, three parameters were used to analyze natural circulation: the power, flow rate, and temperature. The power was controlled by the voltage, and the voltage uncertainty was 3.00%. The uncertainty of heater resistance was 0.14%; thus, total uncertainty in the power was 6.00%. Uncertainty of the heater resistance was 0.14 %, thus, total uncertainty in the power. The flow rate is the flow rate of the coolant, which was used in the heat balance calculation. Uncertainties of the flowmeter, interface, and (analog to digital) AD conversion were 0.30 L/min, 0.04%, and 0.02%, respectively. The total uncertainty of the flow rate was 0.30 L/min. For the temperature, the uncertainty factors were the thermocouple, compensation wire, room temperature, interface, and AD conversion with values 0.40%, 1.50 K, 0.50 K, 0.04%, and 0.02%, respectively. The total uncertainty of the temperature was 1.88–2.63 K. Because the temperature uncertainty contributors include a term related to the reading value, the uncertainty of the temperature was small in the low temperature range in the experiment, which was approximately 20°C. These results were common for the SINCRO-V water, Wood's metal, and SINCRO-2D facility.

Table A-1. Summary of uncertainty analysis

Category	Contributor	Magnitude
Power	Voltage	3.00 %
	Resistance	0.14 %
	Total	**6.00 %**
Flowrate	Flowmeter	0.30 L/min
	I/O interface	0.04 %
	AD conversion	0.02 %
	Total	**0.30 L/min**
Temperature	Thermocouple	0.40 %
	Compensation wire	1.50 K
	Room temperature	0.50 K
	I/O interface	0.04 %
	AD conversion	0.02 %
	Total	**1.88 – 2.63 K**

B. Heat balance test

The SINCRO-V Wood's metal facility had the highest temperature among the facility and easy to lose its heat to the environment. Originally, the heat was intended to be removed only from the cooling surface, which was cooled by boiling heat transfer. It is well known that heat transfer performance under boiling is proportional to the cube of the superheat. In other words, the thermal resistance of the cooling wall significantly decreased as the system temperature increased. The thermal resistance of natural circulation decreased as the temperature difference increased, although the magnitude of decrease is much smaller than that of boiling. Considering the heat transfer characteristics of each surface, the amount of heat loss in the Wood's metal facility was smaller than in the high-power operation; however, the heat loss fraction was smaller during high-power operation. Heat loss was calculated by measuring the time it takes to consume 1 L of water for cooling. Originally, the facility had insulators with uniform thickness on all surfaces. However, insulation performance was poor; hence, insulators were added to the upper part of the facility. After the insulation was increased by more than 90%, as shown in figure B-1, the SINCRO-V experiments were conducted under this condition.

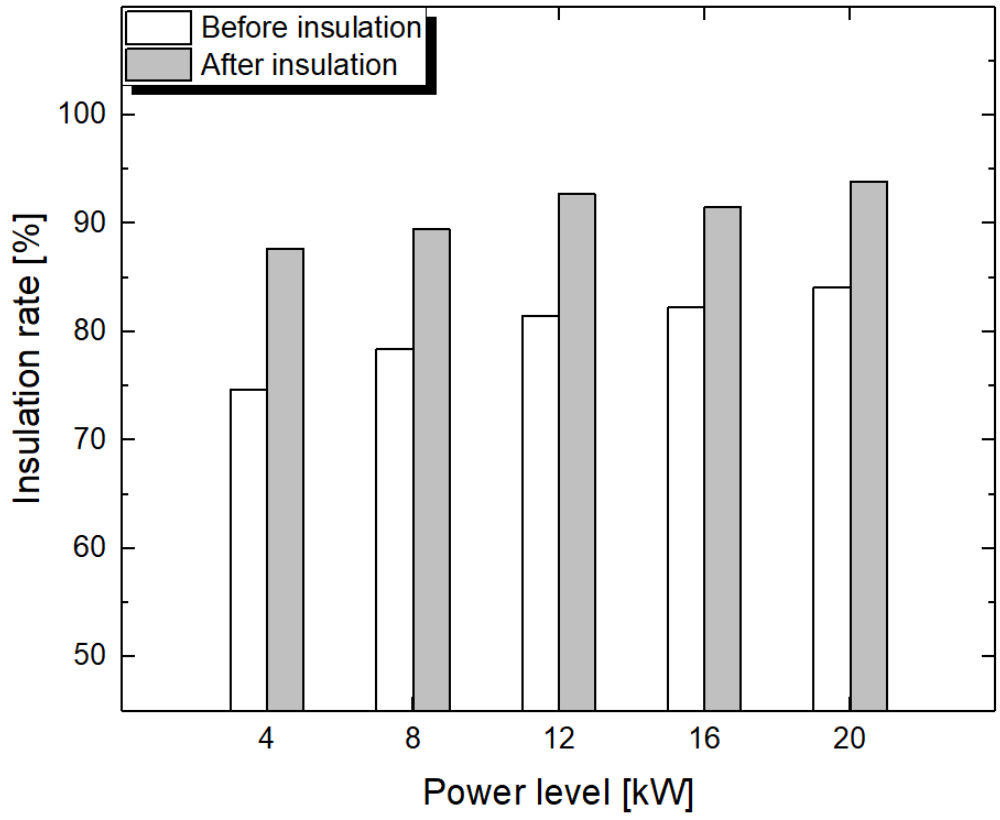

Figure B-1. Insulation rate of the Wood's meatal facility before and after insulation

For the water facilities, it was cooled by the external water-cooling jacket. Therefore, the heat loss in the water facility was calculated by the flow rate and temperature increment of the coolant at the water jacket, like equation (B-1). To minimize uncertainty in the insulation rate and to evaluate the insulation rate conservatively, the maximum power case was selected as a reference case for calculation of the heat loss. It corresponds to 100 W in the SINCRO-V water facility, and 200 W in the SINCRO-2D facility. The result was summarized in table B-1 and B-2. Both facilities showed nice insulation rate.

$$q_{total} = \dot{m} c_p \Delta T_{coolant\,in,out} \qquad \text{(B-1)}$$

Table B-1. Result of the insulation test of the SINCRO-V water

Test	Insulation rate
1	90.3 %
2	85.1 %
3	88.4 %
4	93.7 %
5	94.2 %
Average	**90.3 %**

Table B-2. Result of the insulation test of the SINCRO-2D

Test	Insulation rate
1	96.9 %
2	96.6 %
3	98.7 %
4	101.9 %
5	93.1 %
Average	**97.4 %**

C. Transient similarity

Experimental data were already gathered with time data. In addition to the steady state similarity analysis, transient analysis has been conducted with base case in the SINCRO-V experiment. In fact, there were some weak point for strict and quantitative analysis. First, transient data were obtained with imperfect insulation condition. Figure C-1 shows temperature difference between before and after insulation. The two uppermost points represent temperature of the air between the Wood's metal and the pool cover. Before insulation, two points showed 149°C and 210°C respectively, while showed 194°C and 252°C, after insulation. After insulation, temperature of the air was greatly increased by insulation of the top of the facility, approximately 45°C. However, temperature of the pool was not changed greatly. The maximum temperature was increased to 297°C from 289°C, less than 10°C of the difference. Regard to the minimum temperature, it showed about 3°C of the temperature difference between before and after the insulation. Overall, tendency of the temperature distribution was quite similar. Therefore, data before insulation were used for the transient analysis.

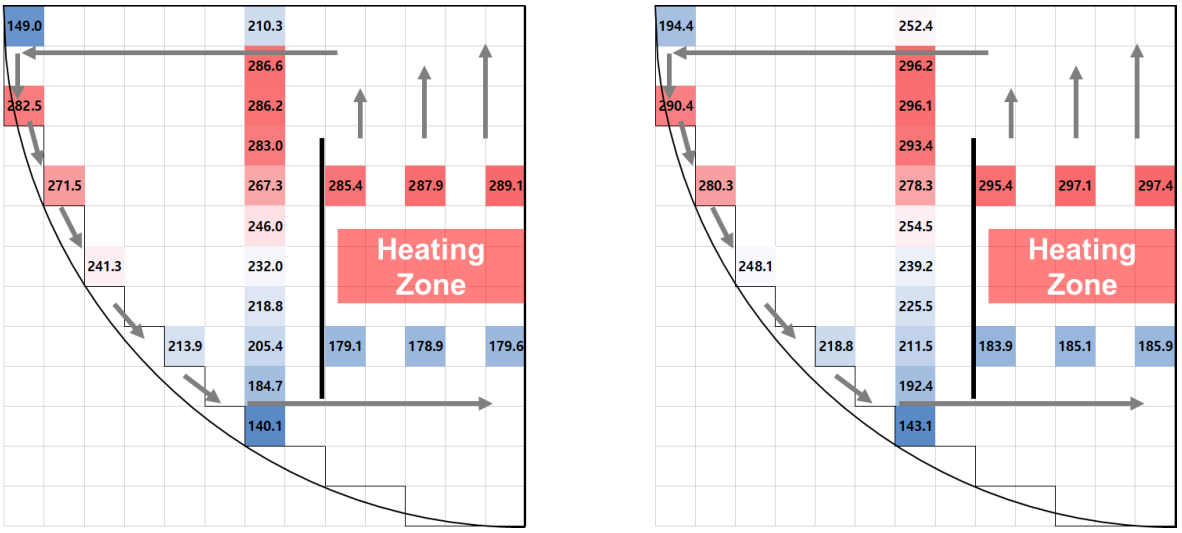

(a) before insulation (b) after insulation

Figure C-1. Temperature comparison before and after insulation

Second one is related to the initial state of the pair of SINCRO-V facilities. For the Wood's metal facility, temperature range of the pool was from 72°C to the 88°C at the beginning, with mild temperature stratification. Regard to the water facility, temperature of the water pool was almost uniform, from 18.4°C to 18.8°C. Although there was 16°C of the temperature difference in Wood's metal facility, it could be tolerable compared to the order of the temperature increase during transient. However, difference of the temperature increment between the initial state and final state was not matched before experiment. Regard to the maximum temperature, approximately 200°C was increased

in the Wood's metal facility while approximately 30°C was increased in the water facility. Because reference temperatures of the two systems were about 8.55 times difference, temperature increment of the water facility during transient was approximately 28 % greater.

$$t_{ref} = \left(\frac{\rho c L^4}{\beta g} \right)^{1/3} Q^{-1/3} \tag{2-9}$$

$$\Delta T_{original} = \frac{\Delta T_{reference,original}}{\Delta T_{reference,model}} \times \Delta T_{model} \tag{2-31}$$

$$t_{original} = \frac{t_{reference,original}}{t_{reference,model}} \times t_{model} \tag{C-1}$$

Last, error already existed in the steady state analysis. In case of present case (1.0% decay heat), 15% was overestimated for the maximum temperature and 18% was underestimated for the minimum temperature. These errors should be into consideration in the transient analysis.

Time scale was interpreted using reference timescale, equation (2-9) in the manuscript. Similar to equation (2-31), which is related to the temperature, time was translated like equation (C-1). Approximately 2.7 seconds in the water facility corresponded to the 10 seconds in the Wood's metal facility.

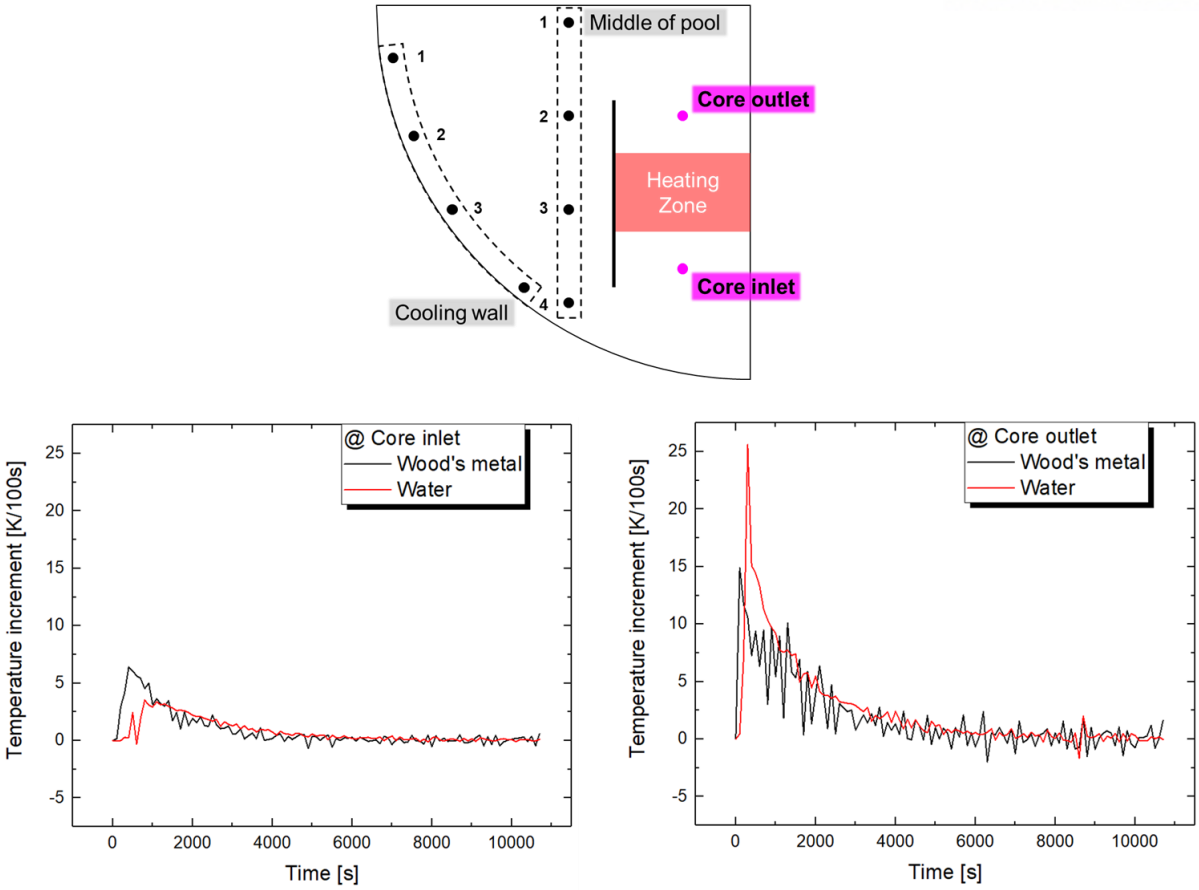

(a) inlet (b) outlet

Figure C-2. Actual, and predicted temperature history of the Wood's metal – inlet and outlet

Figure C-2 to C-4 shows temperature change rate of the actual Wood's metal and predicted temperature by water data. To remove fluctuation of the data, they were summarized in temperature increment per 100 seconds. In C-2, there were temperature history of the core inlet and outlet. Both inlet and outlet, they showed late transient in the initial phase, before 1000 seconds. After 1000 seconds, temperature increment per 100 seconds by actual Wood's metal and water showed good accordance. Red line (Wood's metal temperature predicted by water) follows black line (actual Wood's metal temperature) well. For the inlet, magnitude of the temperature increment was relatively small, and fluctuation was also small. Simulating experiment could predict Wood's metal temperature change quite well for the inlet. However, for outlet, there was large fluctuation in Wood's metal after 1000 seconds, which was caused by strong turbulent upward flow of heated metal from the heater. However here was no fluctuation in the water because thermocouple was installed not directly above the heater in the water facility. Despite of large fluctuation, water experiment follows Wood's metal temperature reasonably.

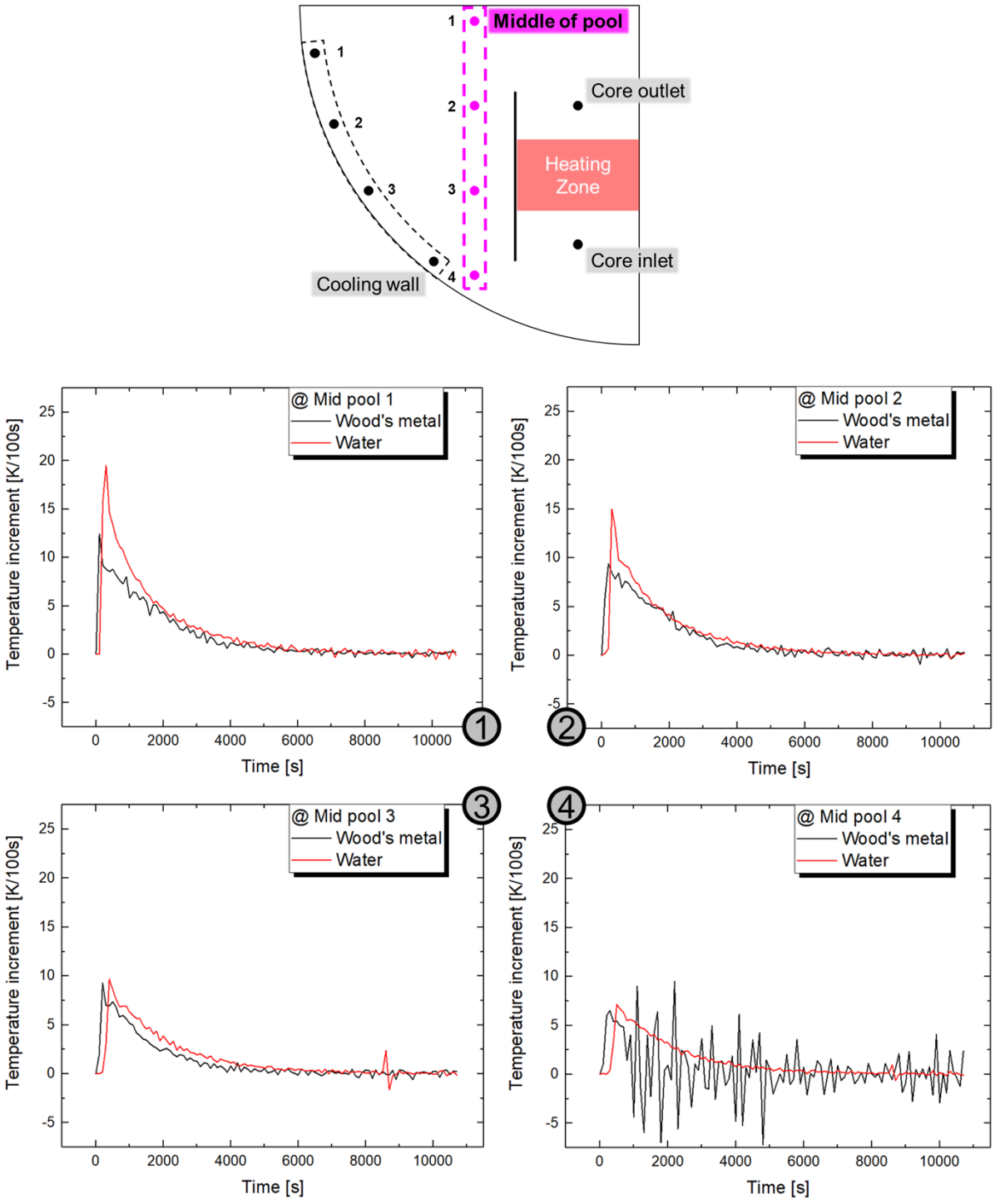

Figure C-3. Actual, and predicted temperature history of the Wood's metal – mid pool

C-3 shows temperature increment history for middle part of the pool. Point 1 was located at the top, and point 4 was located at the bottom. For the point 1, 2, and 3, overestimation in the water

experiment could be recognized by red line slightly above black line. Similar to the core part, initial rapid transient was late in the simulating experiment. Except for the initial transient, simulating experiment showed good accordance with actual temperature. However, regard to point 4, there was strong fluctuation in the Wood's metal experiment, while water experiments was not. It is related to the flow regime of the facilities. There was strong natural circulation flow at the point 1 and 4. However, at point 1, Wood's metal came from heater and there was enough space for mixing. Therefore, averaged temperature of the heated fluid was measured at the point 1 and there was no strong fluctuation. At the point 4, flow detached from the cooling wall and the flow was more turbulent in the Wood's metal. Although there was different temperature behavior by turbulence, overall temperature tendency was well predicted.

Temperature increment history about cooling wall summarized in figure C-4. For the hot region like point 1 and 2, slightly late, but more rapid initial temperature excursion was observed in the simulating experiment. After initial transient, simulating experiment showed good accordance with actual experiment, and stronger initial transient caused overestimation in the steady state analysis. Magnitude of the initial transient was weak enough to neglect itself in the point 3 and 4. Overall, there was no temperature fluctuation in the water simulating experiment, while actual Wood's metal experiment showed strong fluctuation regardless to the observation points. Similar to the point 4 in the mid pool case, these temperature fluctuations were caused by the turbulent downward flow through the cooling wall. Different to point 1 in the mid pool, where temperature also affected by the flow, temperature observation points in the cooling wall region were close to the cooling wall. Thus, temperature change by the cooling wall was reflected into data without mitigation or mixing through distance.

Quantitative error along time interval was summarized in table C-1. And to remove fluctuation, time interval for quantitative analysis was set as 1000 seconds. Because denominator of the error is temperature increment of the Wood's metal in the given time interval, there was large, and absurd errors in the small temperature increment interval, such as second half of the experiment (after 5000 seconds). However, this error summary could provide quantitative error value for the simulating experiment, and the result showed that simulating experiment could reasonably predict transient phenomena in the liquid metal natural circulation, except for initial transient and phenomena related to the flow regime.

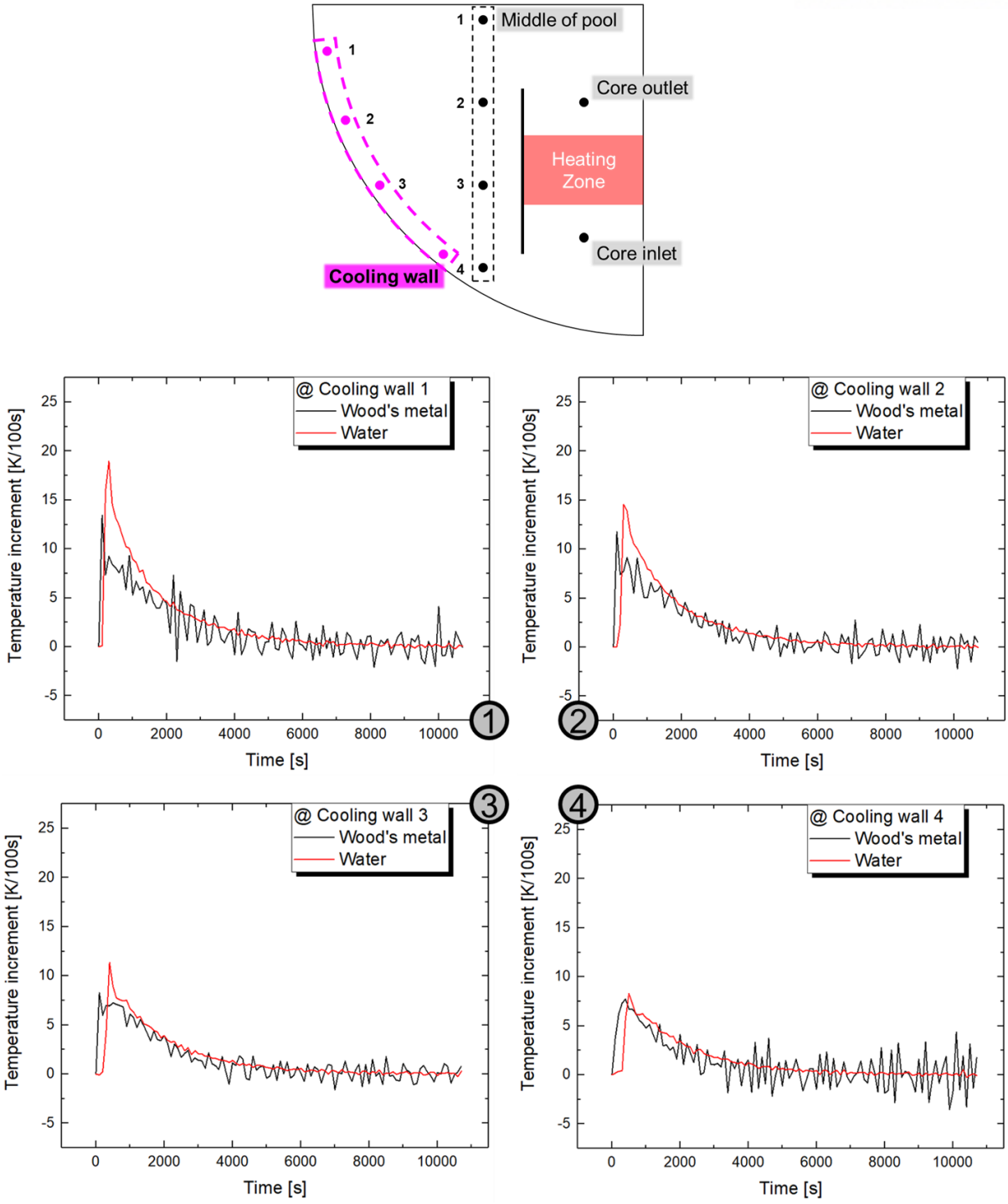

Figure C-4. Actual, and predicted temperature history of the Wood's metal – cooling wall

In summary, overall transient in the Wood's metal natural circulation could be reasonably predicted by the water simulating experiment. However, initial temperature excursion of the water, and fluctuation of the Wood's metal temperature should be into consideration.

Table C-1. Error summary for transient analysis

[%]	Core		Mid pool				Cooling wall			
Time interval	inlet	outlet	1	2	3	4	1	2	3	4
0 – 1000s	39.5	17.9	-8.3	-22.9	37.0	9.0	-9.5	14.6	32.9	-67.7
1000 – 2000s	25.0	14.3	12.2	25.0	20.3	9.5	41.0	386.5	26.8	15.6
2000 – 3000s	24.9	6.3	29.4	52.7	20.7	10.4	43.8	110.0	24.3	24.2
3000 – 4000s	56.2	49.2	81.4	81.8	51.1	45.5	103.5	-629.1	43.0	128.9
4000 – 5000s	49.5	66.2	34.9	184.6	39.2	40.7	81.8	80.5	47.0	120.0
5000 – 6000s	13.6	78.8	74.0	447.2	57.9	72.4	166.6	-14011.8	113.3	121.9
6000 – 7000s	28.4	75.3	295.6	16.7	47.4	41.9	101.8	-269.6	107.4	693.7
7000 – 8000s	24.3	-17.1	120.5	32.6	33.9	83.9	211.3	-324.1	5.3	-630.3
8000 – 9000s	61.1	1.7	-16.9	40.5	127.7	136.0	278.3	-453.2	1128.3	63.6
9000 – 10000s	40.5	69989.6	-230.3	-112.9	189.0	22.8	43.9	-282.3	332.3	172.5
10000 – 10700s	-757.5	74.5	-73.8	-93.5	-102.4	-52.2	-48.8	-86.6	-103.3	-83.5

D. Supplements for the experimental data

This part contains all experimental data for the SINCRO-V and SINCRO-2D experiment. All the data were summarized as figures

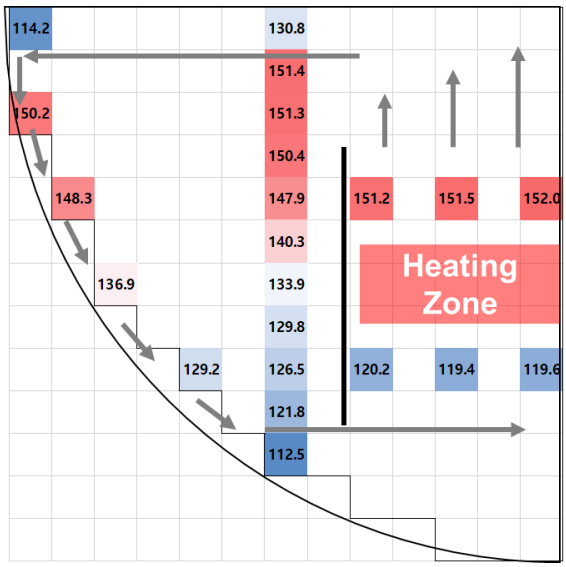

(a) first experiment

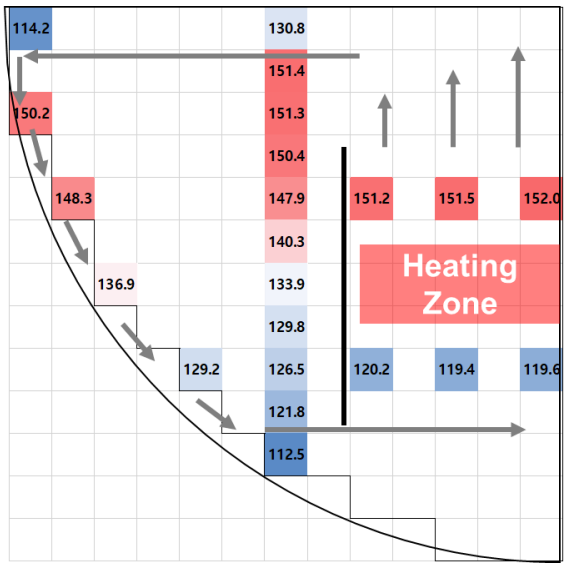

(b) second experiment

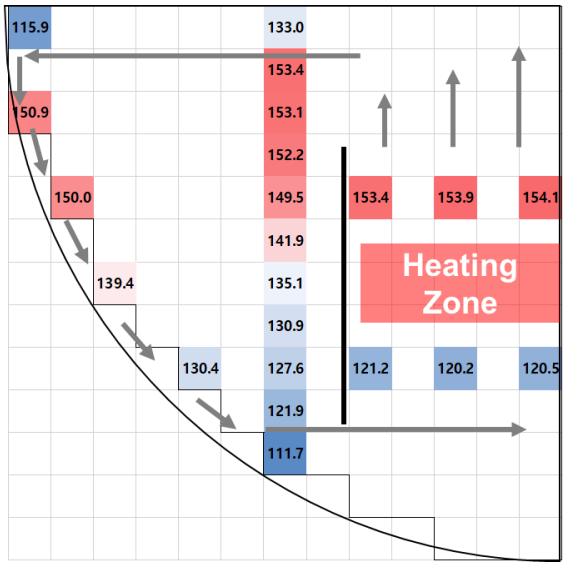

(c) third experiment

Figure D-1. Temperature distribution in SINCRO-V Wood's metal facility – 0.2 %

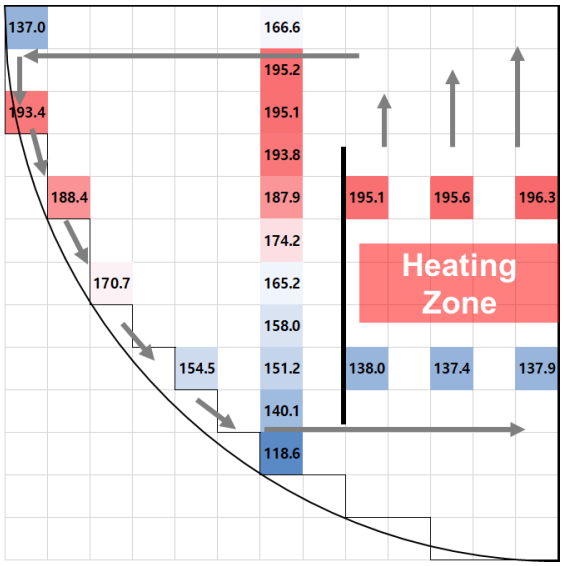

(a) first experiment

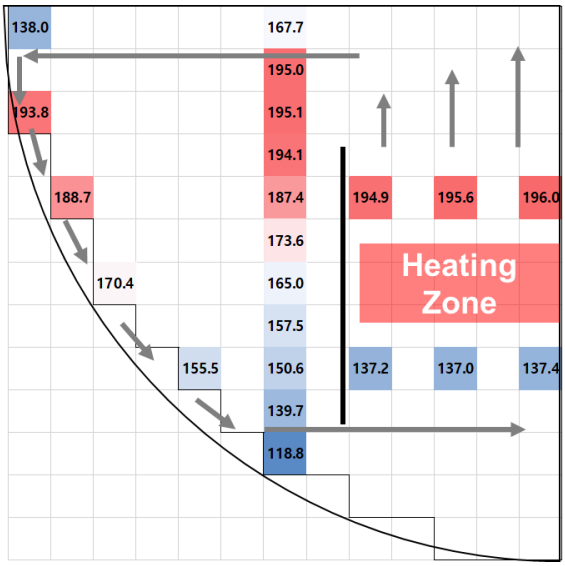

(b) second experiment

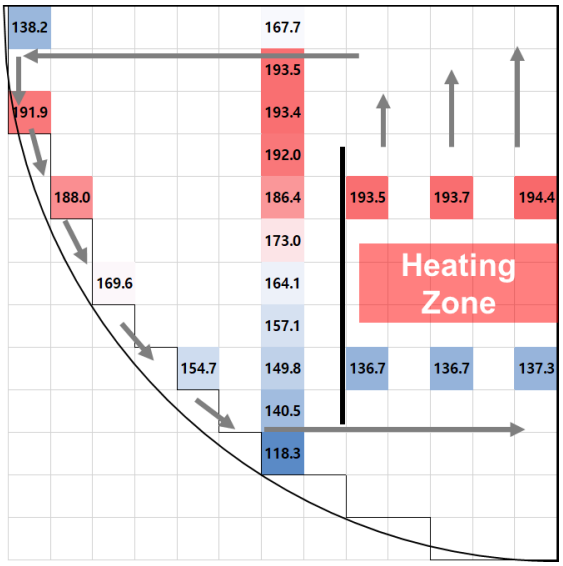

(c) third experiment

Figure D-2. Temperature distribution in SINCRO-V Wood's metal facility – 0.4 %

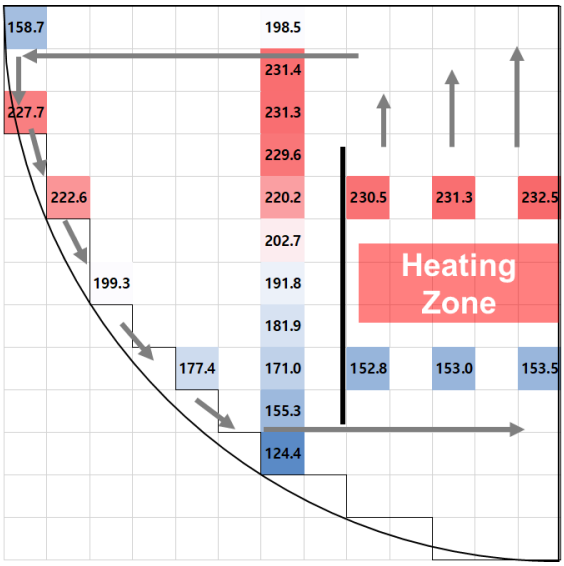

(a) first experiment

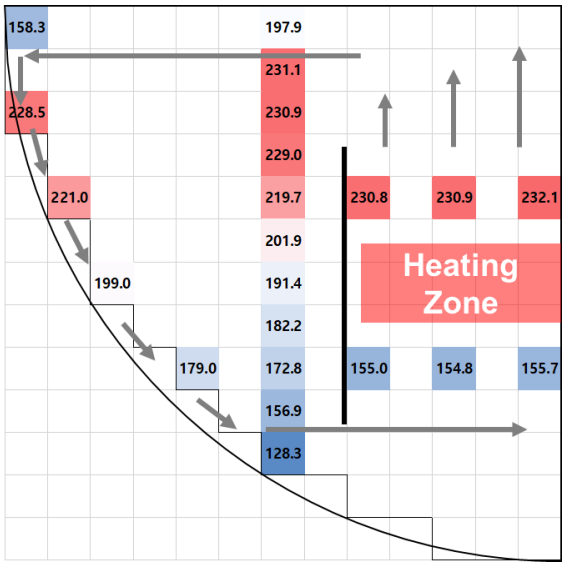

(b) second experiment

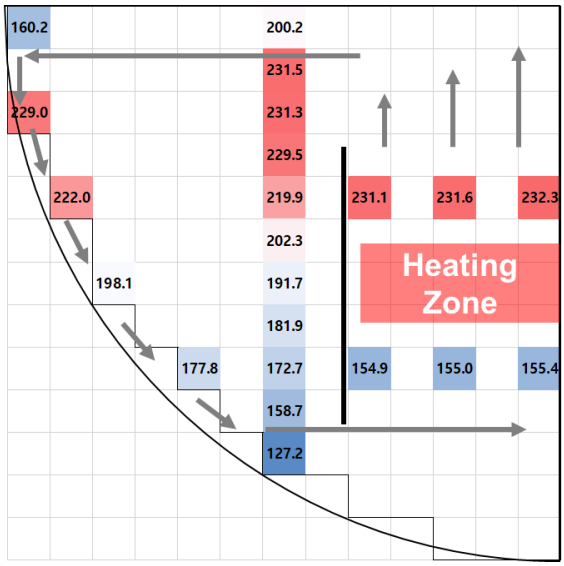

(c) third experiment

Figure D-3. Temperature distribution in SINCRO-V Wood's metal facility – 0.6 %

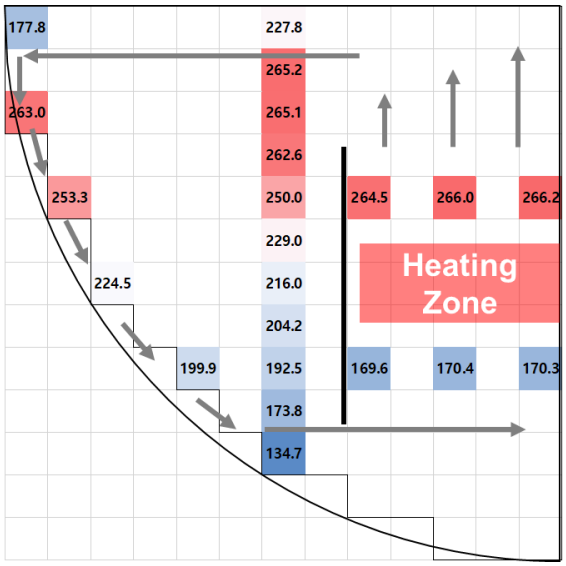

(a) first experiment

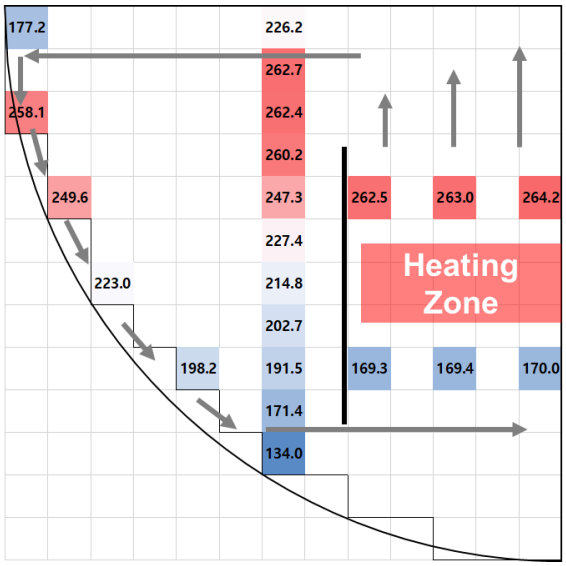

(b) second experiment

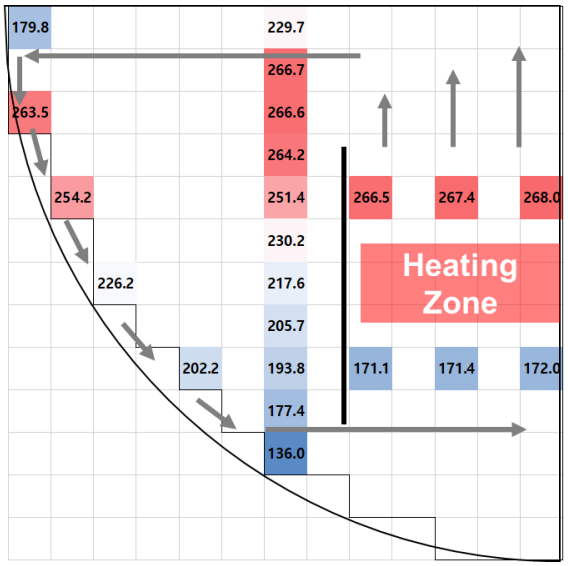

(c) third experiment

Figure D-4. Temperature distribution in SINCRO-V Wood's metal facility – 0.8 %

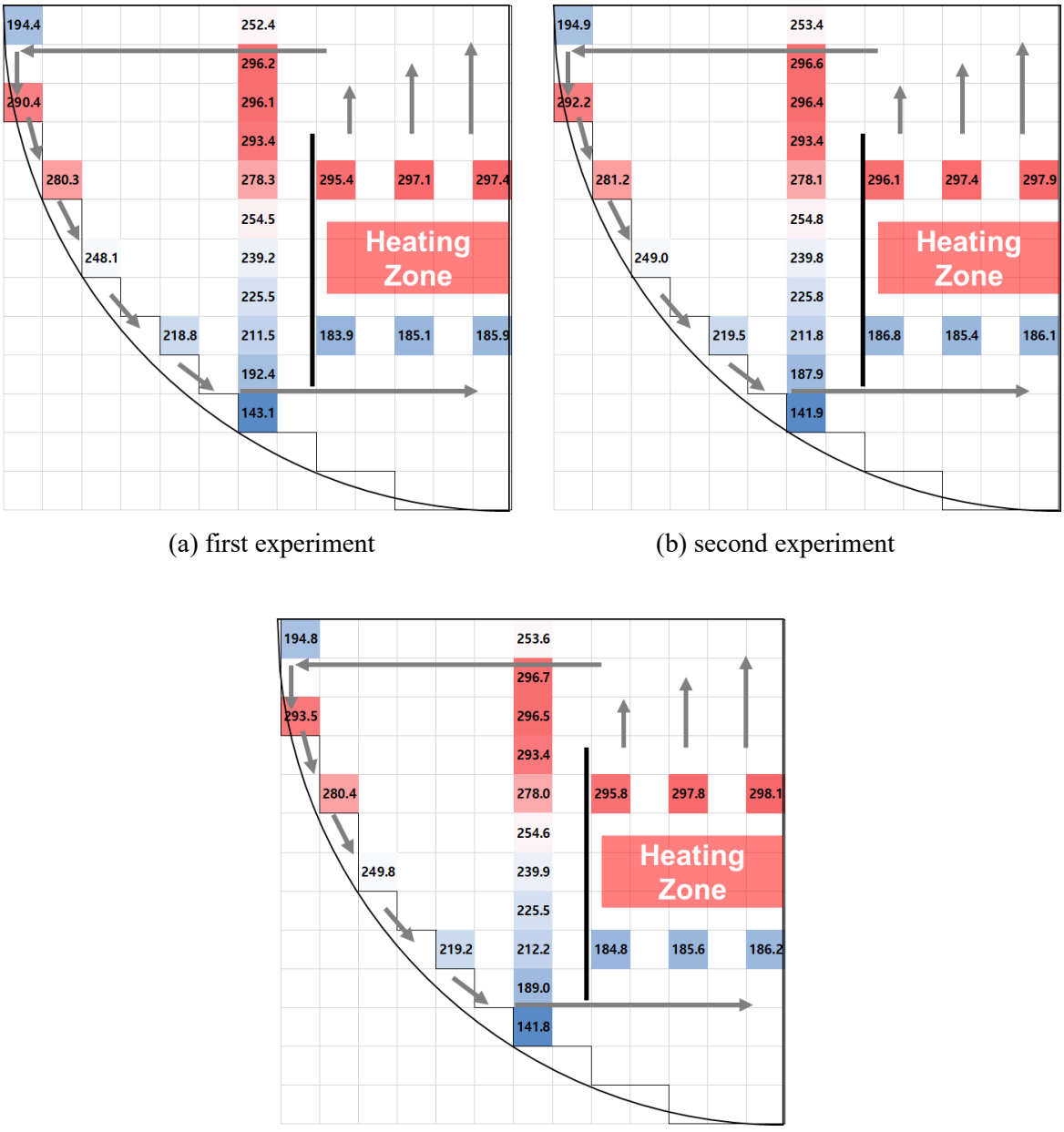

(a) first experiment

(b) second experiment

(c) third experiment

Figure D-5. Temperature distribution in SINCRO-V Wood's metal facility – 1.0 %

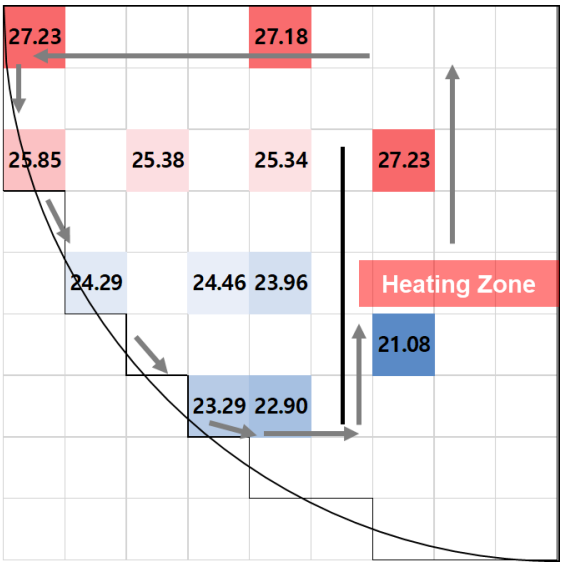

(a) first experiment

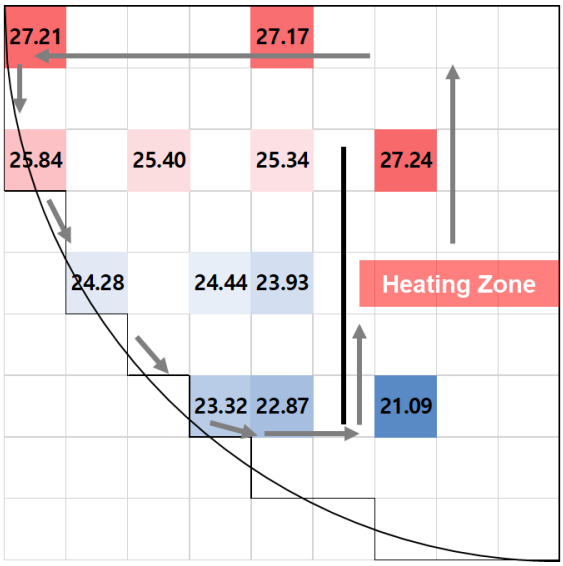

(b) second experiment

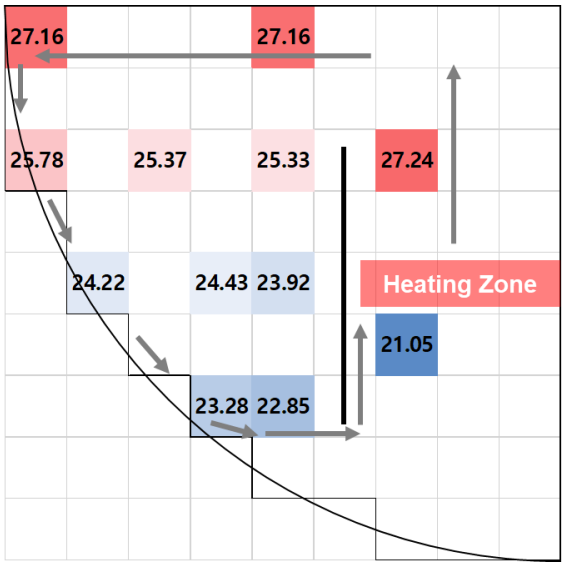

(c) third experiment

Figure D-6. Temperature distribution in SINCRO-V water facility – 0.2 %

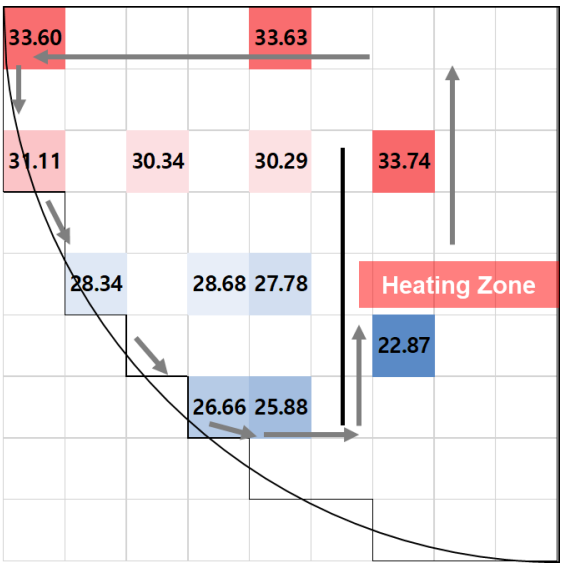

(a) first experiment

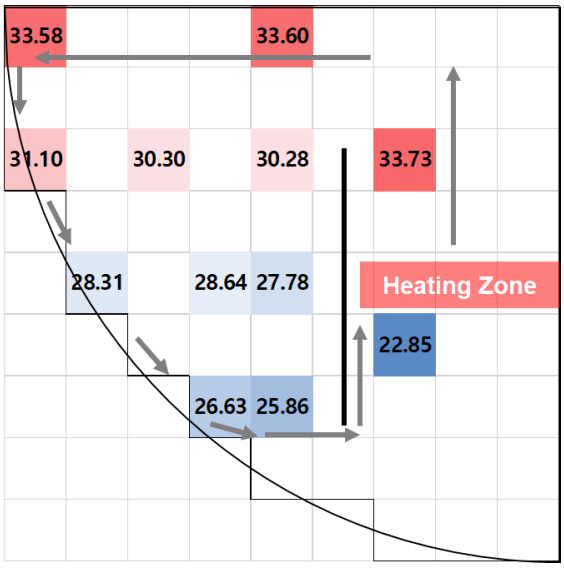

(b) second experiment

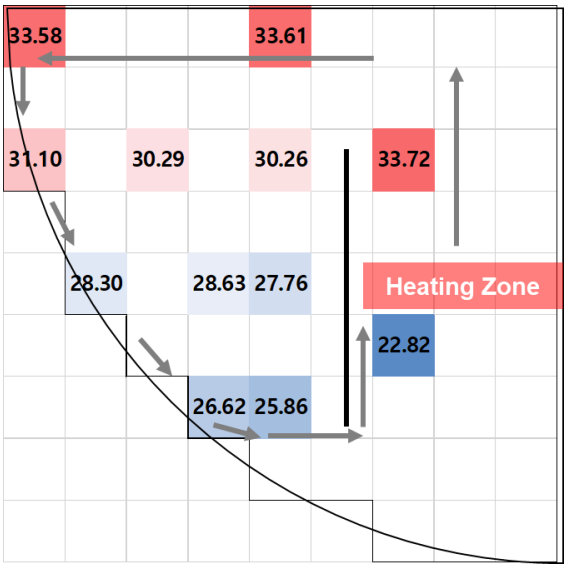

(c) third experiment

Figure D-7. Temperature distribution in SINCRO-V water facility – 0.4 %

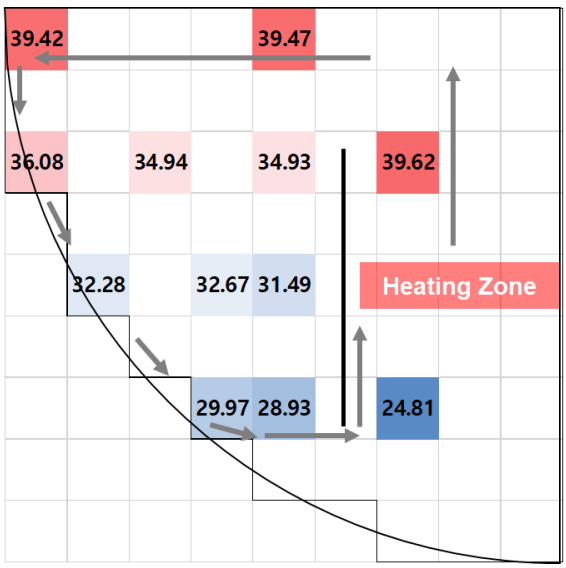

(a) first experiment

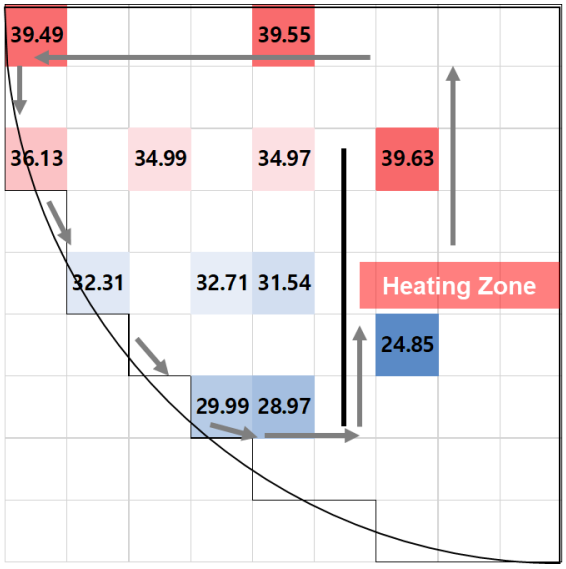

(b) second experiment

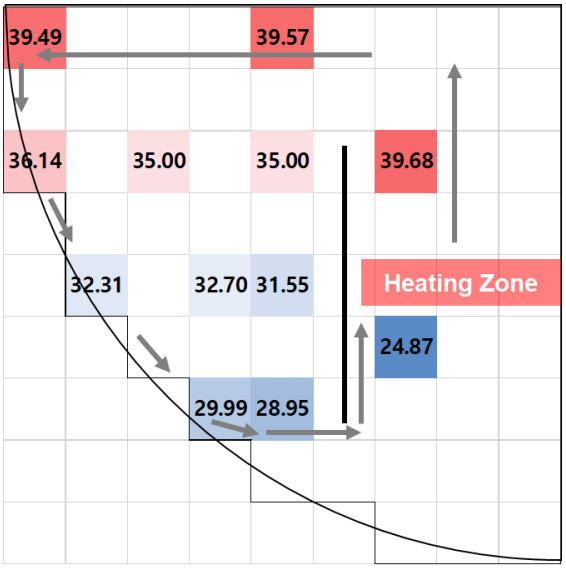

(c) third experiment

Figure D-8. Temperature distribution in SINCRO-V water facility – 0.6 %

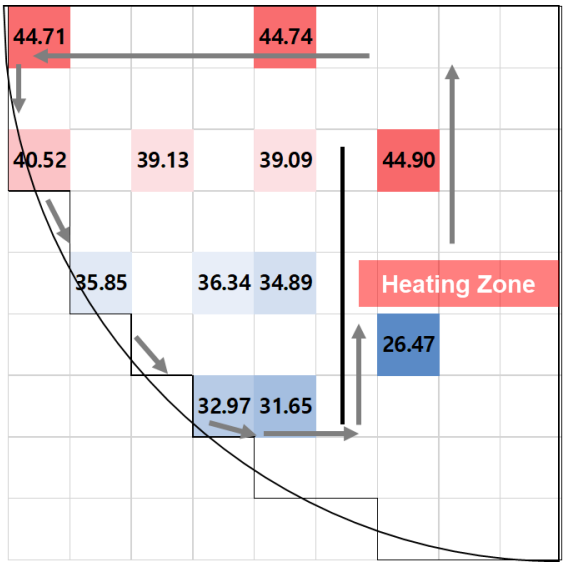

(a) first experiment

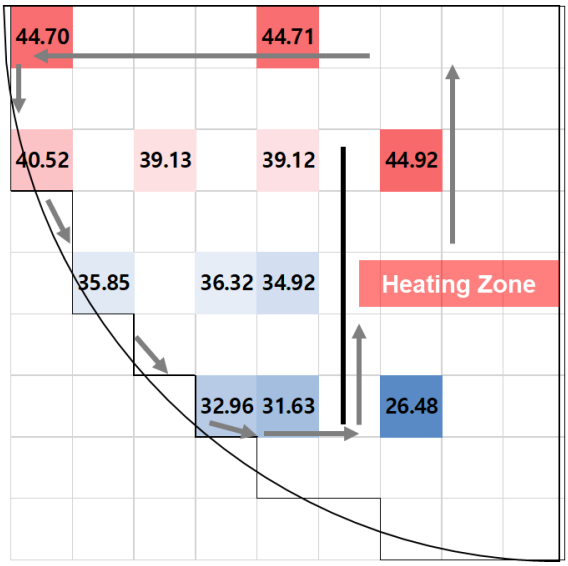

(b) second experiment

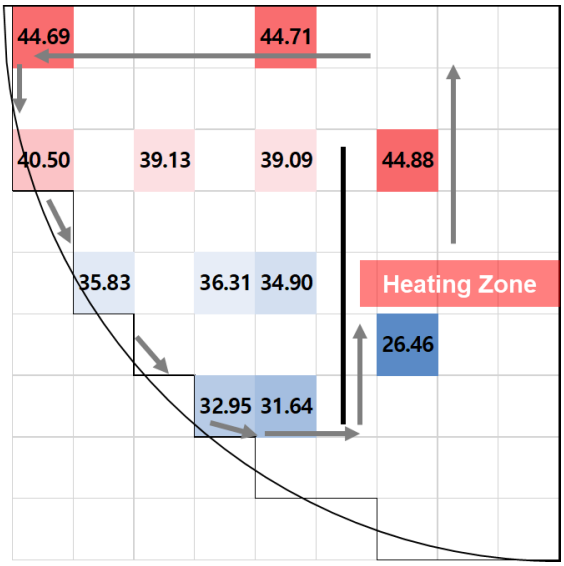

(c) third experiment

Figure D-9. Temperature distribution in SINCRO-V water facility – 0.8 %

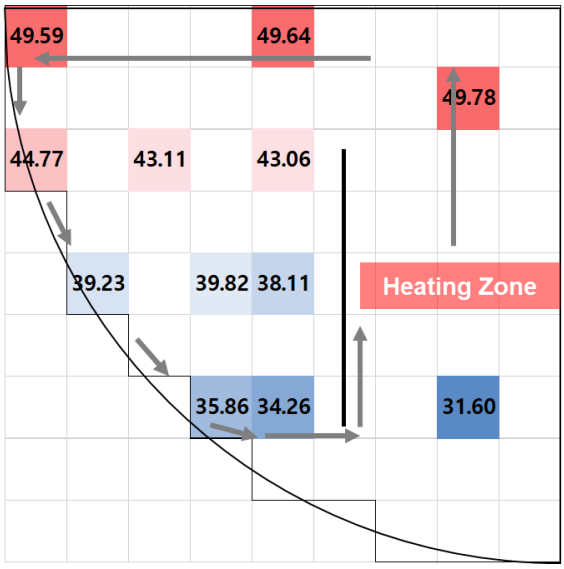

(a) first experiment

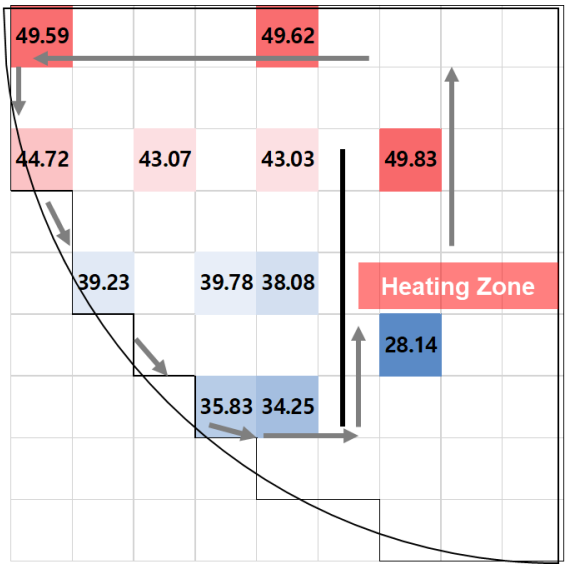

(b) second experiment

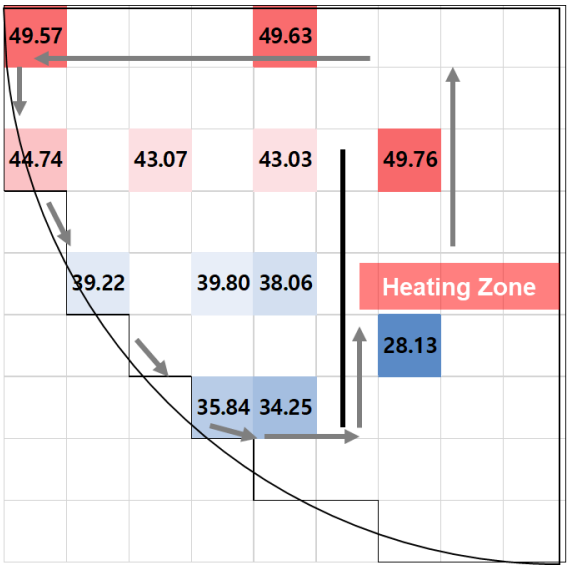

(c) third experiment

Figure D-10. Temperature distribution in SINCRO-V water facility – 1.0 %

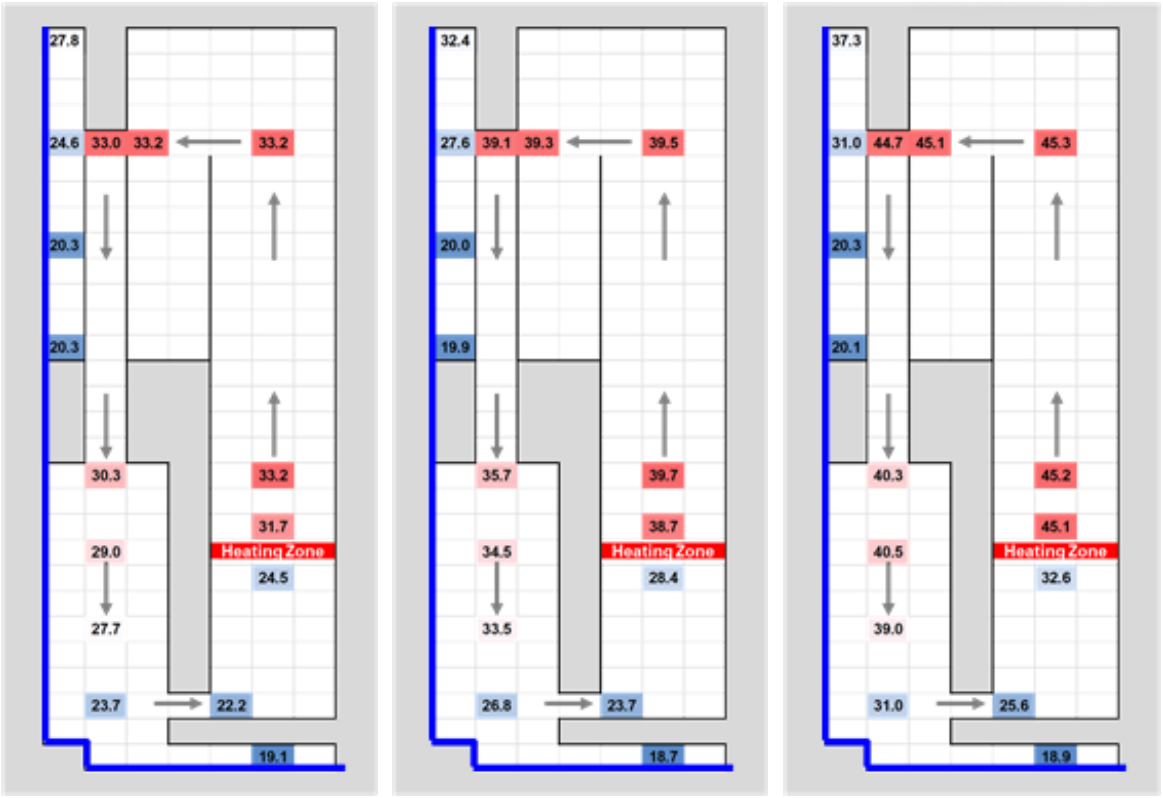

(a) 0.2 % (b) 0.4 % (c) 0.6 %

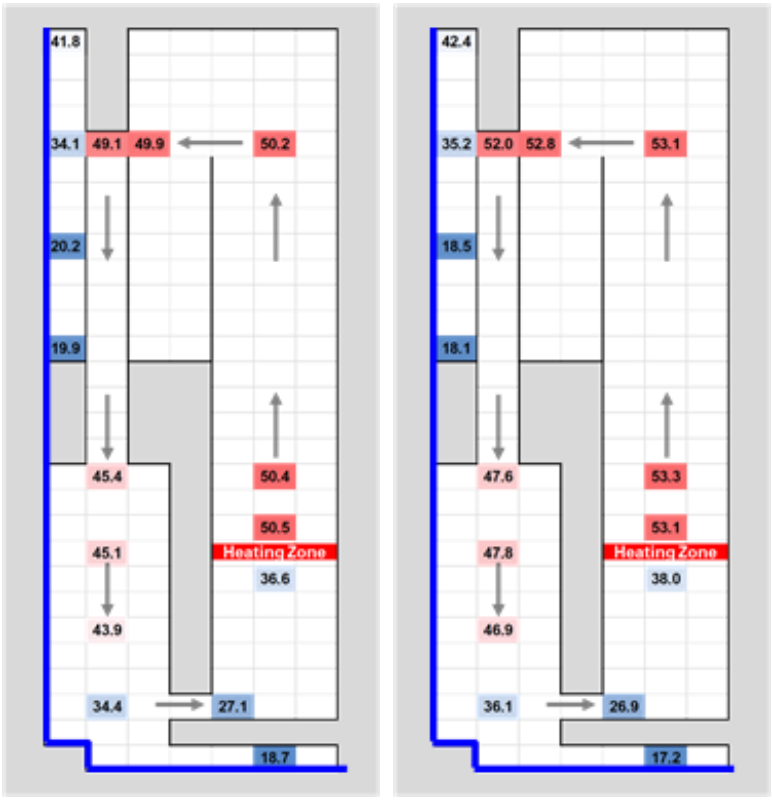

(d) 0.8 % (e) 1.0 %

Figure D-11. Temperature distribution in SINCRO-2D facility – various decay heat with $60\Delta T_{ref}$

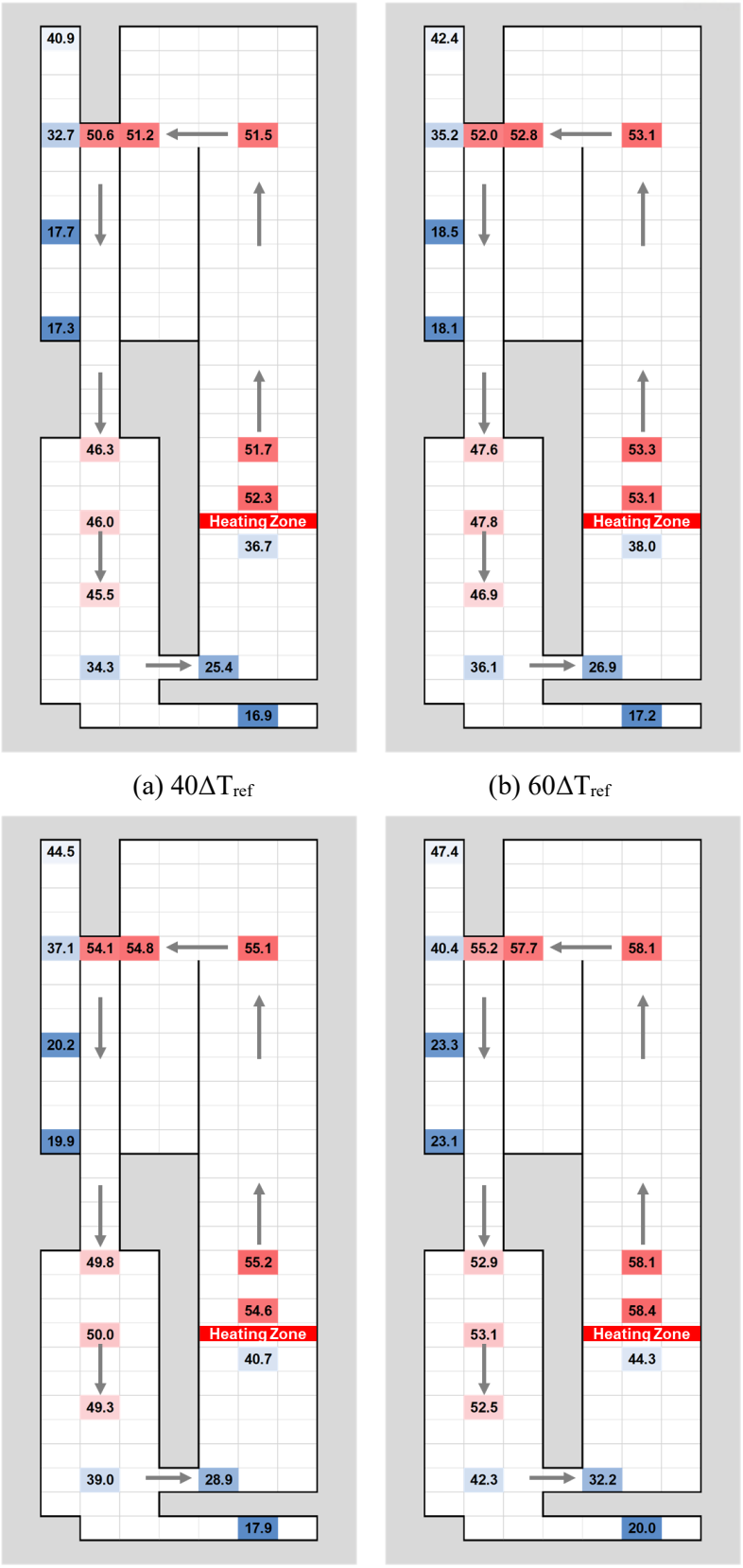

(a) $40\Delta T_{ref}$ (b) $60\Delta T_{ref}$

(c) $80\Delta T_{ref}$ (d) $100\Delta T_{ref}$

Figure D-12. Temperature distribution in SINCRO-2D facility – various B.C. with 1.0 % decay heat

Reference

[1] L. J. Koch, H. O. Monson, W. R. Simmons, M. Levenson, F. Verber, E. Hutter, R. A. Jaross, T. R. Spalding, J. R. Simanton, and A. Lovoff, Construction Design of EBR-II: An Integrated Unmoderated Nuclear Power Plant, No. A/CONF. 15/P/1782. Argonne National Lab., Lemont, III, 1958

[2] H. P. Planchon, J. I. Sackett, G. H. Golden, R. H. Sevy, Implications of EBR-II Inherent Safety Demonstration Test, Nuclear Engineering and Design 101 (1987) 75-90.

[3] W. K. Lehto, R. M. Fryer, E. M. Dean, J. F. Koenig, L. K. Chang, D. Mohr, E. E. Feldman, Safety Analysis for the Loss-of-flow and Loss-of-Heat sink without Scram Tests in EBR-II, Nuclear Engineering and Design 101 (1987) 35-44.

[4] C. E. Lahm, J. F. Koenig, P. R. Betten, J. H. Bottcher, W. K. Lehto, B. R. Seidel, EBR-II Driver Fuel Qualification for Loss-of-flow and Loss-of-heat-sink Tests without Scram, Nuclear Engineering and Design 101 (1987) 25-34.

[5] E. E. Feldman, D. Mohr, L. K. Chang, H. P. Planchon, E. M. Dean, P. R. Betten, EBR-II Unprotected Loss-of-heat-sink Predictions and Preliminary Test Results, Nuclear Engineering and Design 101 (1987) 57-66.

[6] D. Mohr, L. K. Chang, E. E. Feldman, P. R. Betten, H. P. Planchon, Loss-of-primary-flow-without-scram Tests: Pretest Predictions and Preliminary Results, Nuclear Engineering and Design 101 (1987) 45-56.

[7] USDOE, Fast Flux Test Facility Overall Conceptual Systems Design Description, United States Department of Energy BNWL-500, 1. 1967.

[8] D. W. Wootan, R. P. Omberg, T. Sofu, and C. Grandy, Passive Safety Testing at the Fast Flux Test Facility Relevant to New LMR Designs, Proceedings of the International Conference on Fast Reactor and Related Fuel Cycles, June 26-29, 2017 – Yekaterinburg, Russia.

[9] T. R. Beaver, H. G. Johnson, and R. L. Stover, Transient Testing of the FFTF for Decay Heat Removal by Natural Circulation, Proceedings of International Topical Meeting on Liquid Metal Fast Reactor Safety and Related Design and Operational Aspects, July 19-23, 1982 – Lyon, France.

[10] H. Ninokata, A. Yamaguchi, and A. Deguchi, An Analytical Investigation of Decay Heat Removal Performance of an LMFBR under Adverse Thermal Conditions, Science and Technology of Fast Reactor Safety, (1987) 281-287.

[11] S. Yoshikawa, A. Yamaguchi, I. Maekawa, and H. Ninokata, An Integrated Analysis of Natural Circulation Test in Joyo using SSC-L and COMMIX-1A, Proceedings of the International Topical Meeting on Fast Reactor Safety, 1, (1985) 293-300.

[12] K. Nabeshima, N. Doda, H. Oshima, T. Mori, H. Ohira, and T. Iwasaki, Analysis of Natural Circulation Test in the Experimental Fast Reactor Joyo, Proceedings of the NURETH-16, Chicago, IL,

August 30-September 4, 2015.

[13] M. Sawada, H. Arikawa, and N. Mizoo, Experiment and Analysis on Natural Convection Characteristics in the Experimental Fast Reactor Joyo, Nuclear Engineering and Design 120 (1990) 341-347.

[14] K. Kawashima, T. Saito, and S. An, Decay Heat Removal System of Monju, Proceedings of Meetings of Specialists on the Reliability of Decay Heat Removal Systems for Fast Reactors. Summary report 1975.

[15] T. Ishizu, H. Endo, Y. Shindo, and K. Haga, An Evaluation of Passive Safety Features of the Japanese Prototype LMFBR Monju, Proceedings of the NURETH-11, Avignon, France, October 2-6, 2005.

[16] A. Hunsbedt, P. M. Magee, Design and performance of the PRISM natural convection decay heat removal system, Proceedings of the International Topical Meeting on Safety of Next Generation Power Reactors, Seattle, Washington May 1-5 1988.

[17] G. J. Van Tuyle, G. C. Slovic, B. C. Chan, R. J. Kennett, H. S. Cheng, and P. G. Kroeger, Summary of Advanced LMR Evaluations – PRISM and SAFR, NUREG/CR-5364 BNL-NUREG-52197, 1989.

[18] K. Kasza, C. Grandy, Y Chang, and H Khalil, Argonne Liquid-Metal Advanced Burner Reactor: Components and In-Vessel System Thermal- Hydraulic Research and Testing Experience Pathway Forward, ANL/NE--07/21 2007.

[19] J. Yoo, J. Chang, J. Y. Lim, J. S. Cheon, T. H. Lee, S. K. Kim, K. L. Lee, and H. K. Joo, Overall System Description and Safety Characteristics of Prototype Gen IV Sodium Cooled Fast Reactor in Korea, Nuclear Engineering and Technology 48 (2016) 10595-1070.

[20] A. D. Shin, Y. W. Choi, and M. H. Bae, Preliminary Assessment of the Loss of Flow Accident for PGSFR, Proceedings of the Korean Nuclear Society Autumn Meeting, Pyeongchang, Korea, October 30-31, 2014

[21] K. L. Lee, K. S. Ha, J. H. Jeong, C. W. Choi, T. K. Jeong, S. J. Ahn, S. W. Lee, W. P. Chang, S. H. Kang, J. Y. Yoo, A Preliminary Safety Analysis for the Prototype Gen-IV Sodium-Cooled Fast Reactor, Nuclear Engineering and Technology 48 (2016) 1071-1082.

[22] C. W. Choi, T. K. Jeong, and S. J. An, Thermal-hydraulic analyses of passive reactor vault cooling system (RVCS) in PGSFR using MARS-LMR, Annals of Nuclear Energy 117 (2018) 333–342.

[23] F. Varaine, G. Rodriguez, D. Settimo, J. M. Hamy, H. Hayafune, S. Romdhane, R. P. Benard, A. Remy, T. Chauveau, L. Vandendriesche, Mochida, T. Itsuka, D. Robertson, M. Lefrancois, M. Fukuie, and J. L. Mazel, Status of the ASTRID Sodium Fast Reactor Project : from Conceptual Design to Basic Design Phase, Proceedings of ICAPP 2017 Fukui and Kyoto (Japan), April 24-28, 2017.

[24] H. Edouard, T. Mihara, A. Dauphin, A. Ide, and J. F. Dirat, ASTRID Nuclear Island Design Update in French-Japanese Joint Team Development of Decay Heat Removal Systems, Proceedings of ICAPP 2018, Charlotte, United States Apr 2018.

[25] F. Auberta, B. Baudea, P. Gauthéa, M. Marquèsa , N. Pérota, F. Bertranda, C. Vaglio-Gaudard, V. Rychkov, M. Balmain, Implementation of probabilistic assessments to support the ASTRID decay heat removal systems design process, Nuclear Engineering and Design 340 (2018) 405–413.

[26] L. Cinotti, C. F. Smith, and H. Sekimoto, Lead-Cooled Fast Reactor (LFR): overview and perspectives, Proceedings of the Gen-IV International Forum Symposium, Paris (France) 9-10 September 2009.

[27] A. Alemberti, V. Smirnov, C. F. Smith, and M. Takahashi, Overview of Lead-cooled Fast Reactor Activities, Progress in Nuclear Energy 77 (2014) 300-307.

[28] A. Alemberti, M. L. Frogheri, S. Hermsmeyer, L. Ammirabile V. Smirnov, M. Takahashi, C. F. Smith, Y. Wu, and I. S. Hwang, Lead-cooled Fast Reactor (LFR) Risk and Safety Assessment White Paper, Gen-IV International Forum 2014.

[29] I. Sato, Y. Tobita, K. Konishi, K. Kamiyama, J. Toyooka, R. Nakai, S. Kubo, S. Kotake, K. Koyama, Y. Vassiliev, A. Vurim, V. Zuev and A. Kolodeshnikof, Safety Strategy of JSFR Eliminating Severe Recriticality Events and Establishing In-Vessel Retention in the Core Disruptive Accident, Journal of NUCLEAR SCIENCE and TECHNOLOGY, Vol. 48, No. 4, p. 556–566 (2011)

[30] S. Kotake, Y. Sakamoto, T. Mihara, S. Kubo, N. Uto, Y. Kamishima, K. Aoto, and M. Toda, Development of Advanced Loop-Type Fast Reactor in Japan, Nuclear Technology 170 (2010) 133-147.

[31] H. Zhao, and H. Zhang, An Innovative Hybrid Loop-Pool Design for Sodium Cooled Fast Reactor, No. INL/CON-07-12657. Idaho National Laboratory (INL), 2007.

[32] C. G. Park, J. B. Kim, and J. H. Lee, Design Study of an IHX Support Structures for a Pool-type Sodium-cooled Fast Reactor, Nuclear Engineering and Technology, 41, (2009) 1323-1332.

[33] F. Gauché, Generation IV reactors and the ASTRID prototype: Lessons from the Fukushima accident, Comptes Rendus Physique Vol. 13, Issue 4 (2012) 365-371.

[34] C. Jammes, N. Chapoutier, P. Filliatrea, J. P. Jeannot, F. Jadot, D. Verrier, A. C. Scholer, and B. Bernardine, Neutron flux monitoring system of the French GEN-IV SFR: Assessment of diverse solutions for in-vessel detector installation, Nuclear Engineering and Design 270 (2014) 273–282.

[35] M. Angelucci, D. Martelli, G. Barone, I. Di Piazza, and N. Forgione, STH-CFD Codes Coupled Calculations Applied to HLM Loop and Pool Systems, Science and Technology of Nuclear Installations, (2017) 13p.

[36] G. Wu, M. Jin, J, Chen, Y. Bai, and Y. Wu, Assessment of RVACS performance for small size lead-cooled fast reactor, Annals of Nuclear Energy 77 (2015) 310–317.

[37] S. Yeom, S. H. Ryu, D. Kim, and T. H. Lee, The Effect of Duct Level on the Performance of Reactor Vault Cooling System in the PGSFR, Proceedings of the Korean Nuclear Society Autumn Meeting Gyeongju, Korea, October 29-30, 2015

[38] S. H. Ryu, S. Yeom, and T. H. Lee, The Effect of Air Separator Geometry on the RVCS in PGSFR, Proceedings of the Korean Nuclear Society Autumn Meeting Gyeongju, Korea, October 29-30, 2015

[39] S. Grewal and E. Gluekler, Water Simulation of Sodium Reactors, Chemical Engineering Communications 17 (1982) 3443-360.

[40] Y. Ieda, H. Kamide, H. Ohshima, S. Sugawara, and H. Ninokata, Strategy of Experimental Studies in PNC on Natural Convection Decay Heat Removal, Proceedings of IAEA-IWGFR Specialists' Meeting on "Evaluation of Decay Heat Removal by Natural Convection", O-arai, Japan, 1993.

[41] Y. Eguchi, H. Takeda, T. Koga, N. Tanaka, K. Yamamoto, Quantitative prediction of natural circulation in an LMFR with a similarity law and a water test, Nuclear Engineering and Design 178 (1997) 295–307.

[42] H. Hoffman, D. Weinberg, Y. Ieda, K. Marten, H. Tschöke, H. H. Frey, and Kurt Dres, Thermohydraulic Investigations of Decay Heat Removal Systems by Natural Convection for Liquid-Metal Fast Breeder Reactors, Nuclear Technology 88 (1989) 75-88.

[43] H. Hoffman, D. Wienberg, and R. Webstar, Investigation on Natural Convection Decay Heat Removal for the EFR – Status of the Program, Proceedings of IAEA-IWGFR Specialists' Meeting on "Passive and Active Safety Features of LMFRs", Oarai, Japan, 1991.

[44] D. Wienberg, H. Hoffman, H. Ohira, and G. Schnetgöke, The Status Study Using RAMONA and NEPTUN Models on Decay Heat Removal by Natural Convection for the European Fast Reactor, Proceedings of IAEA-IWGFR Specialists' Meeting on "Evaluation of Decay Heat Removal by Natural Convection in Fast Reactor", Mito, Japan, 1993.

[45] D. Wienberg, K. Rust, and H. Hoffmann, Overview Report of RAMONA-NEPTUN Program on Passive Decay Heat Removal, Report FZKA 5667, Forschungszentrum Karlsruhe, 1996.

[46] N. Tanaka, S. Moriya, S. Ushijima, T. Koga, and Y. Eguchi, Prediction Method for Thermal Stratification in a Reactor Vessel, Nuclear Engineering and Design 120 (1990) 395-402.

[47] M. Akutsu, Y. Okabe, K. Satoh, H. Kamide, K. Hayashi, N. Naohara, K. Iwashige, and Y. Shibata, Study of Thermal-Hydraulic Characteristics during Decay Heat Removal in a Pool-Type Fast Breeder Reactor, Nuclear Technology 98 (1992) 14-26.

[48] H. Takeda, and T. Koga, Study on Similarity Rule for natural Circulation Water Test of LMFBR, Proceedings of IAEA-IWGFR Specialists' Meeting on "Evaluation of Decay Heat Removal by Natural Convection in Fast Reactor", Mito, Japan, 1993.

[49] H. Takeda, T. Koga, and O. Watanabe, Experimental and computational simulation for natural circulation in an LMFBR, Nuclear Engineering and Design 140 (1993) 331-340.

[50] K. Rust, H. Tschöke, and D. Weinberg, Influence of the position and number of decay heat exchangers on the thermal hydraulics of a slab test facility: A comparison of analytical and experimental data, Experimental Thermal and Fluid Science 9 (1994) 413-425.

[51] V. M. Mente, G. K. Pandey, I. Banerjee, S. Ajesh Kumar, G. Padmakumar, and K.K. Rajan, Experimental studies in water for safety grade decay heat removal of prototype fast breeder reactor, Annals of Nuclear Energy 65 (2014) 114–121

[52] T. Murakami, Y. Eguchi, K. Oyama, and O. Watanabe, Reduced-scale water test of natural circulation for decay heat removal in loop-type sodium-cooled fast reactor, Nuclear Engineering and Design 288 (2015) 220–231.

[53] A. Ono, A. Kurihara, M. Tanaka, H. Oshima, and H. Kamide, Study on Reactor Vessel Coolability of Sodium-cooled Fast Reactor under Severe Accident Condition – Water Experiments using a Scale Model -, ICAPP 2017, Fukui and Kyoto, Japan, 2017.

[54] P. Planquarta, and K. van Tichelen, Experimental investigation of accidental scenarios using a scale water model of a HLM reactor, Nuclear Engineering and Design 346 (2019) 10-16.

[55] D. H. Han, and J. H. Choi, Liquid Metal Reactor Design Technology Development, KAERI/RR-2507/2004, 2004.

[56] R. Radu, P. Ilie, T. Minoru, and R. Mereu, Breakup and Solidification Behaviour of Liquid Metal Jet in Water Environment, Proceedings of International Conference Nuclear Energy for New Europe, Portorož, Slovenia, September 14− 17, 2015. SVN, 2015.

[57] M. M. Rahman, T. Hino, K. Morita, T. Matsumoto, K. Nakagawa, K. Fukuda, and W. Maschek et al., Experimental Study on Freezing Behavior of Molten Metal on Structure, Memoirs of the Faculty of Engineering, Kyushu University, 65(2) June 2005

[58] L. Guo, Y. Kawano, S. Zhang, T. Suzuki, K. Morita, and K. Fukuda, Numerical Simulation of Rheological Behavior in Melting Metal using Finite Volume Particle Method, Journal of Nuclear Science and Technology 47(11) (2010) 1011-1022.

[59] K. H. Bang, J. M. Kim, and D. H. Kim, Experimental Study of Melt Jet Breakup in Water, Journal of Nuclear Science and Technology, 40(10) (2003) 807-813.

[60] R. Secareanu, R. Mereu, M. Takahashi, F. Inzoli, and I. Prisecaru, Experimental and numerical study of freezing and flow characteristics of Wood's Metal injection in a water pool, Applied Thermal Engineering 103 (2016) 1261-1277.

[61] S. S. Son, P. O. Na, and K. W. Yi, The effect of crystal rotation direction on the thermal and velocity fields of a Czochralski system with a low Prandtl number, Journal of Crystal Growth 292 (2006) 272-281.

[62] B. I. Kazandzhan, V. M. Matveev, T. B. Savich, A. M. Umarov, Experimental-study of the electrical conductivity, density, and viscosity of a wood alloy, TVT, 1989, Volume 27, Issue 2, 269–273

[63] B. E. Schubert, and D. Floreano, Electronic Supplementary Information (ESI): Variable stiffness material based on rigid low-melting-point-alloy-microstructures embedded in soft poly(dimethylsiloxane) (PDMS), RSC Advances 46 (2013) 24671-24679

[64] S. Kondo, S. Konishi, M. Isozaki, S. Imahori, A. Furutani, and D. J. Brear, Experimental study on simulated molten jet-coolant interactions, Nuclear Engineering and Design 155 (1995) 73-84.

[65] H. K. Joo, J. W. Yoo, Y. I. Kim, J. W. Jang, M. H. Jang , Y. J. Kim, J. Y. Lim, S. R. Choi, S. H. Yoon, and M. J. Lee, NSSS Design and Validation of Prototype Gen-IV Sodium Cooled Fast Reactor - Mechanical Design of Prototype Gen-IV Sodium Cooled Fast Reactor, (KAERI/RR--4059/2015). Korea, Republic of (2016)

[66] M. H. Lee, D. W. Jerng, and In Cheol Bang, Simulating Sodium Pool Natural Circulation in RVACS Operation using CFD, Proceedings of the International Congress on Advances in Nuclear Power Plants (ICAPP) 2018, Charlotte, NC, April 8-11, 2018.

[67] A. Kraus, and R. Hu, CFD Simulation of Natural Convection Cooling after a Loss-of Flow Transient, Proceedings of the NURETH-16, Chicago, IL, August 30-September 4, 2015.